GEO 225 Week 5 Lecture # 3

Earthquake focal mechanisms — played an important early role in development of plate tectonic theory.

In classical field geology, offset of features used to determine sense of motion on a fault.

Example — offset streams on SA fault in Carrizo Plain ⇒ right lateral motion.

The mid-ocean ridges were observed to be offset by major strike-slip faults.

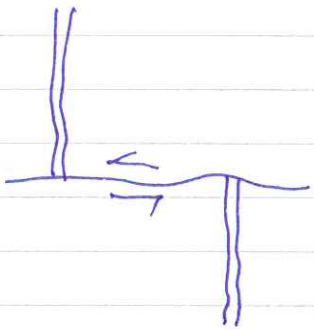

if this were an ordinary strike-slip fault offsetting the ridge topography like a stream this would be left lateral

Transform fault hypothesis of J. Tuzo Wilson

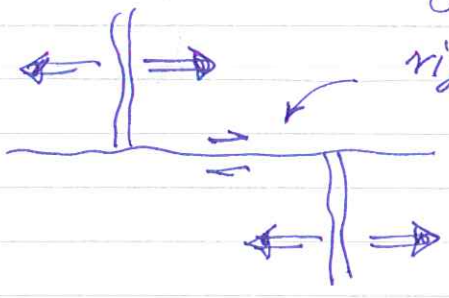

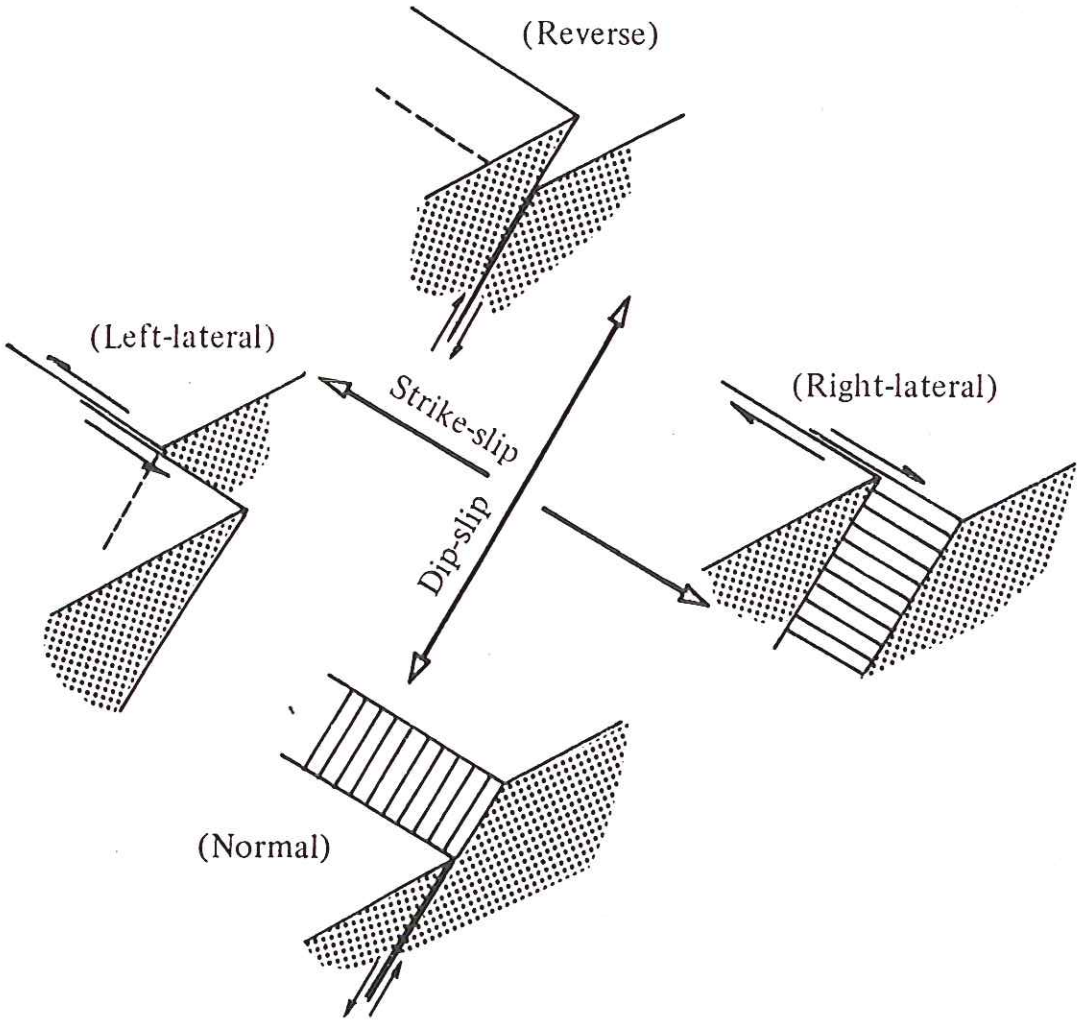

Fig. 4.2. Basic models of fault slipping.

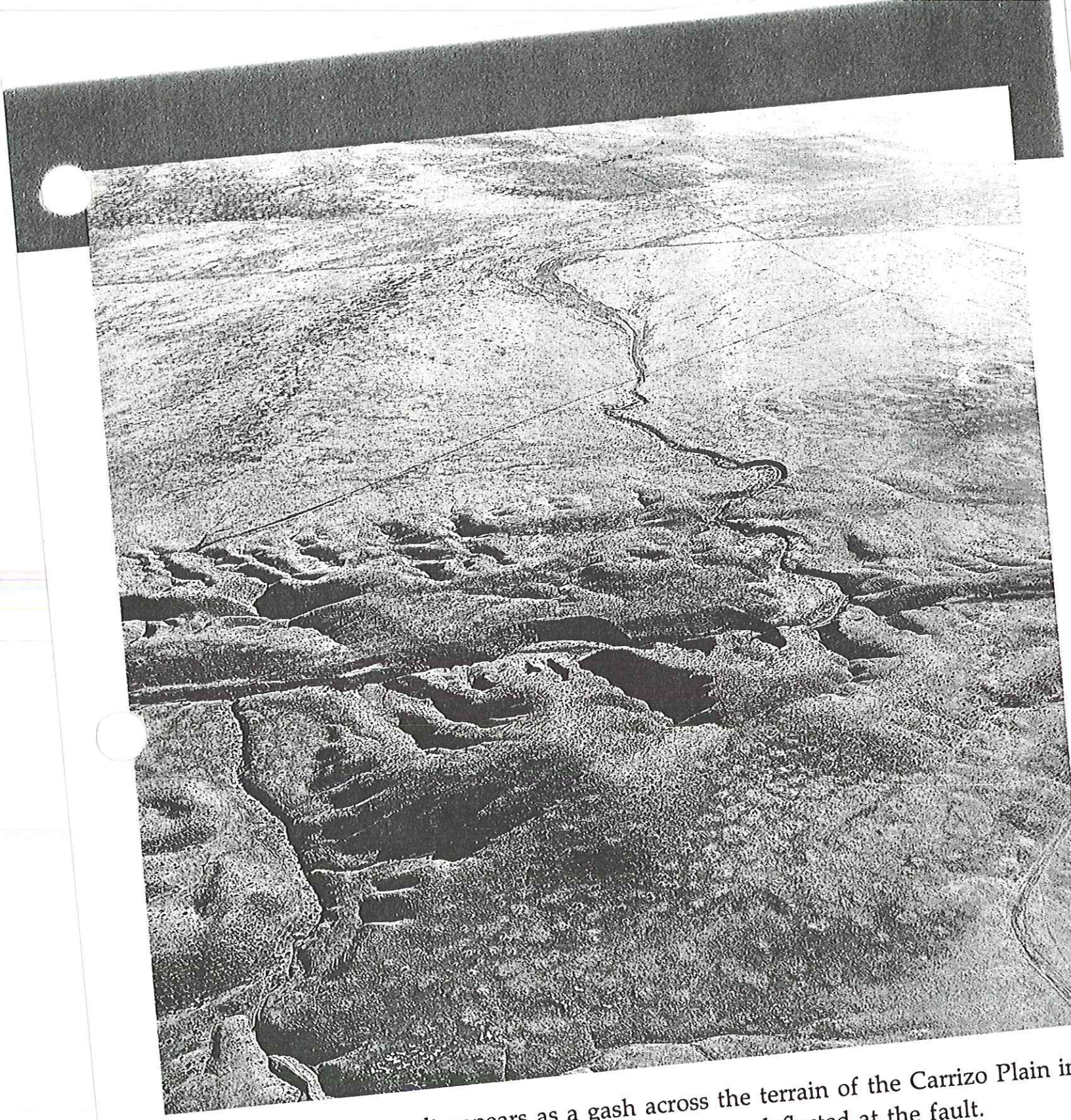

The San Andreas Fault appears as a gash across the terrain of the Carrizo Plain in Central California. Note the offset streams deflected at the fault.

right lateral

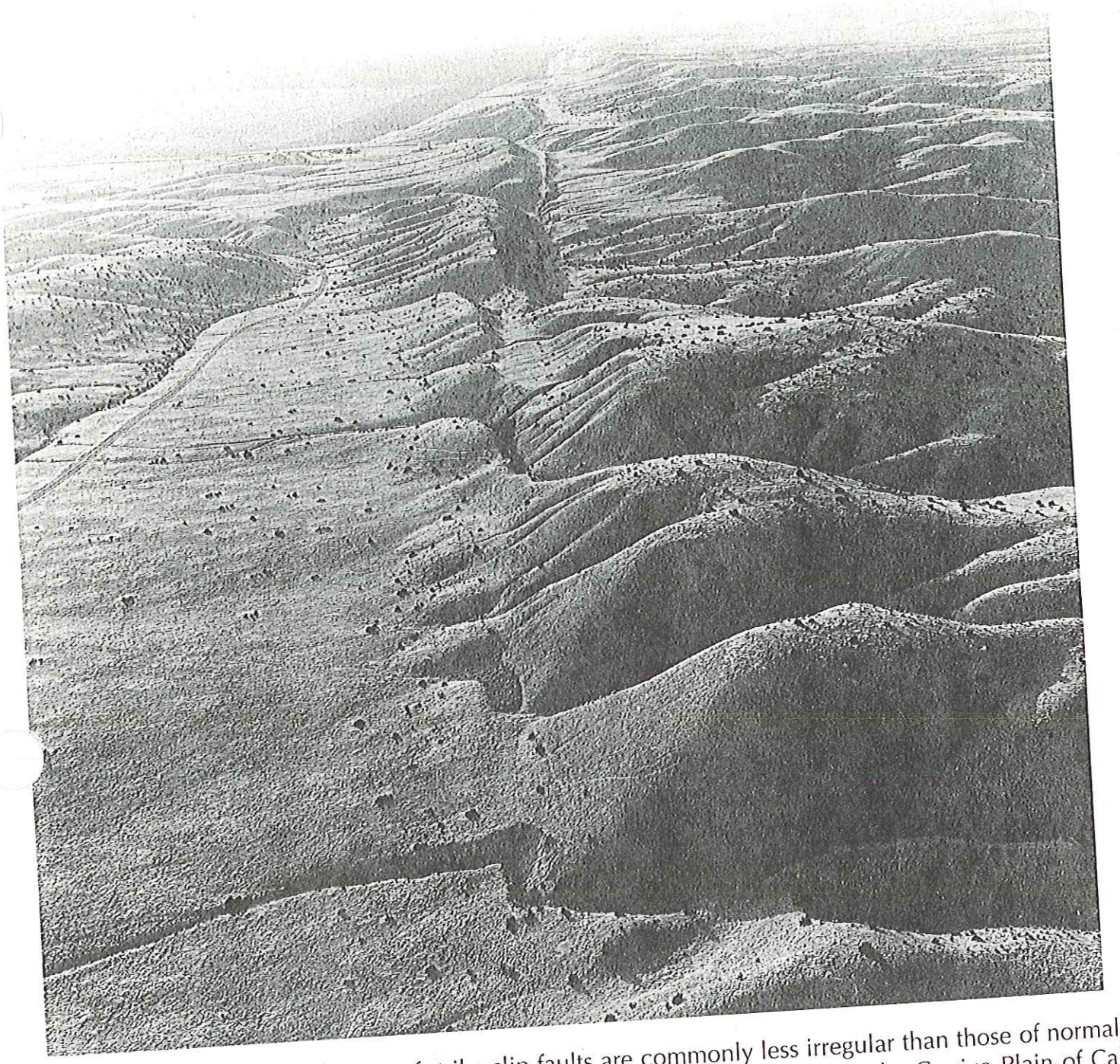

Figure 8–23. The surficial traces of strike-slip faults are commonly less irregular than those of normal a reverse faults. The extremely linear trace of the right-lateral San Andreas fault, in the Carrizo Plain of Cali nia, is a good example. View is toward the northwest, and closest channel is offset 16 m. Photo by C. R. Al (1967).

right lateral

Seismology provides a test of this hypothesis

Prediction (1):

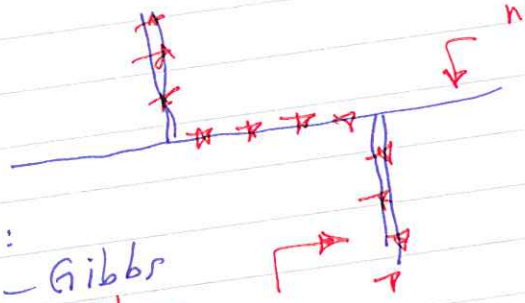

Example: Charlie–Gibbs fracture zone

These quakes in Iceland due to spreading

N. Atlantic

Rese
on
extensi
part
where
plates
moving
the same

Prediction (2): "first motion" of P waves

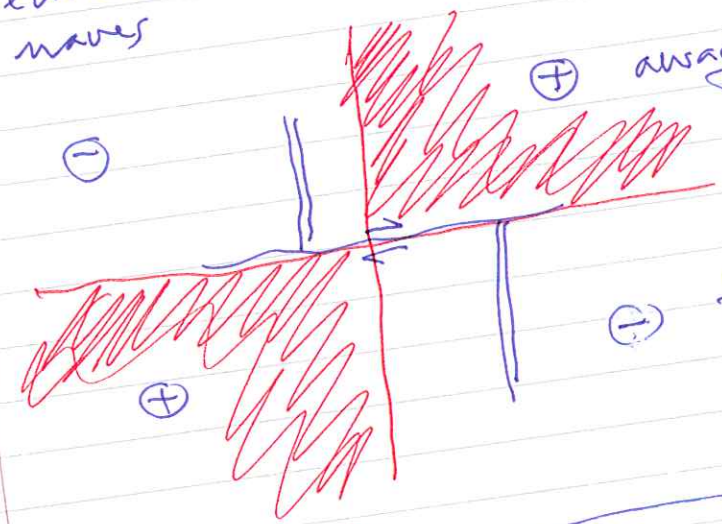

in this qua

quadran

Ca

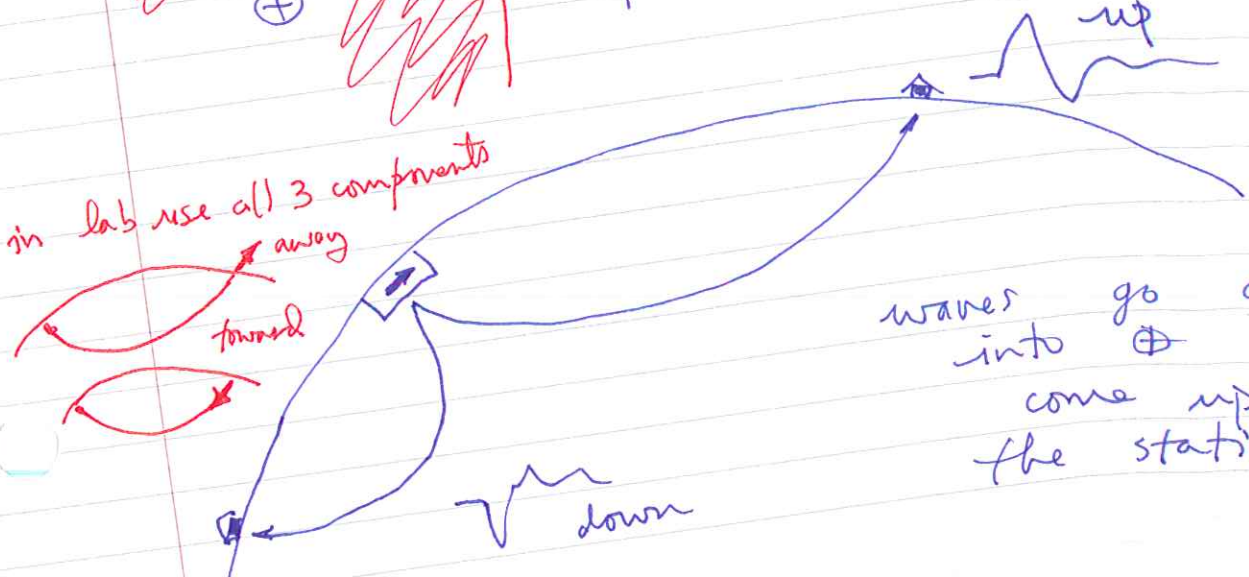

waves go do
into ⊕ an
come up
the station

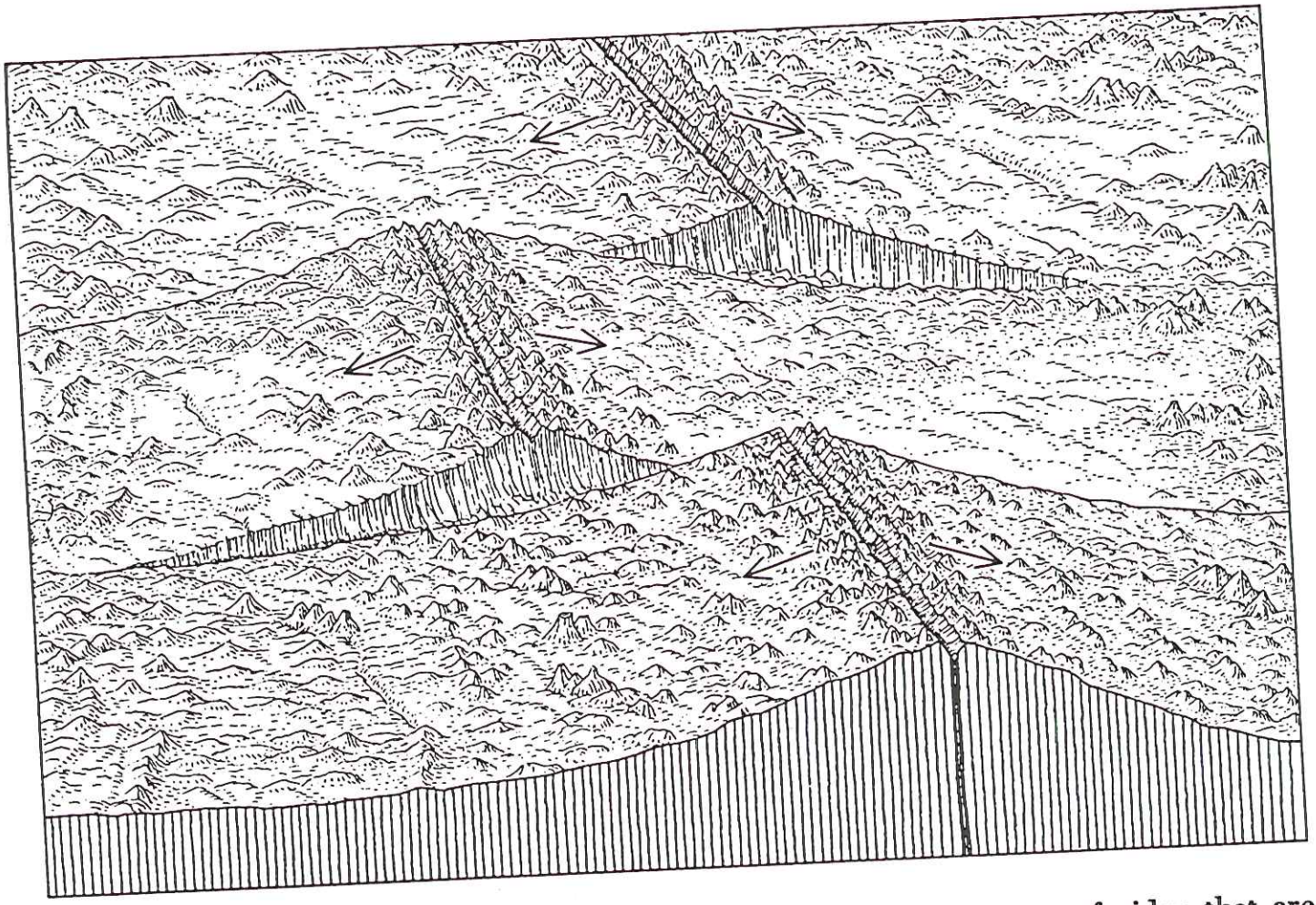

RIDGE-RIDGE TRANSFORM FAULT appears between two segments of ridge that are displaced from each other. Mountains are built, earthquakes shake the plate edges and volcanoes erupt in such an area because of the forces generated as plates, formed at the spreading centers under the ridges, slide past each other in opposite directions. On outer slopes of the mid-ocean ridges, however, this intense seismic activity appears to subside.

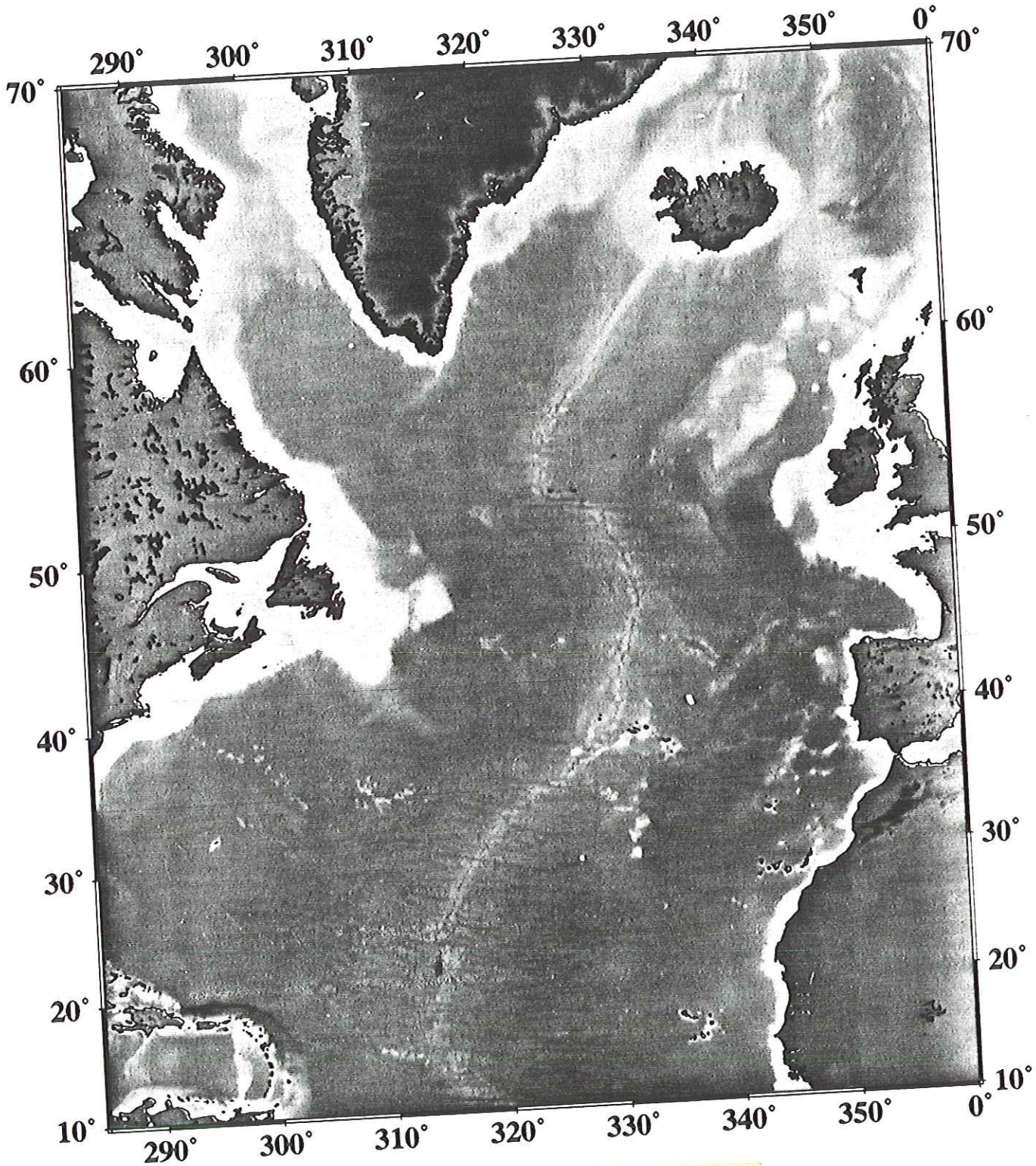

be good to get map from Jason

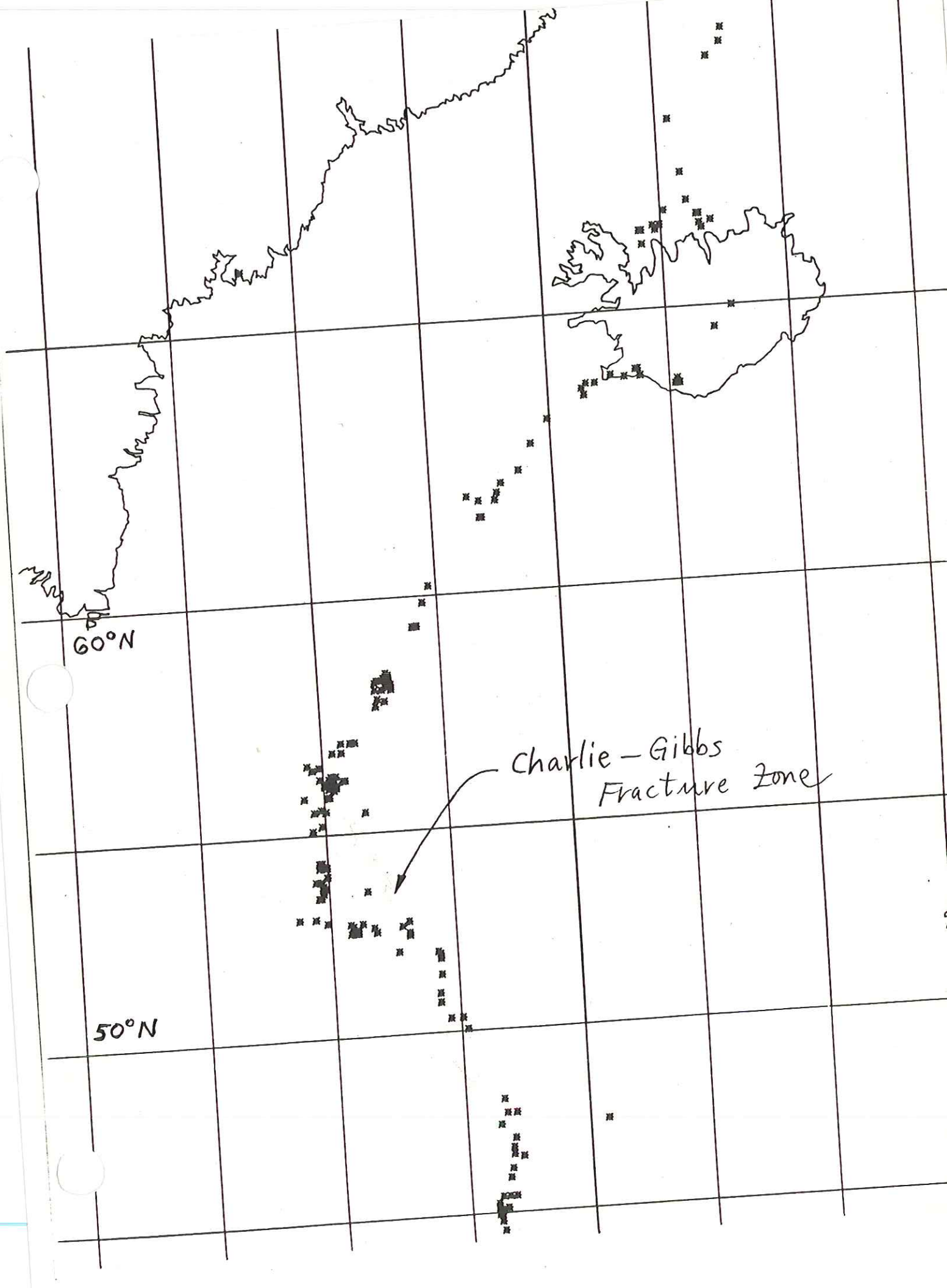
60°N
Charlie – Gibbs
Fracture Zone
50°N

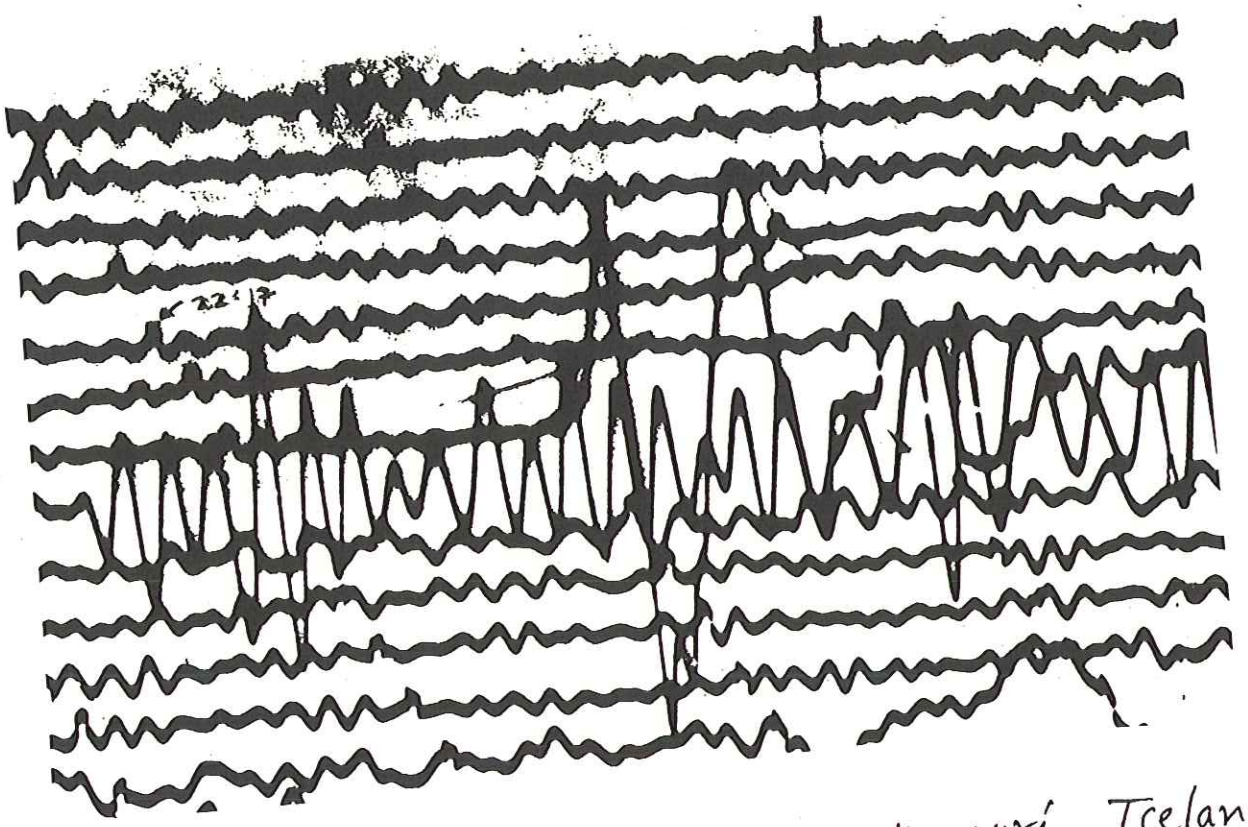

Akureyri, Iceland

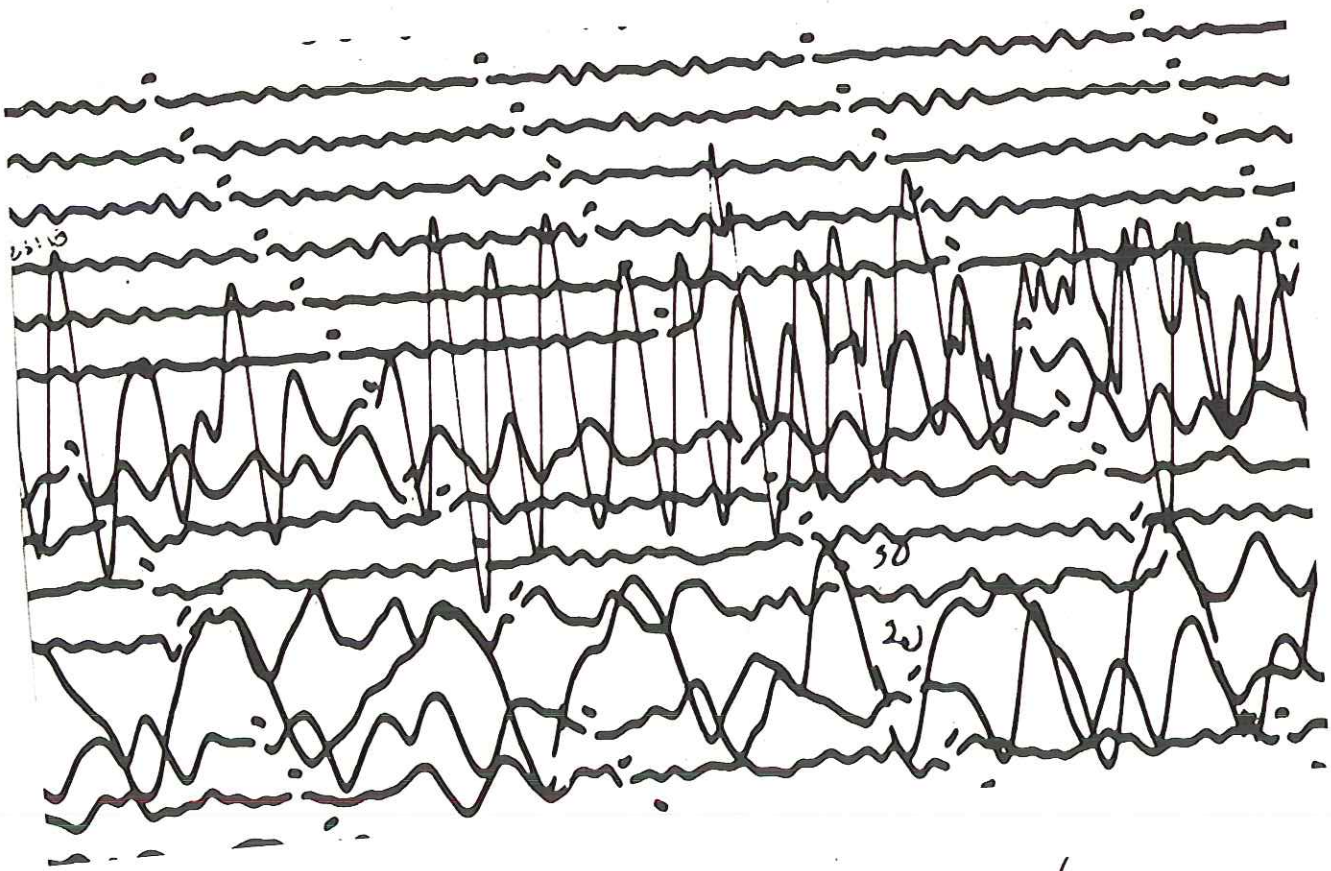

Copenhagen

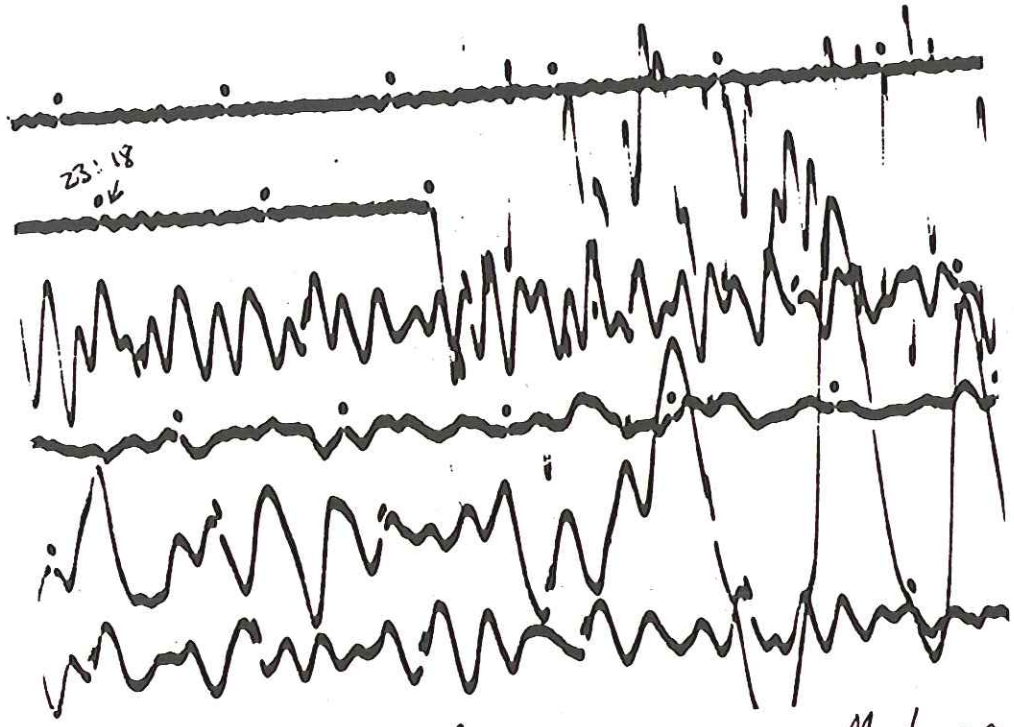

Malaga

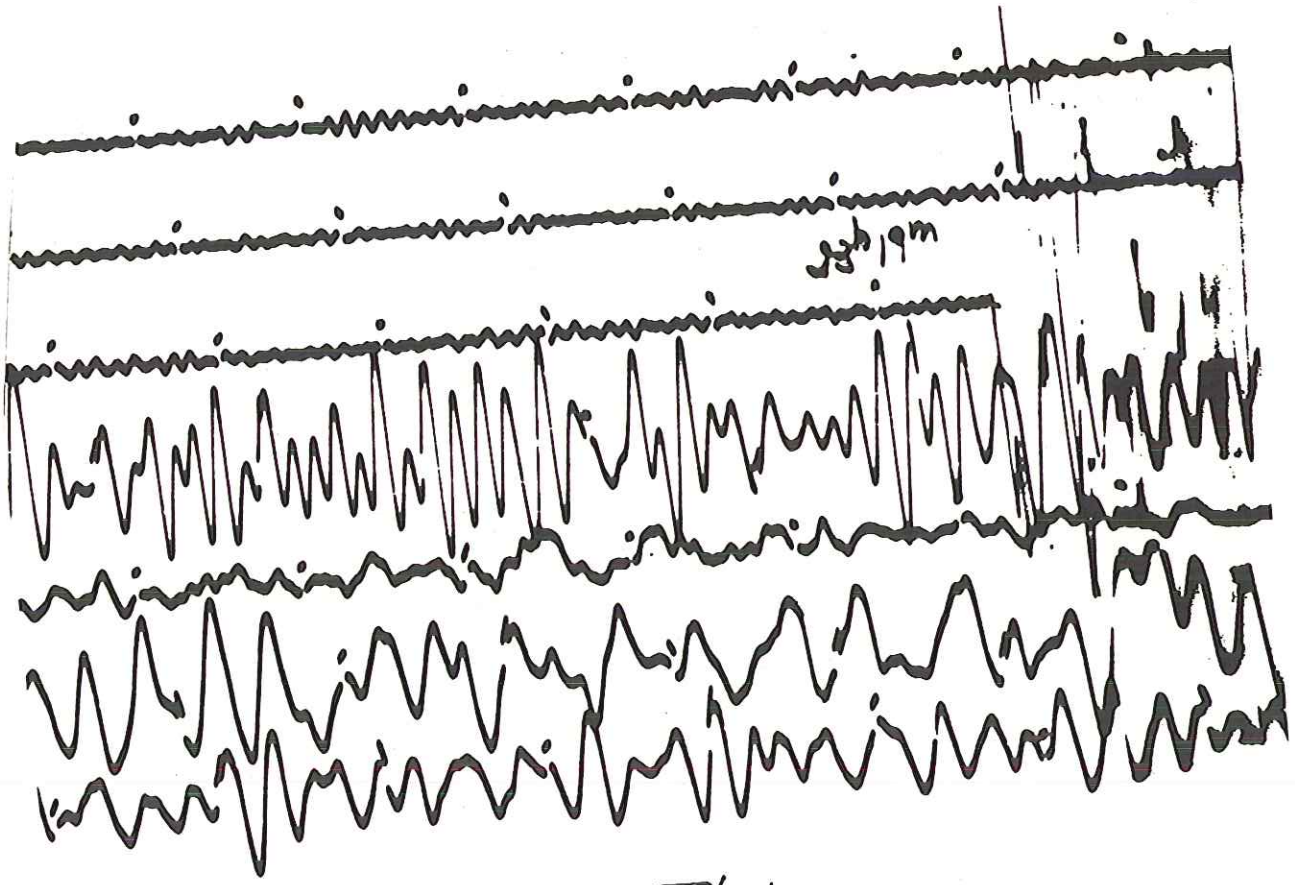

Toledo

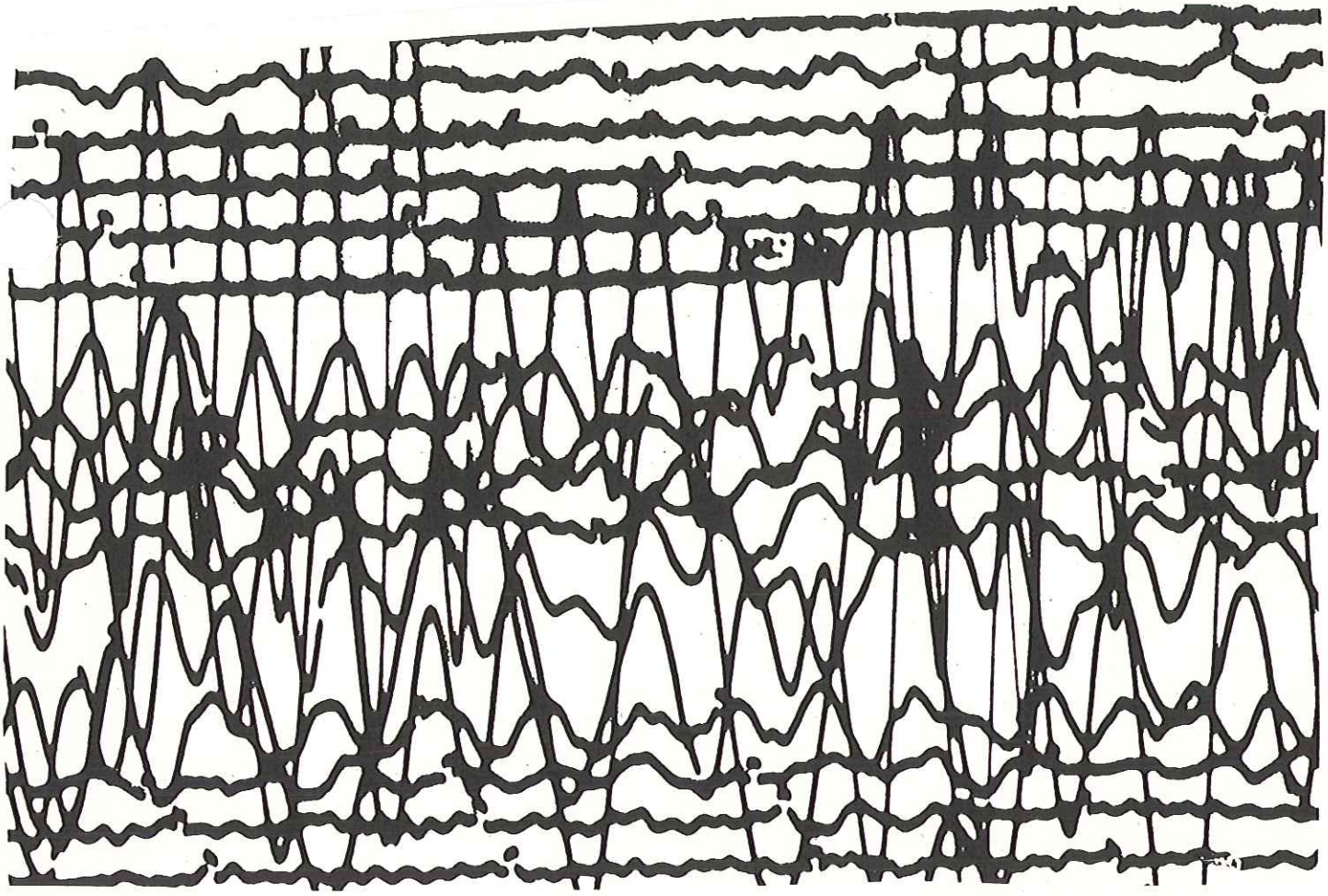

Caracas

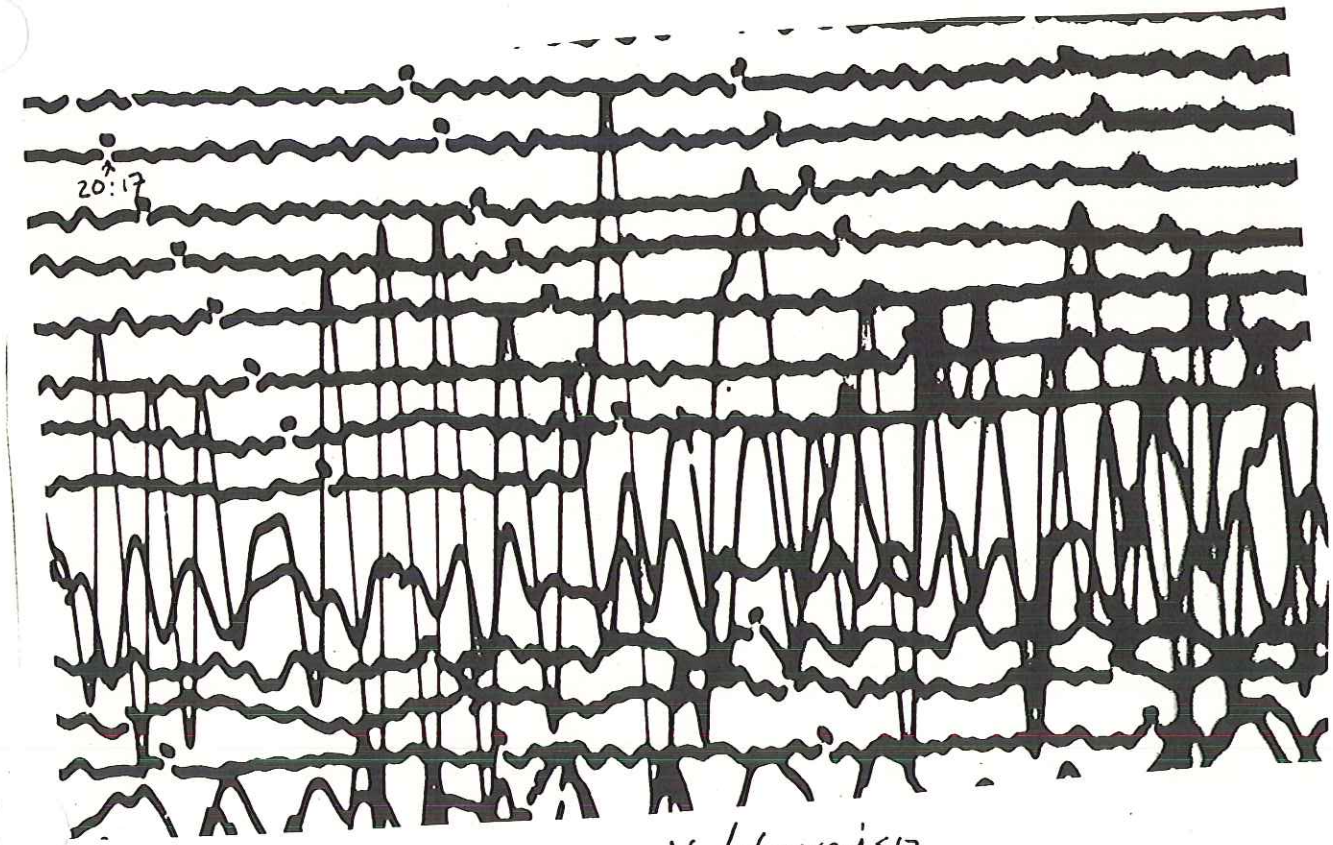

Valparaiso

Example: 1967 quake on Charlie—Gibb fracture zone

up: Iceland
Copenhagen

down: Malaga
Toledo

up: Caracas
Valparaiso

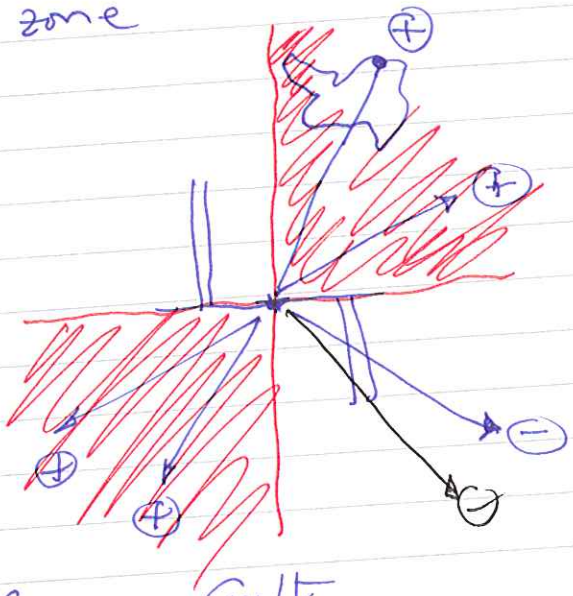

Consistent with transform fault hypothesis.

The conventional method of plotting an earthquake focal mechanism

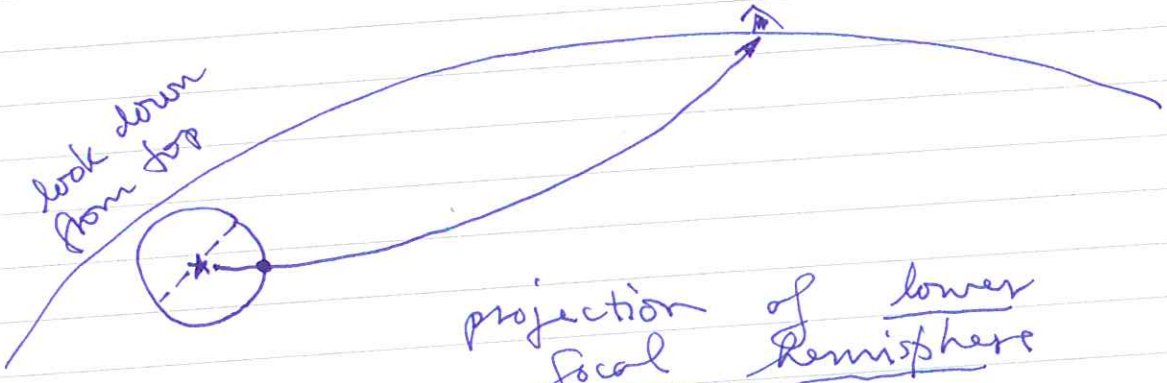

projection of lower focal hemisphere

Beach balls:

strike slip fault

either // or \\

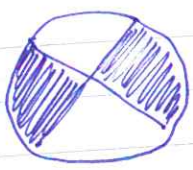

black: first mot up

fault plane – auxiliary plane
ambiguity

Not an issue if ∃ other evidence for which is fault plane, e.g. Charlie – Gibbs fracture zone.

Thrust fault:

A very shallow thrust – common in subduction zones

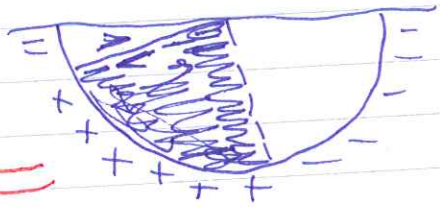

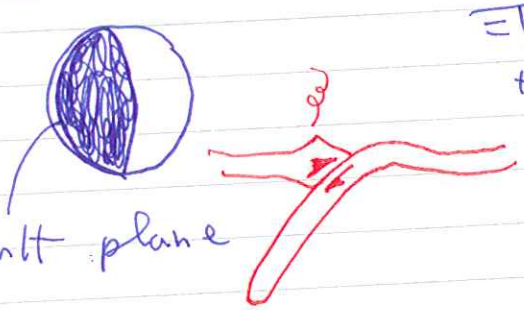

Comment about white on blackboard – possible confusion

Normal fault:

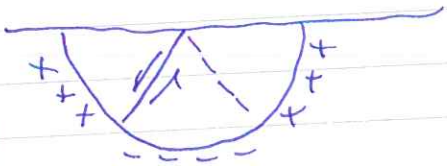

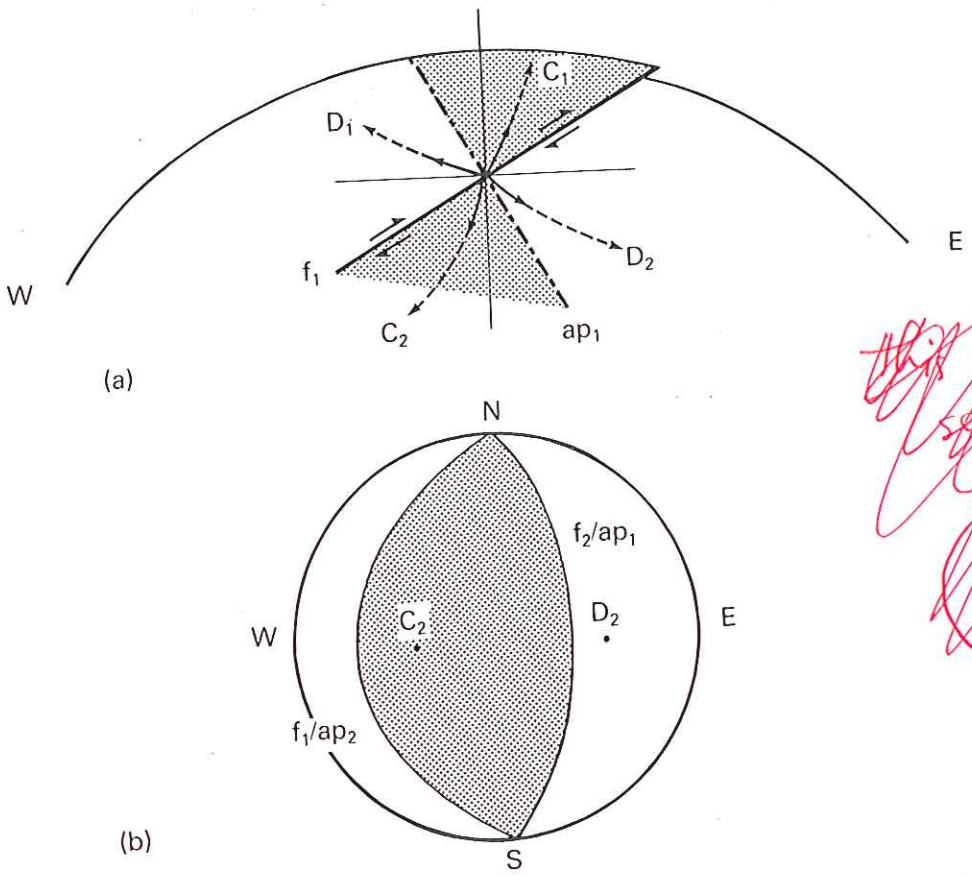

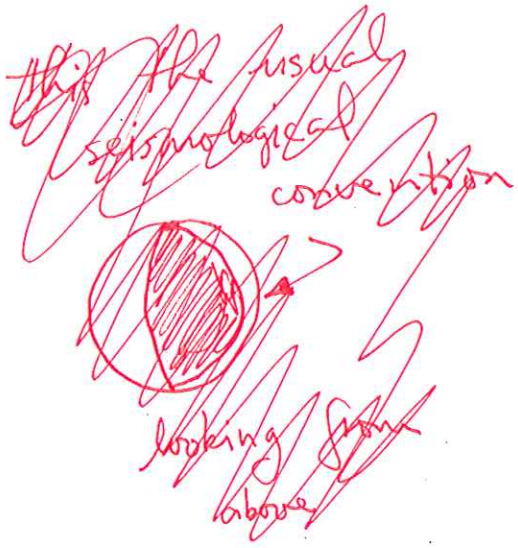

Fig. 2.8 Ambiguity in the focal mechanism solution of a thrust fault. Shaded areas represent regions of compressional first motions (C), unshaded areas represent regions of dilational first motions (D). f refers to a fault plane, ap to an auxilliary plane. Changing the nature of the nodal planes as in (a) and (c) does no alter the pattern of first motions shown in (b), the projection of the lower hemisphere of the focal sphere

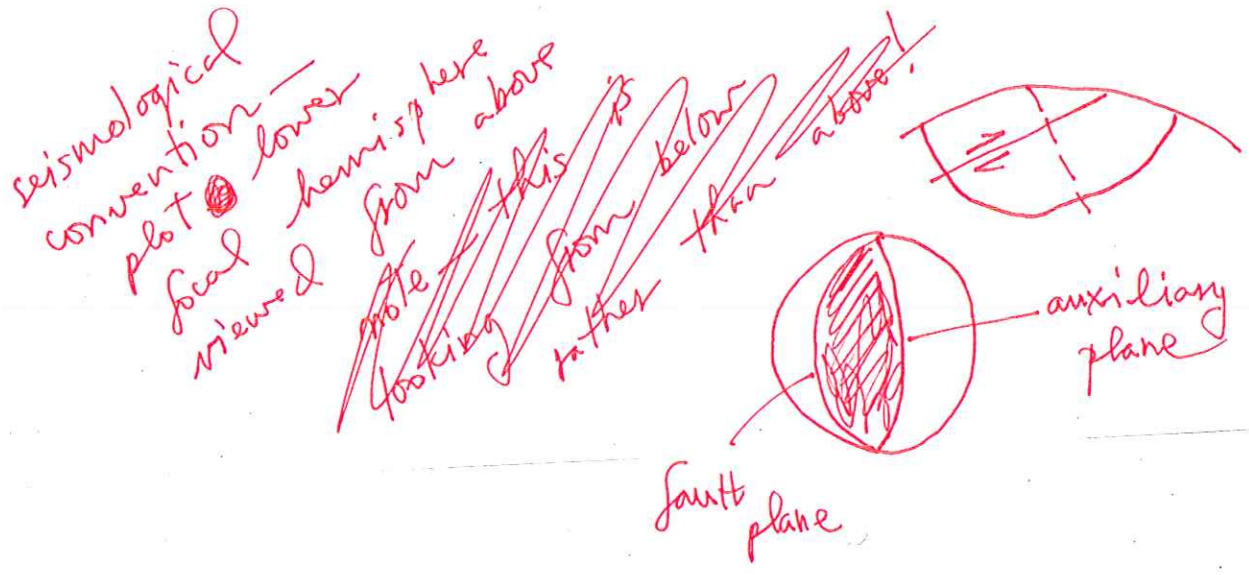

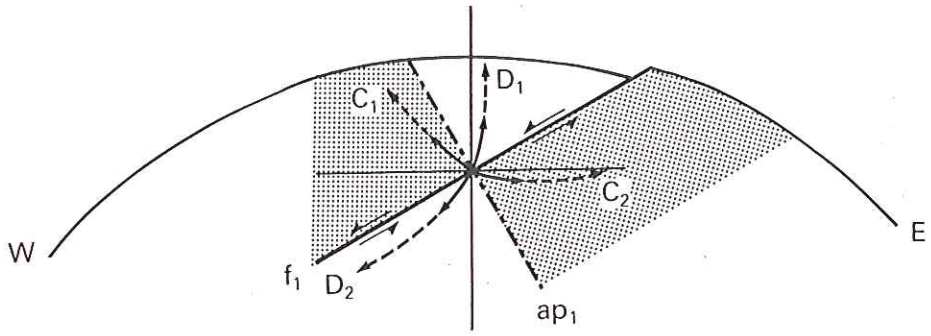

(a)

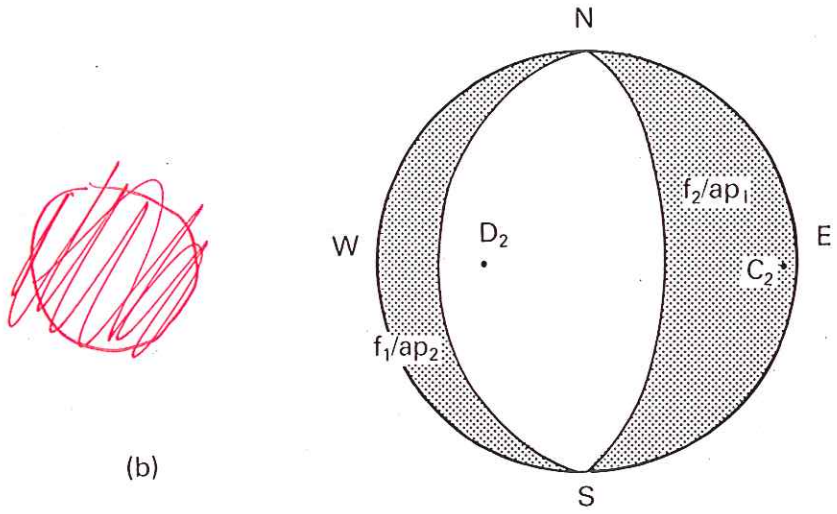

(b)

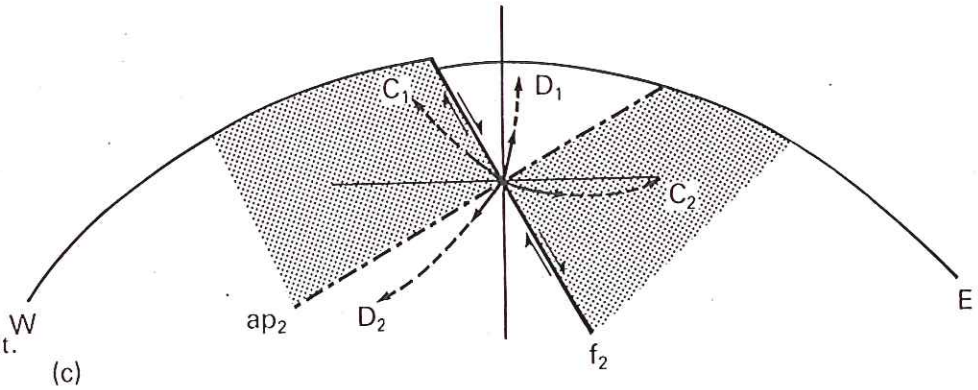

(c)

Fig. 2.9 Ambiguity in the focal mechanism solution of a normal fault. Legend as for Fig. 2.8.

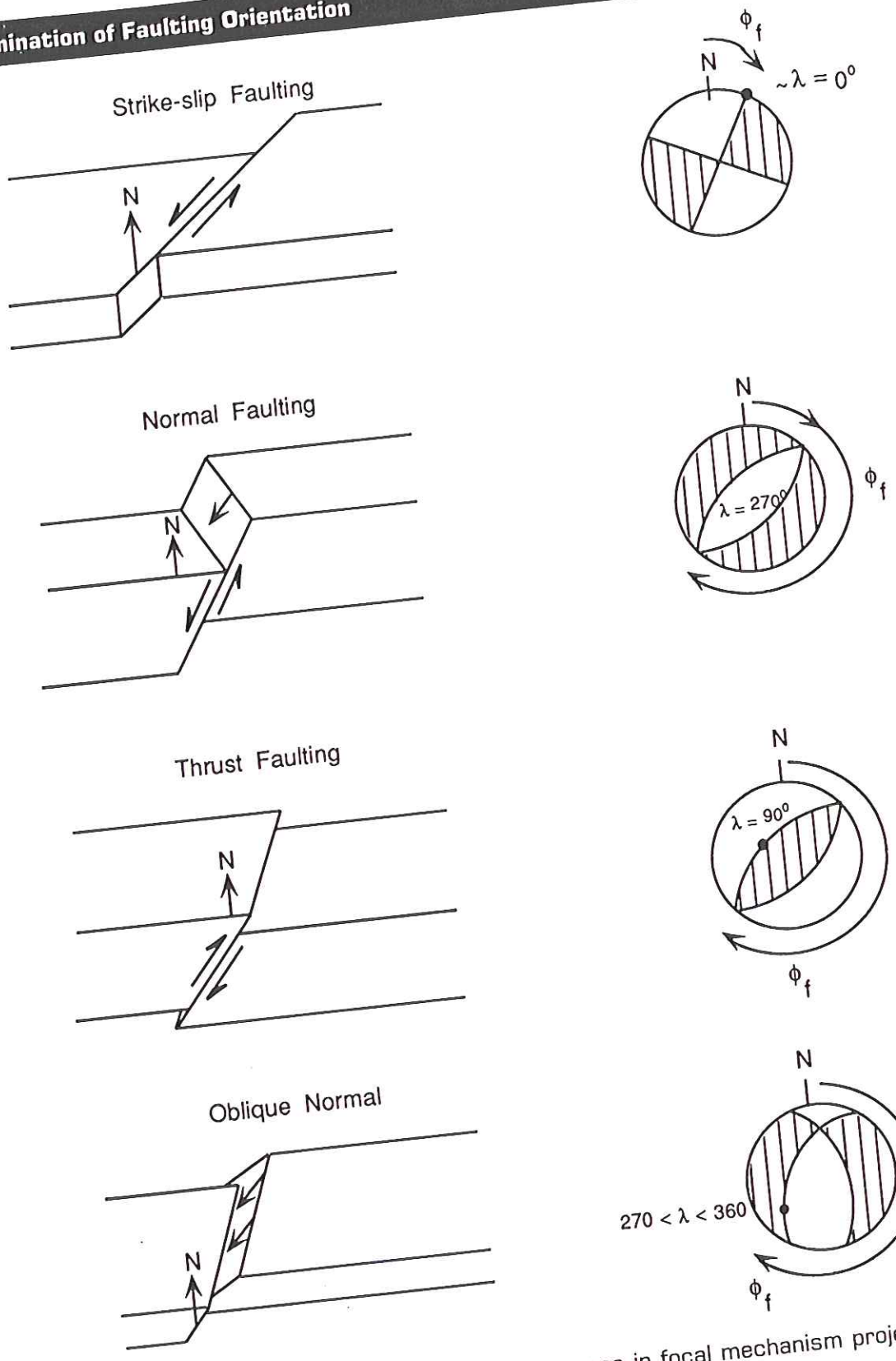

FIGURE 8.26 Basic fault types and their appearance in focal mechanism projections. Dark regions indicate compressional *P*-wave motions.

— Ten Thousand Beachballs —

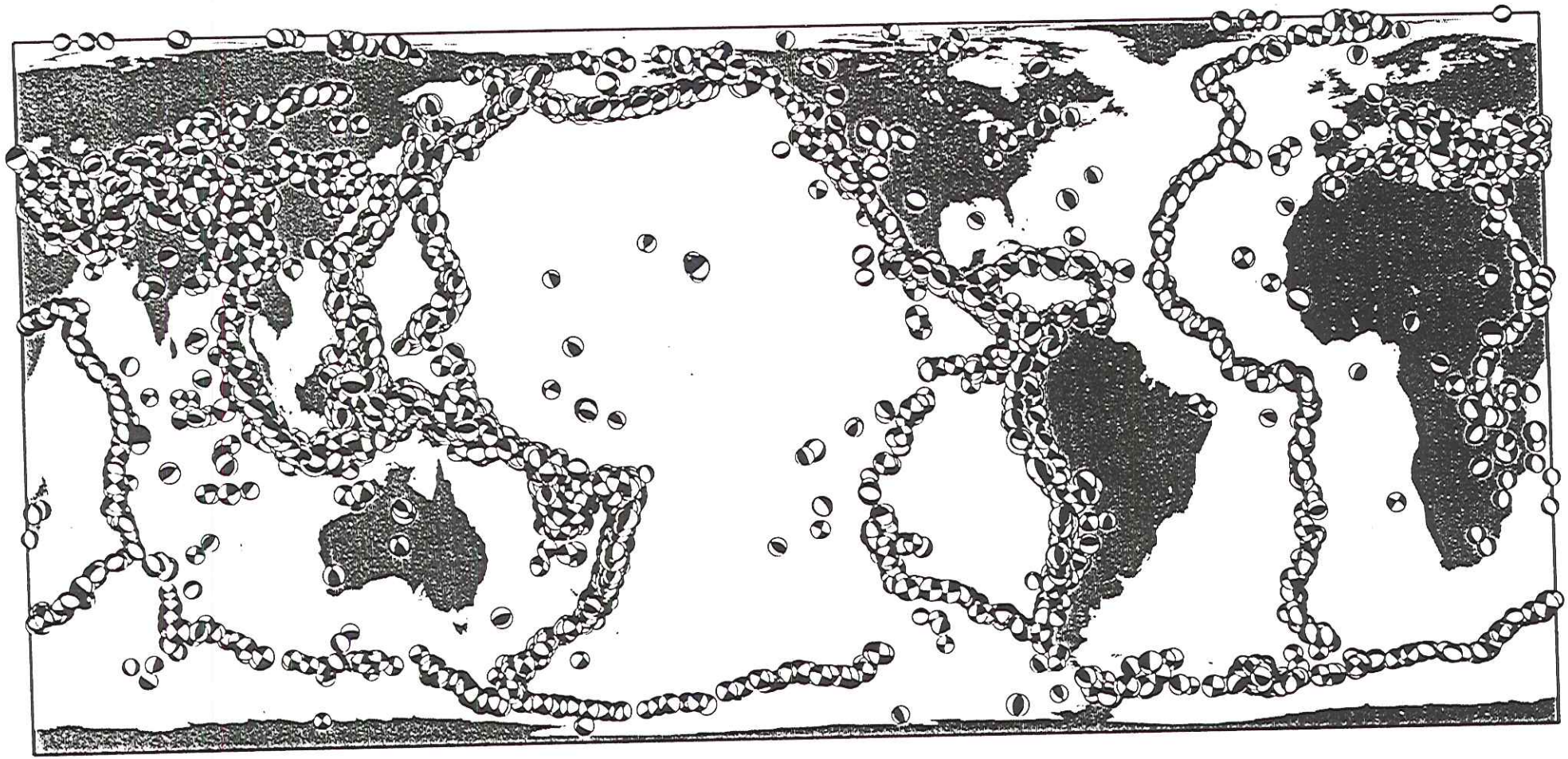

igure 5.8. Epicentral locations and source mechanisms of 10,219 earthquakes in the Harvard CMT catalogue, with focal epths less than 50 km, during the period 1976–1997. The size of each beachball is proportional to the logarithm of the eismic moment M_0. The world map is a cylindrical equal-area projection, with landmasses shaded. (Courtesy of E. Larson.)

Examples — (1) central Atlantic transform faults.

(2) Normal faulting along mid-ocean ridges

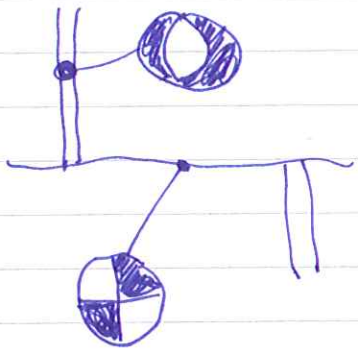

(3) Thrust mechanisms along ~~Himalaya~~ Himalayan front

⇒ extensional faulting in Tibet

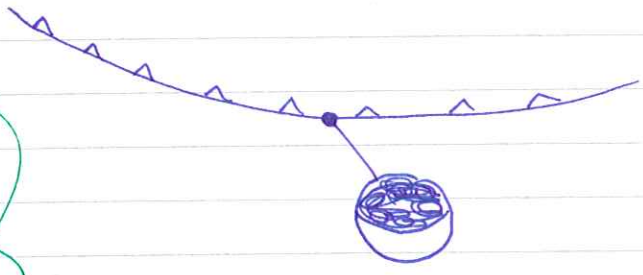

Do this before Himalaya

(4) Normal faulting on outer rise (Aleutians)

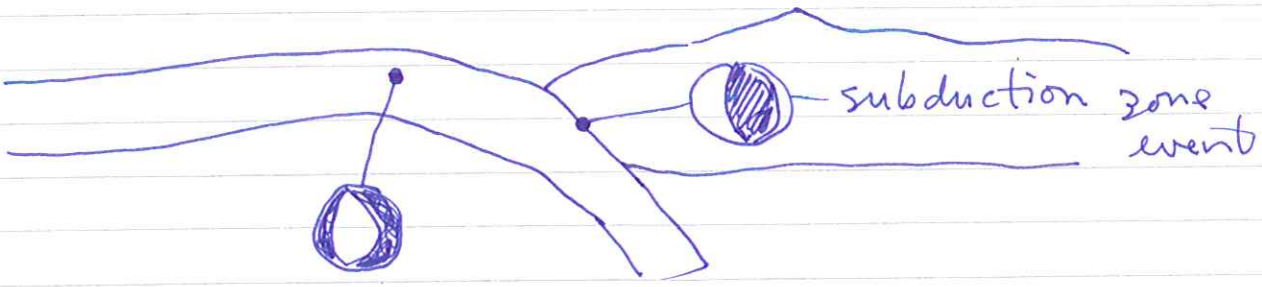

(5) Ekström *fish-eyes*:

volcanic sing faults

examples from Iceland

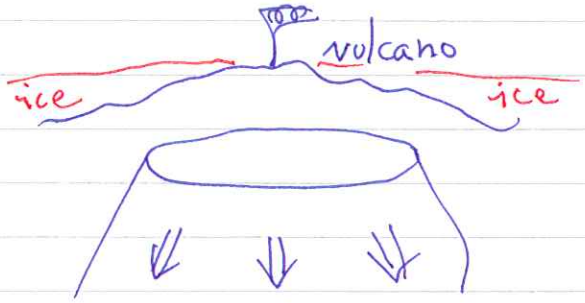

Aside — modern method of determining focal mechanisms does *not* rely solely on first motions — but rather full waveform fitting.

Have even been four-de-force determinations using a single station

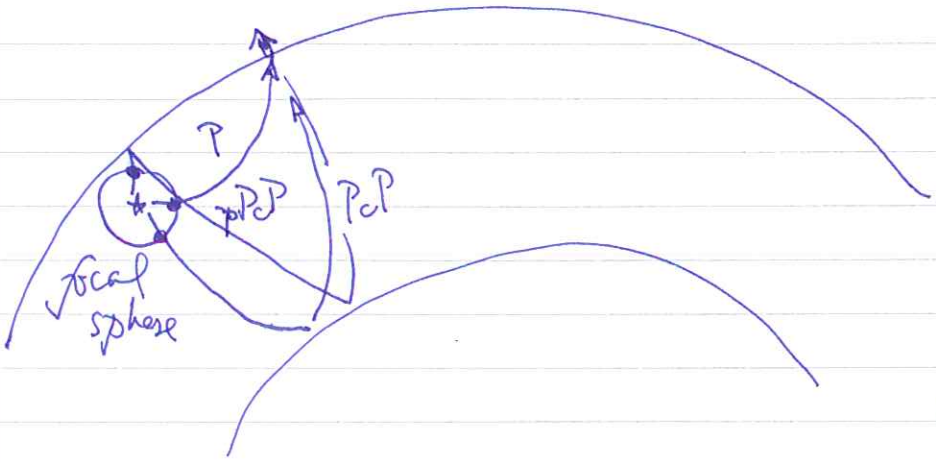

different waves provide samples of different points on the focal sphere

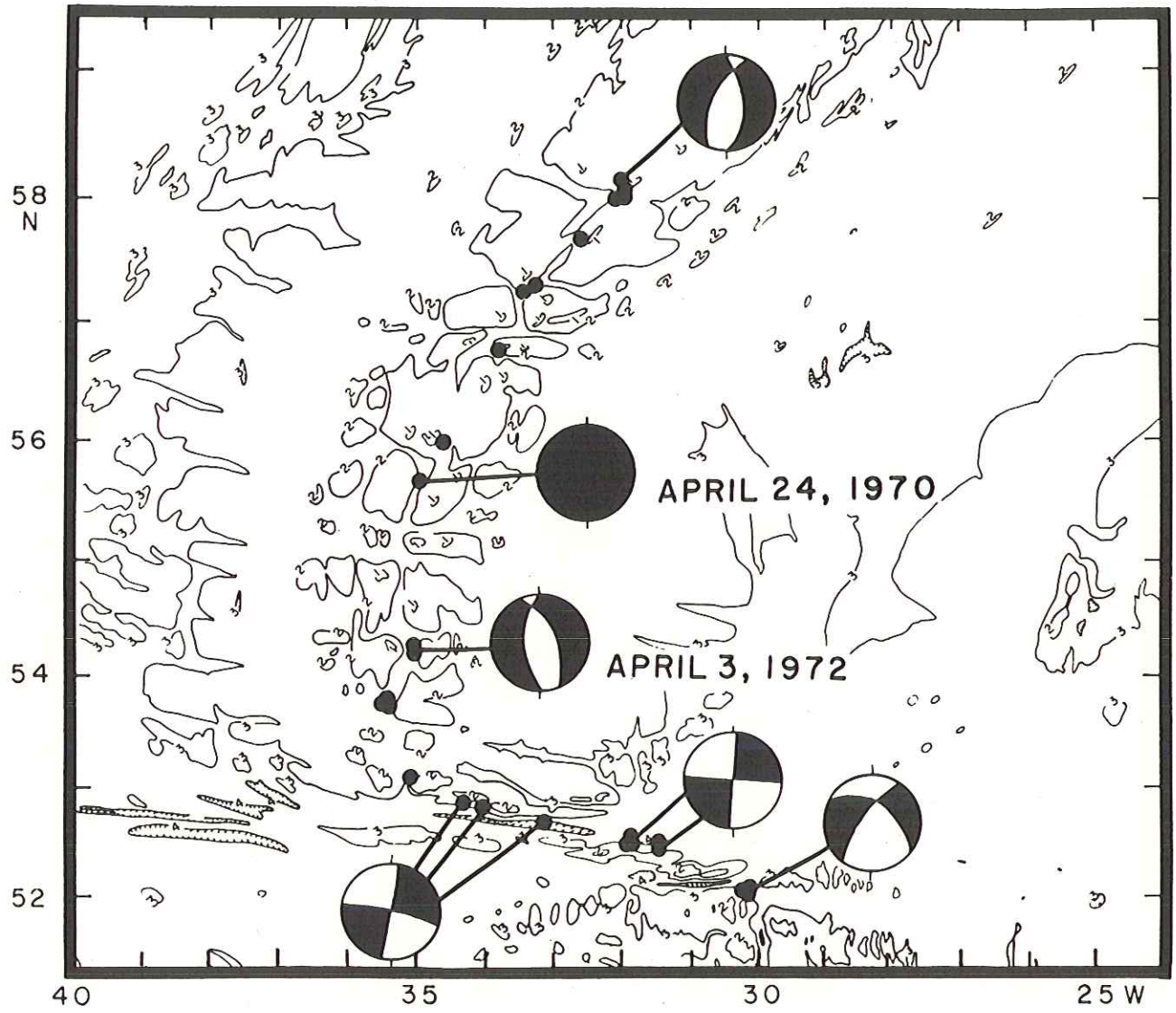

Fig. 1. Bathymetric map of the southern Reykjanes Ridge and Gibbs Fracture Zone. Contours are at 1-km intervals. Earthquakes of m_b greater than 5.0 recorded by the WWSSN from 1962 to 1978 are shown by dots. Fault plane solutions are from *Einarsson* [1979]. Bathymetry from NAVOCEANO World Relief Map, NA-4, May 1977.

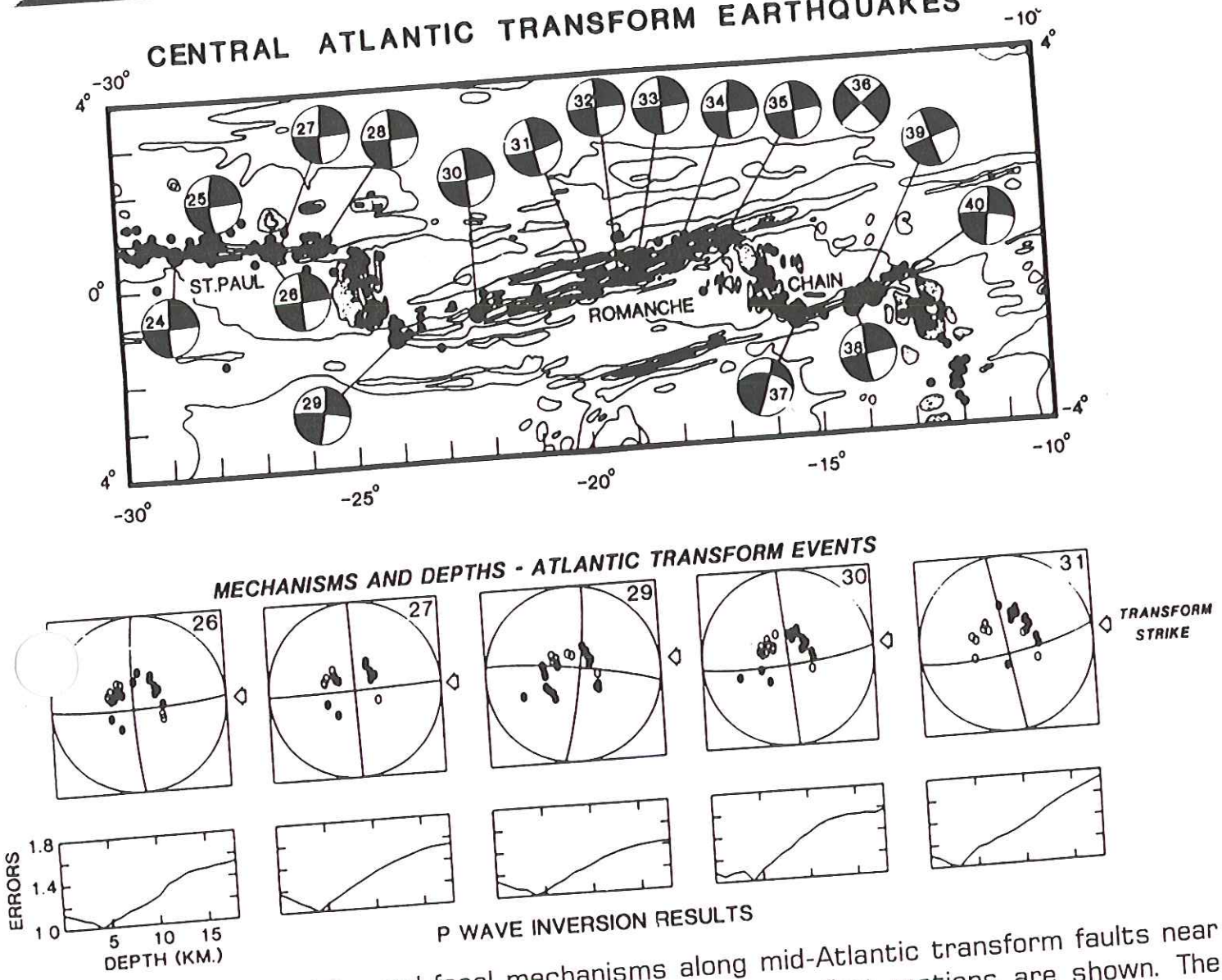

FIGURE 11.15 Seismicity and focal mechanisms along mid-Atlantic transform faults near the equator. Some of the focal mechanisms with *P*-wave first motions are shown. The waveform inversion depths are also shown (most depths are approximately 4 km). (Modified from Engeln *et al.*, *J. Geophys. Res.* **91**, 548–577, 1986; © copyright by the American Geophysical Union.)

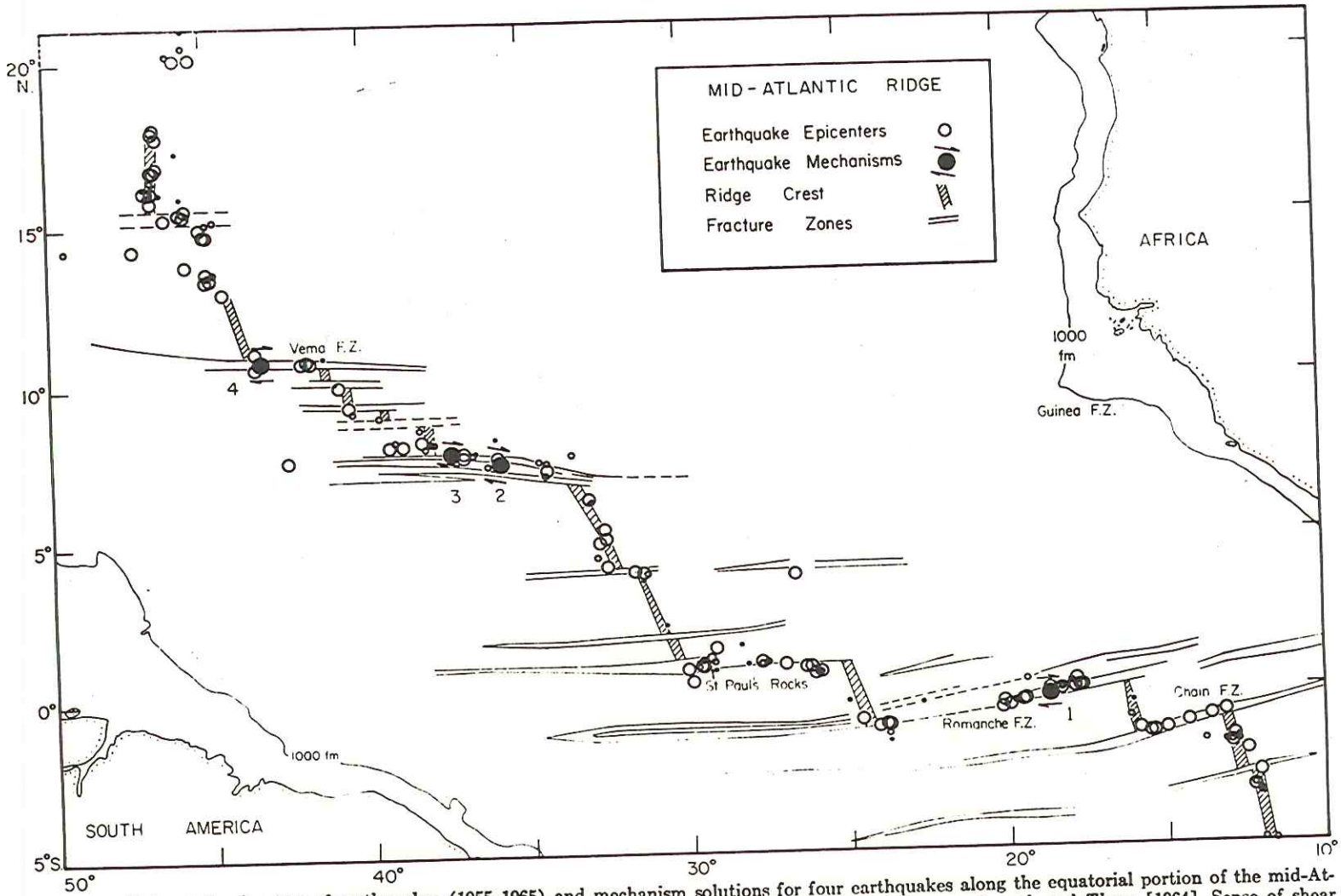

Fig. 4. Relocated epicenters of earthquakes (1955–1965) and mechanism solutions for four earthquakes along the equatorial portion of the mid-Atlantic ridge. Ridge crests and fracture zones from *Heezen, Bunce, Hersey, and Tharp* [1964] and *Heezen, Gerard, and Tharp* [1964]. Sense of shear displacement and strike of inferred fault plane are indicated by the orientation of the set of arrows beside each mechanism. Numbers beside mechanism solutions refer to data in Table 1. Large circles denote more precise epicentral determinations; smaller circles, poorer determinations.

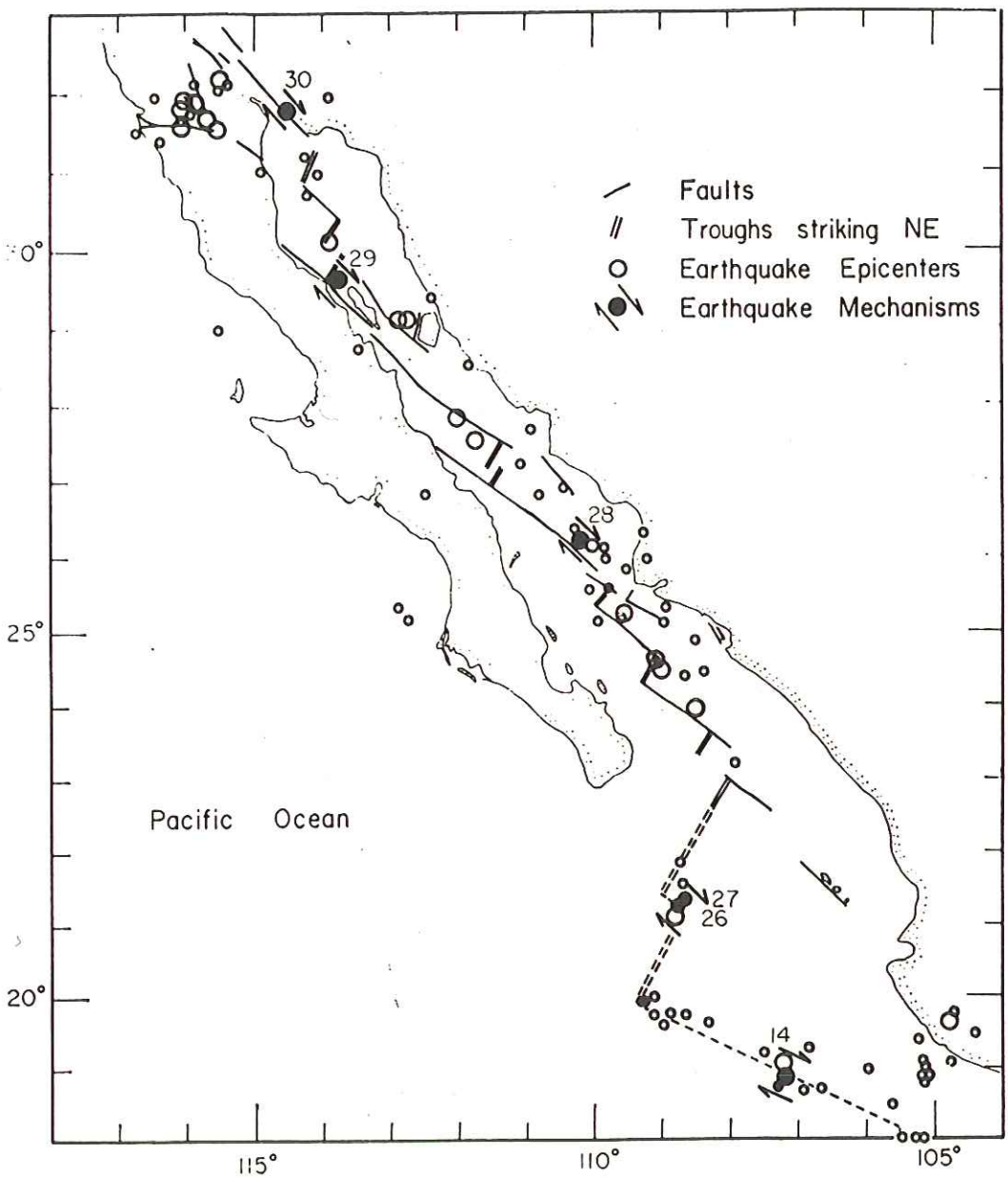

Fig. 6. Structural features of the Gulf of California [after *Sykes*, 1968]. Relocated epicenters of earthquakes for the period 1954 to 1962. Seismicity and focal mechanisms support the hypothesis of spreading by ocean-ridge–transform-fault mechanism.

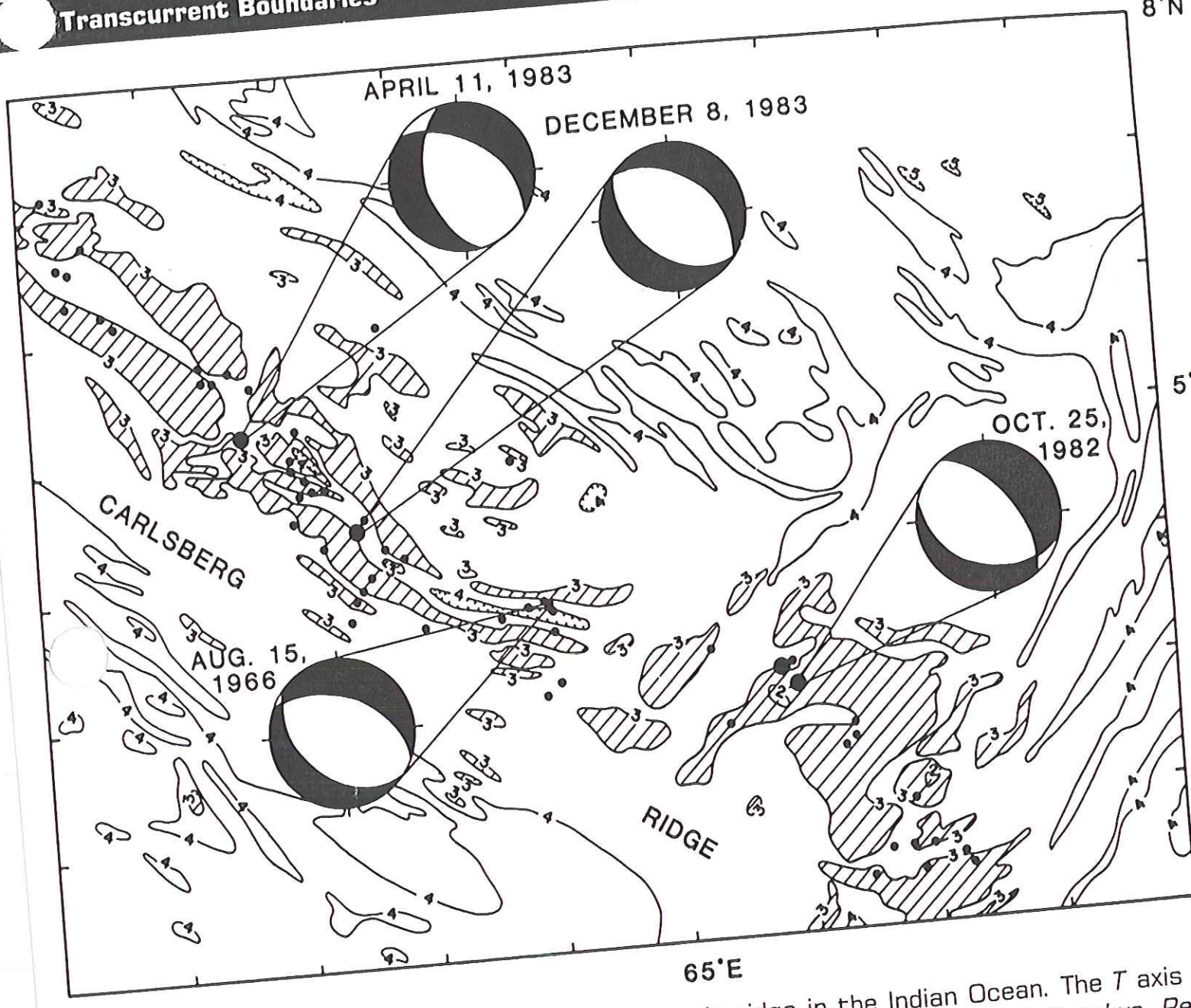

FIGURE 11.9 Focal mechanism along a midoceanic ridge in the Indian Ocean. The *T* axis oriented parallel to the direction of spreading. (From Huang and Solomon, *J. Geophys. Re* **92**, 1361–1382, 1987; © copyright by the American Geophysical Union.)

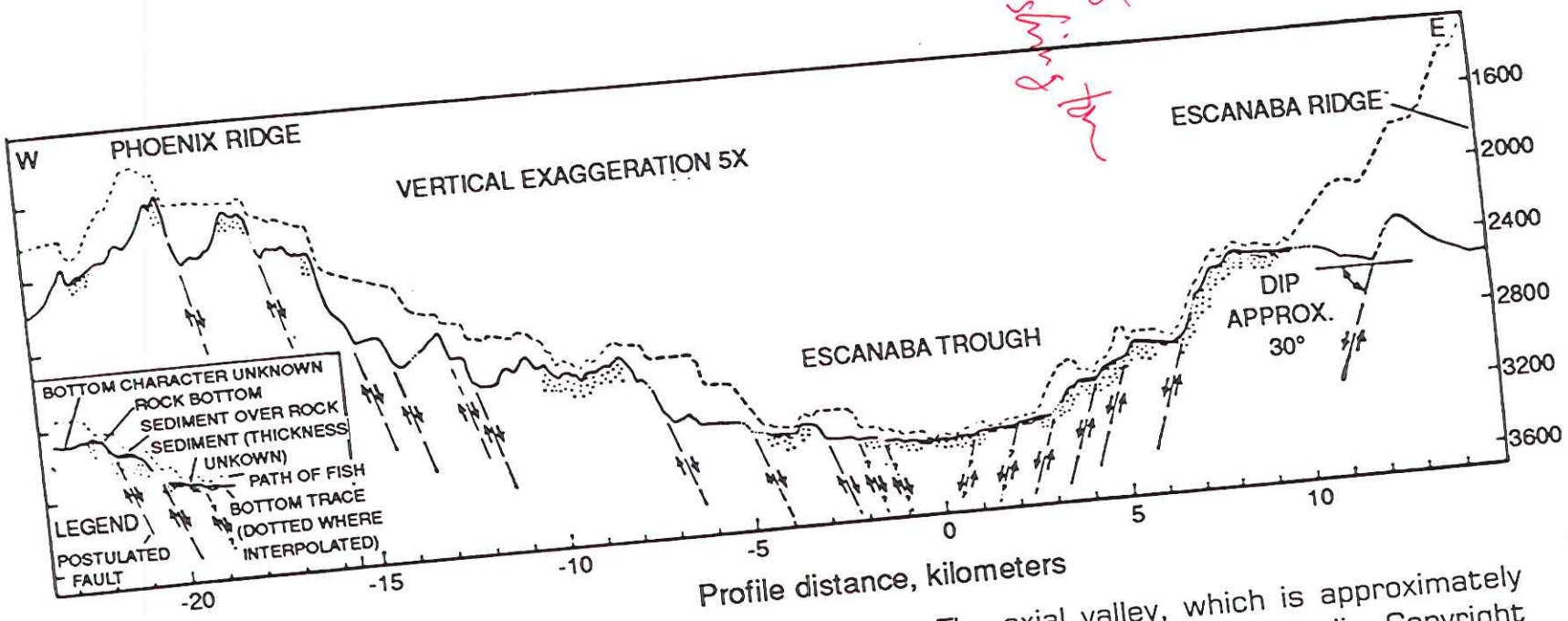

FIGURE 11.8 Topography across the Gorda Rise. The axial valley, which is approximately 30 km across, is bounded by a series of normal faults. (After Atwater and Mudie. Copyright © 1968 by the AAAS.)

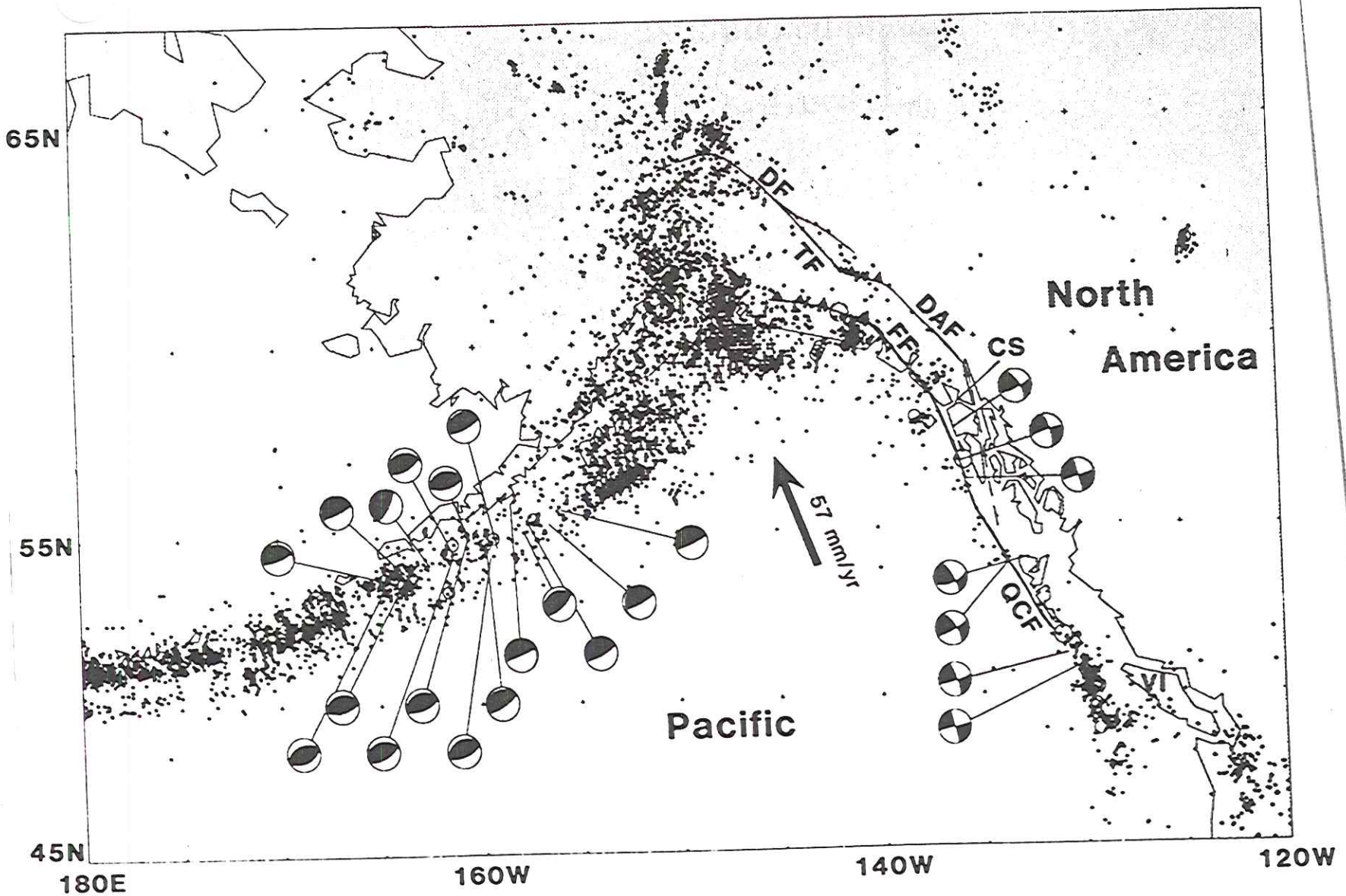
65N
55N
45N
180E
160W
140W
120W
DF
TF
FF
DAF
CS
QCF
VI
North
America
Pacific
57 mm/yr

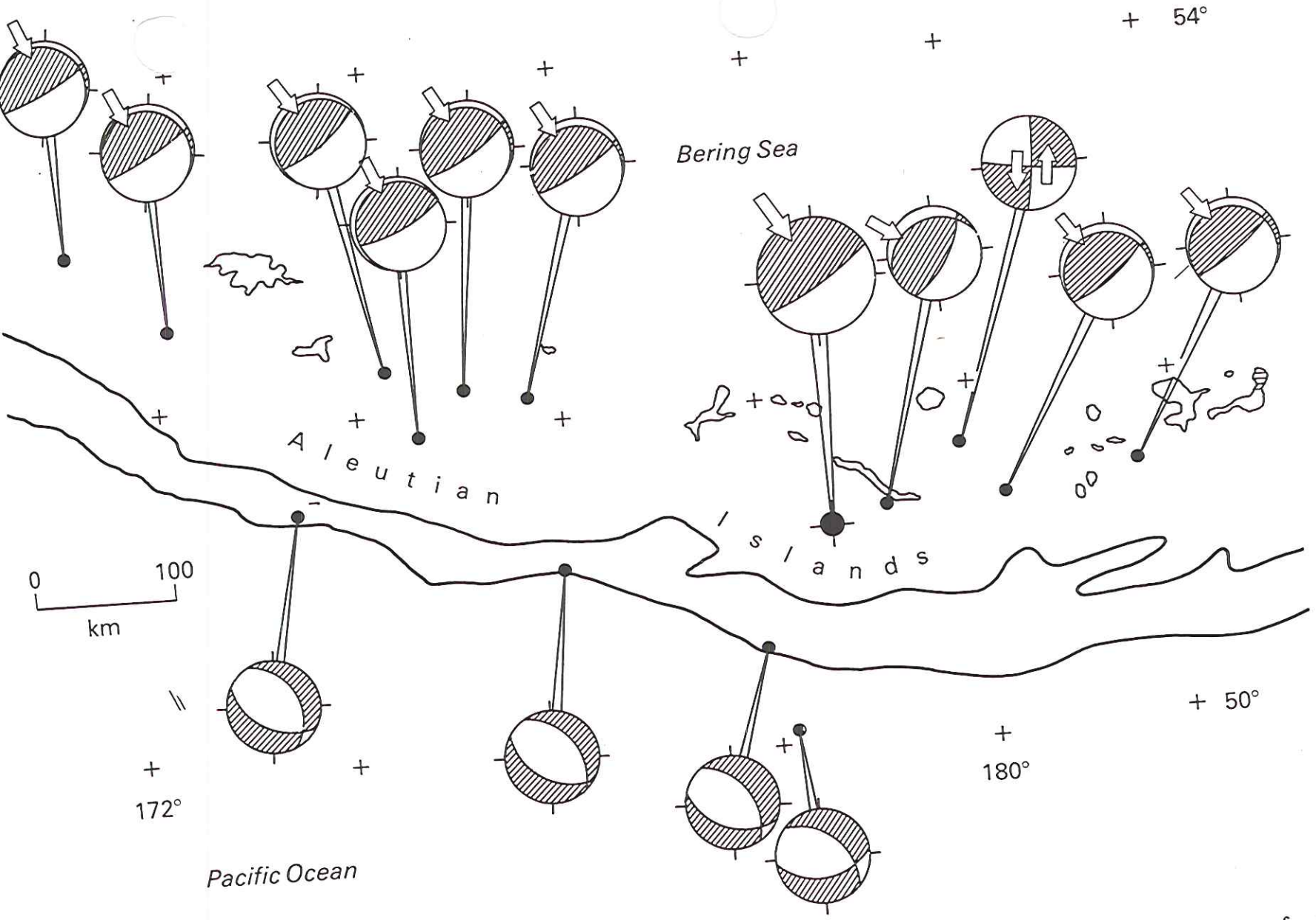

Fig. 8.12 Focal mechanism solutions of earthquakes in the Aleutian arc, compressional quadrant shaded (redrawn from Stauder, 1968, *Journal of Geophysical Research*, **73**, with permission from the American Geophysical Union).

Farther to the W along the Aleutian Chain

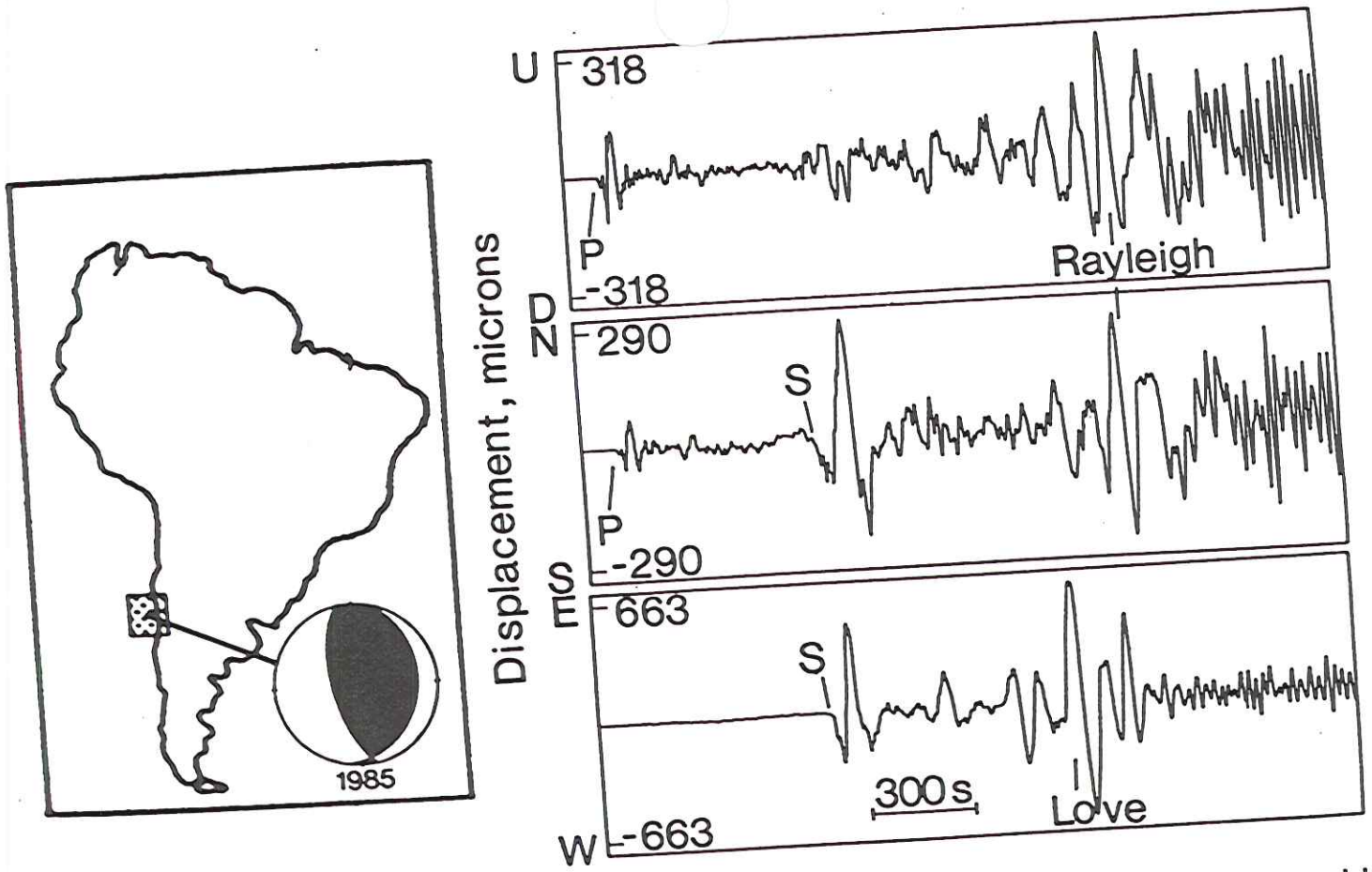

FIGURE 1.1 Recordings of the ground displacement history at station HRV (Harvard, Massachusetts) produced by seismic waves from the March 3, 1985, Chilean earthquake, which had the location shown in the inset. The three seismic traces correspond to vertical (U–D), north–south (N–S), and east–west (E–W) displacements. The direction to the source is almost due south, so all horizontal displacements transverse to the raypath appear on the east–west component. The first arrival is a *P* wave that produces ground motion along the direction of wave propagation. The *S* motion is large on the horizontal components. The Love wave occurs only on the transverse motions of the E–W component, and the Rayleigh wave occurs only on the vertical and north–south components. These are consistent with the predictions of Figure 1.2. (Modified from Steim, 1986.)

Himalayan Front – highest mountains in the world

continent – continent collision

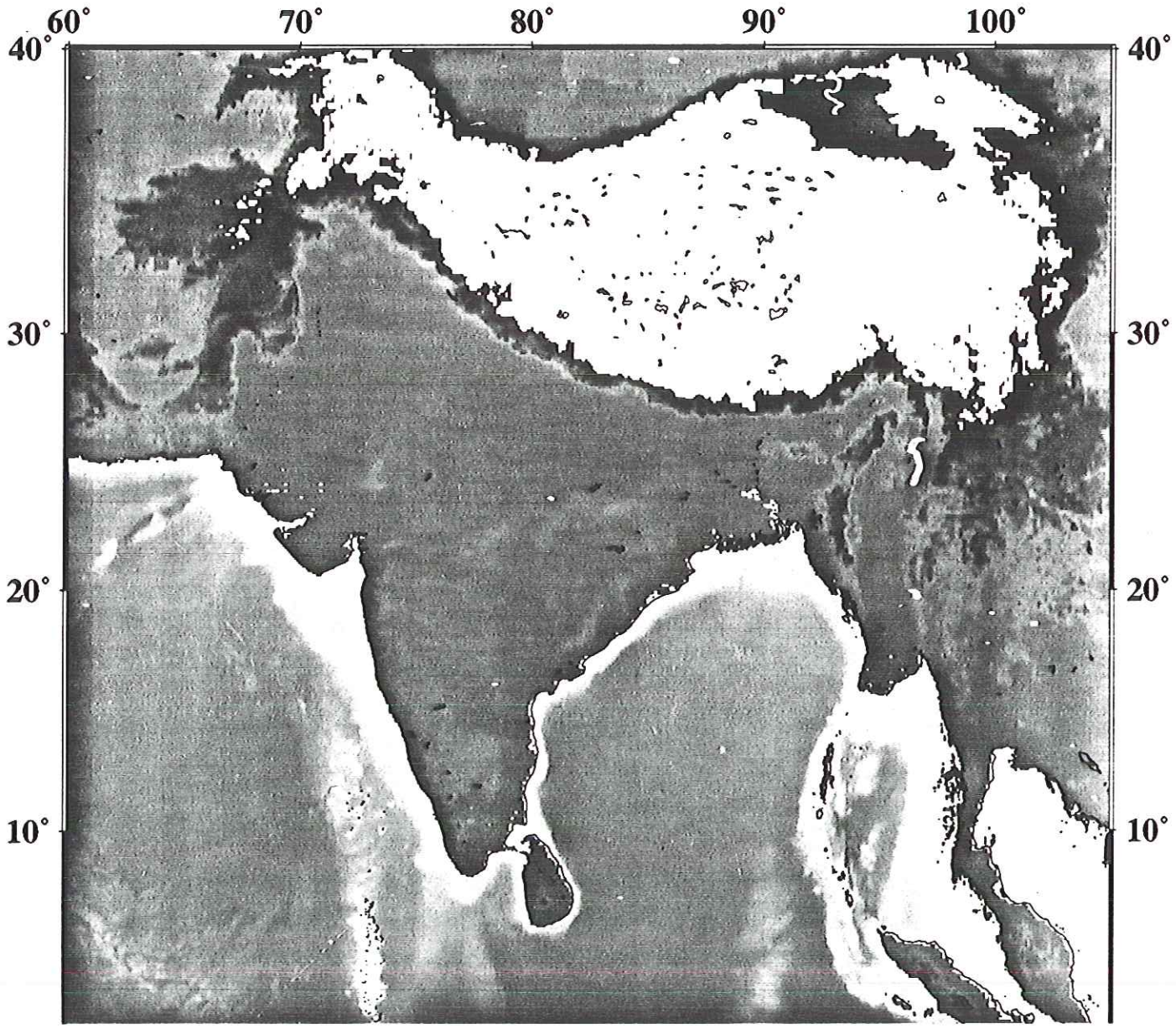

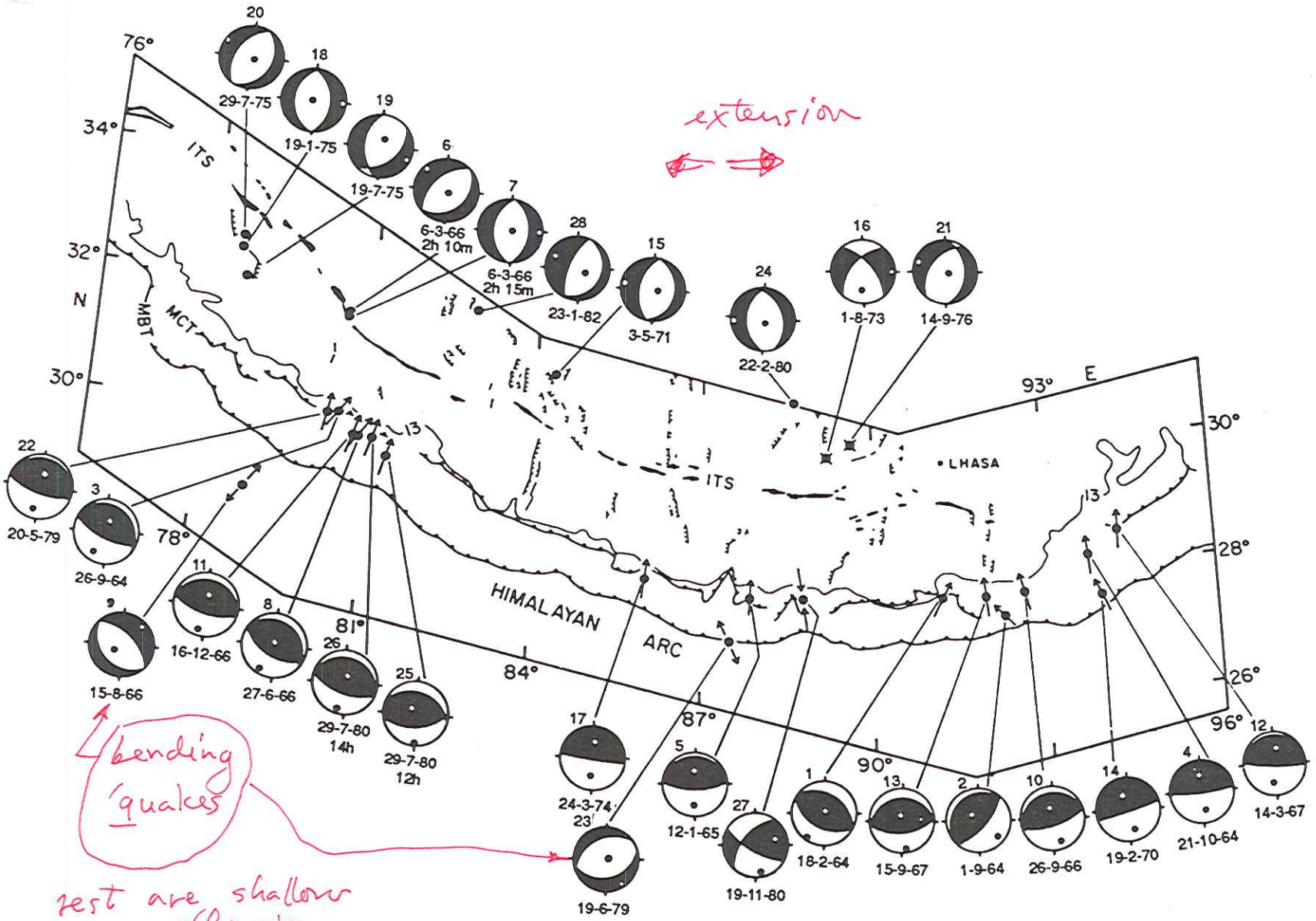

FIGURE 11.39 Focal mechanism and aftershock areas for events along the India–Eurasia collision zone. Note the east–west extension in the Tibetan Plateau, in contrast to the

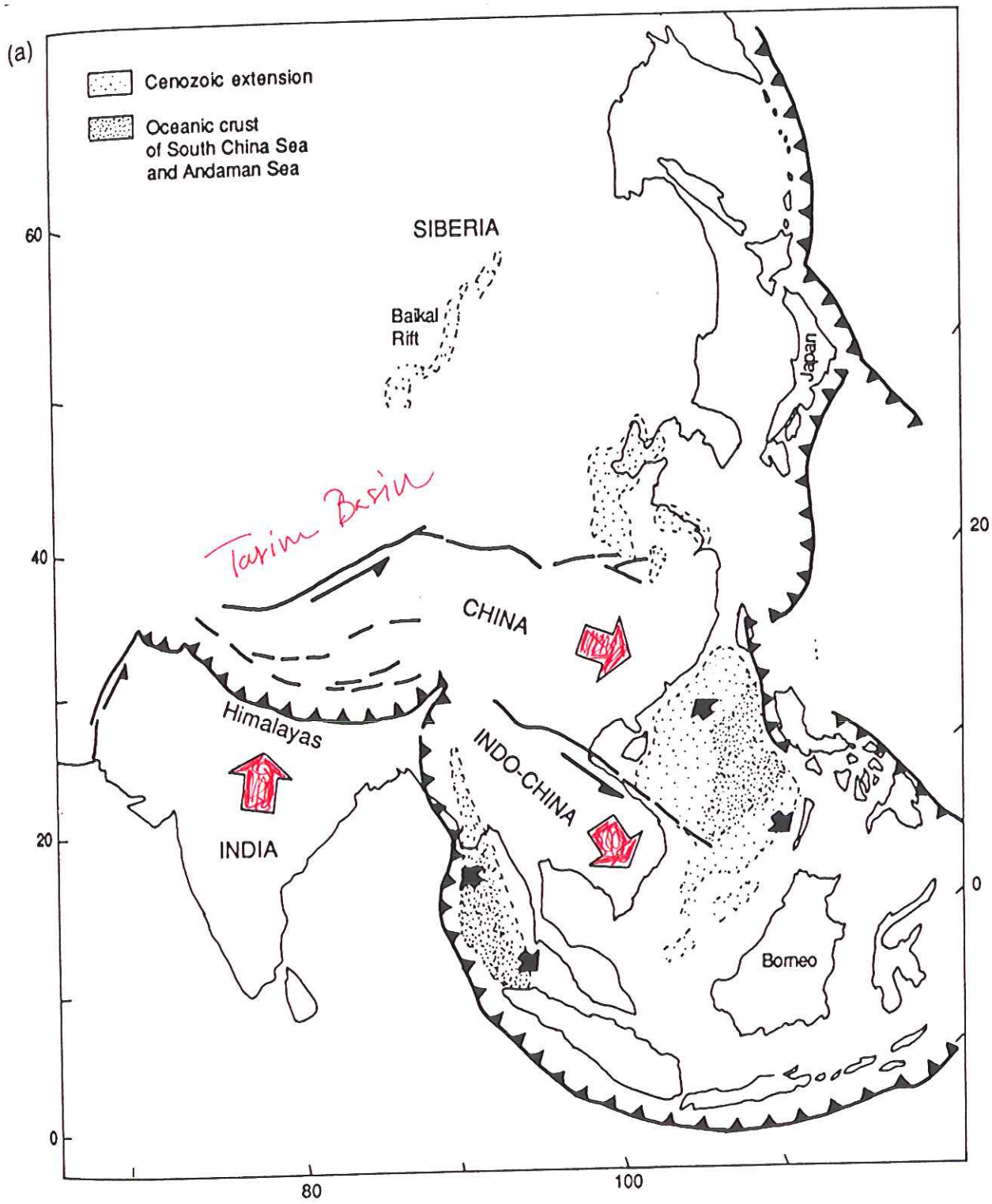

getting squeezed like a watermelon seed

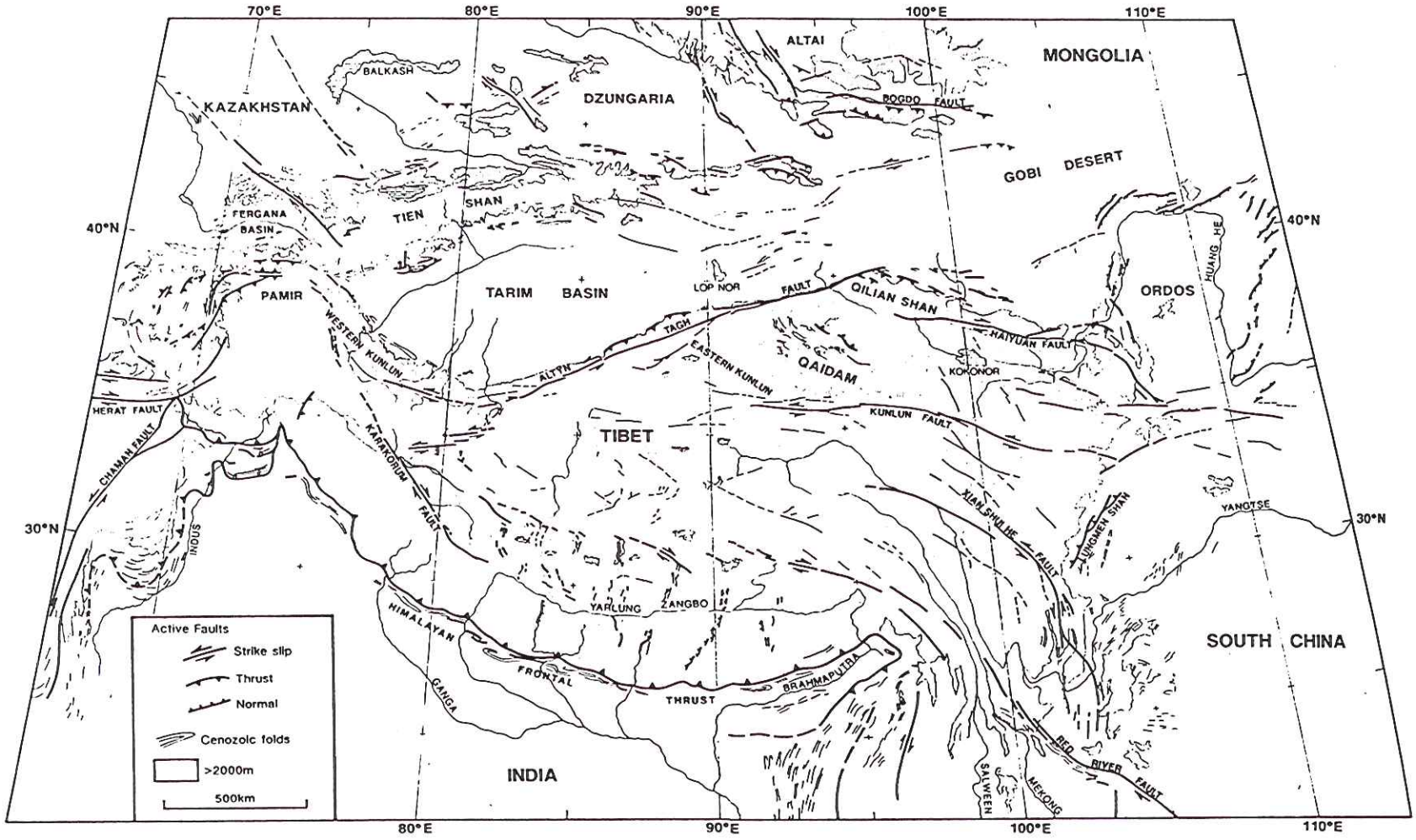

Figure 10–22. Active tectonic map of part of central Asia, showing major regions of active reverse faulting. These include the Himalayan frontal thrust system (cf. Fig. 10–3), the Pamirs, the southern and northern foothills of the Tien Shan (Tianshan), the Qilian Shan between the Altyn Tagh and Haiyuan strike-slip faults, and the Lungmen Shan at the eastern edge of the Tibetan Plateau. After Avouac and Tapponnier (1993).

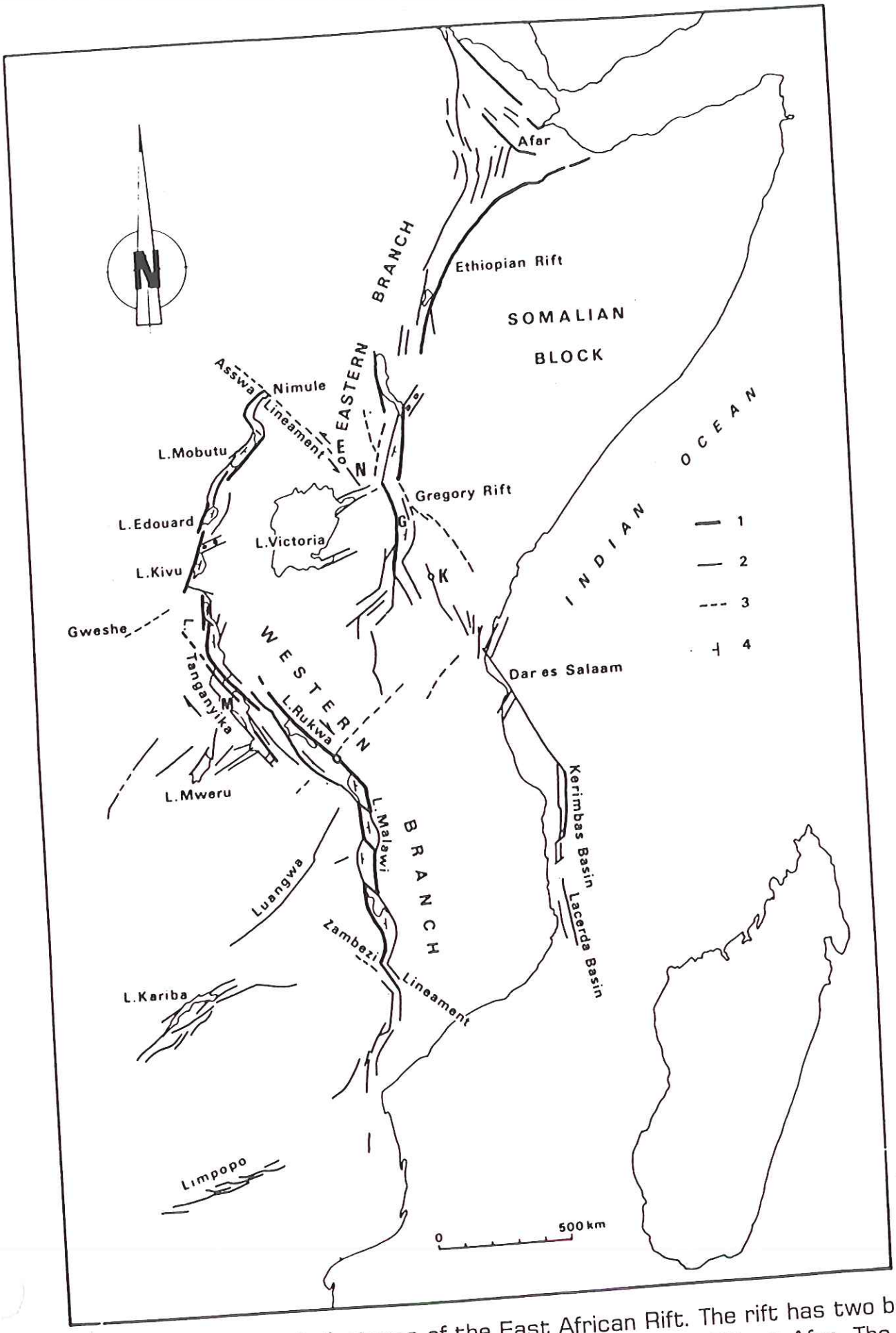

FIGURE 11.10 Major tectonic features of the East African Rift. The rift has two branches which merge in Ethiopia; the East African Rift joins the Red Sea Rift at Afar. The Red Se was formerly continental, but now it is completely floored by oceanic crust. (Reprinted fro Skarawicz, I., 1989, pp. 203–214, with kind permission from Elsevier Science Ltd., Th

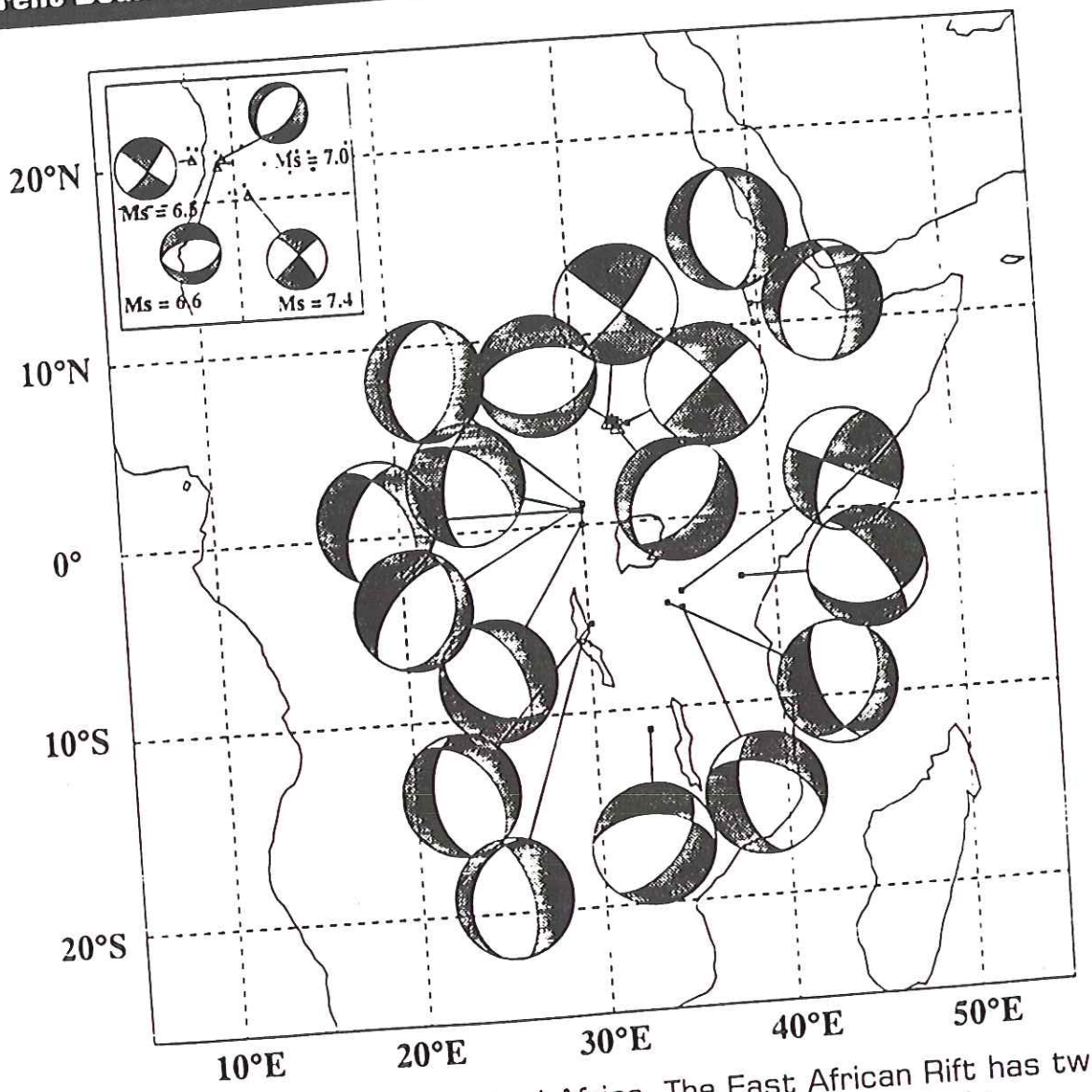

FIGURE 11.11 Focal mechanisms in central Africa. The East African Rift has two arms, as indicated by the trends of the focal mechanisms. (From Gao *et al.*, 1994.)

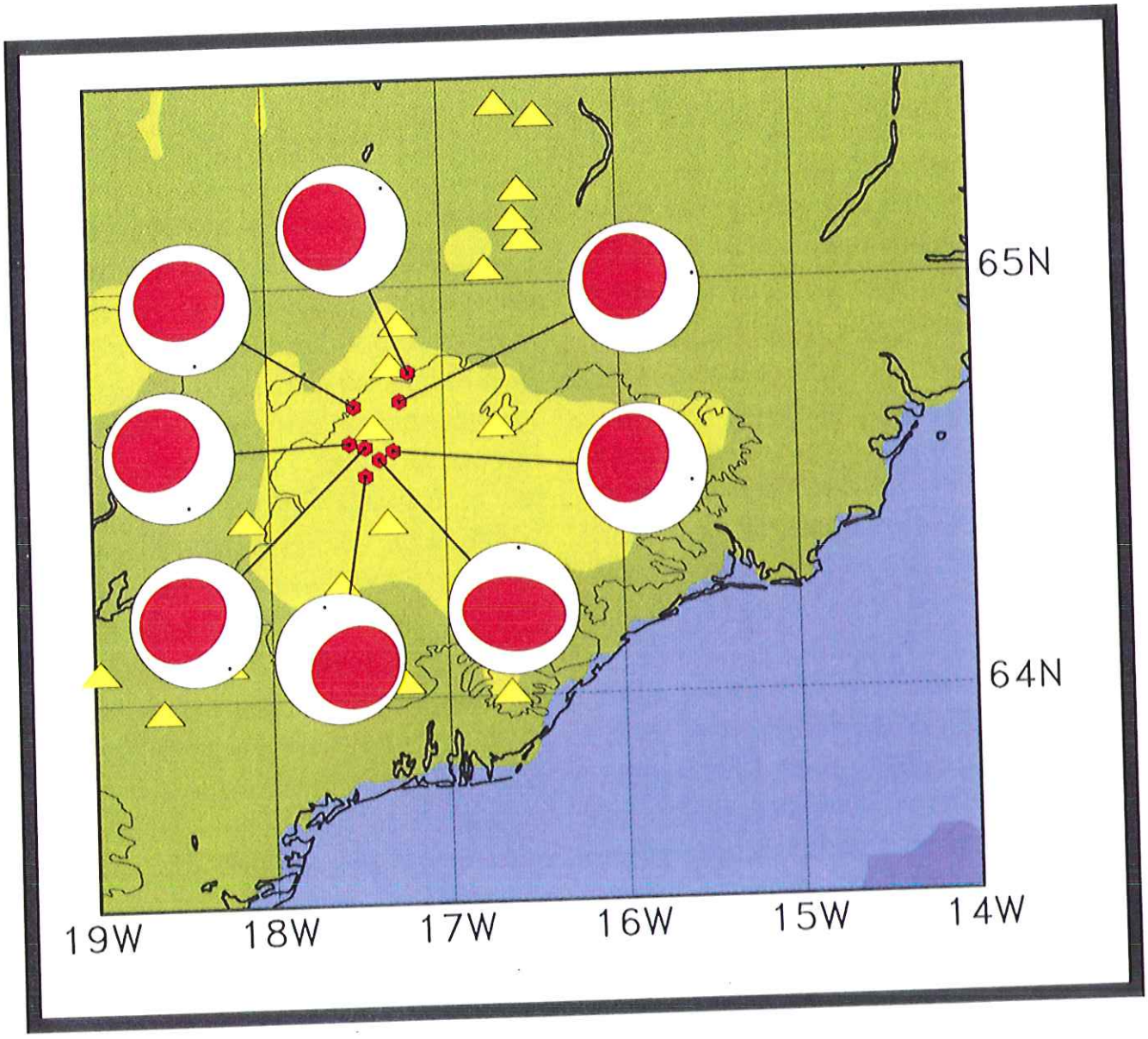
65N
64N
19W
18W
17W
16W
15W
14W

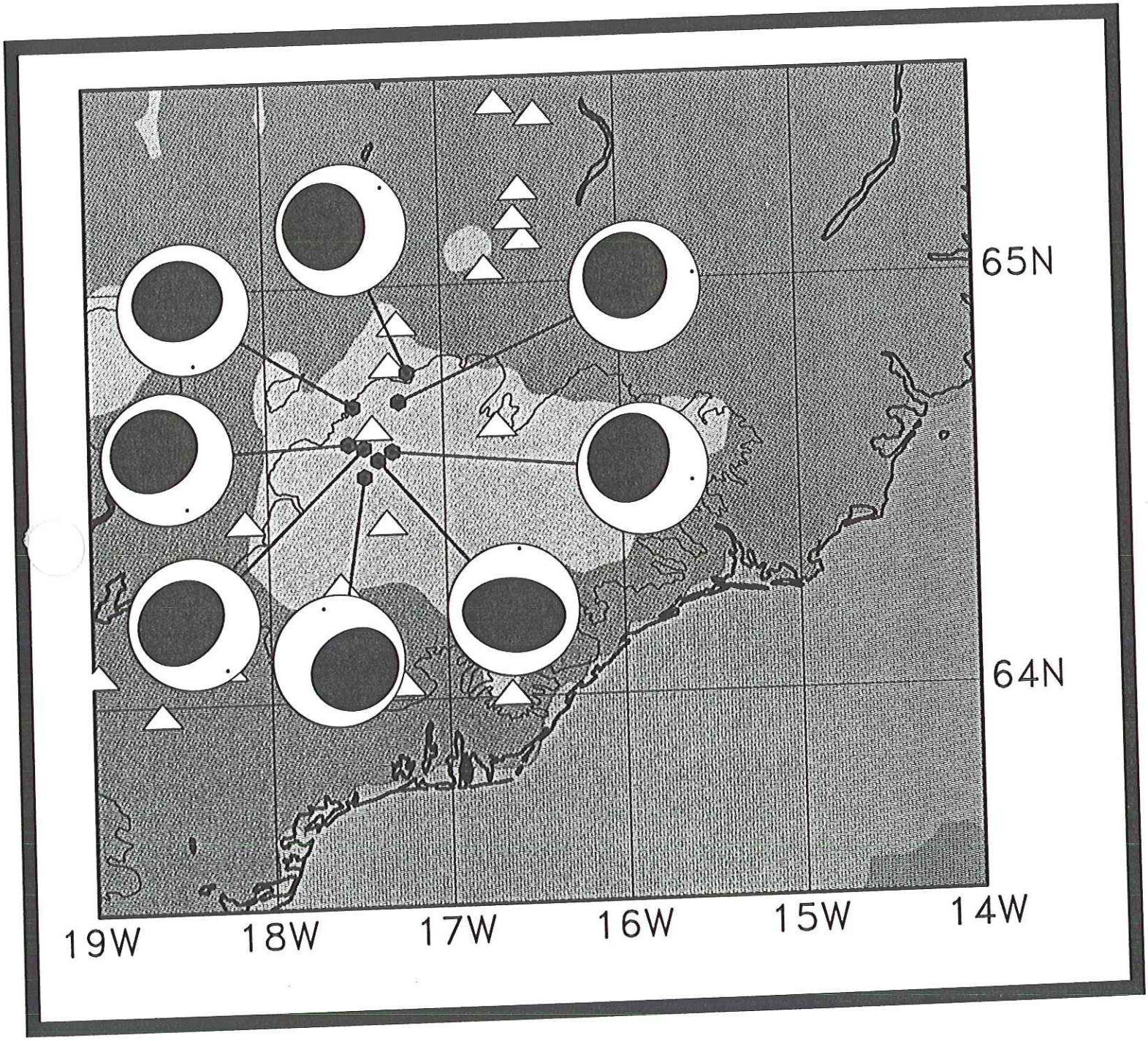

under Vatnajokull

Bardarbunga volcano

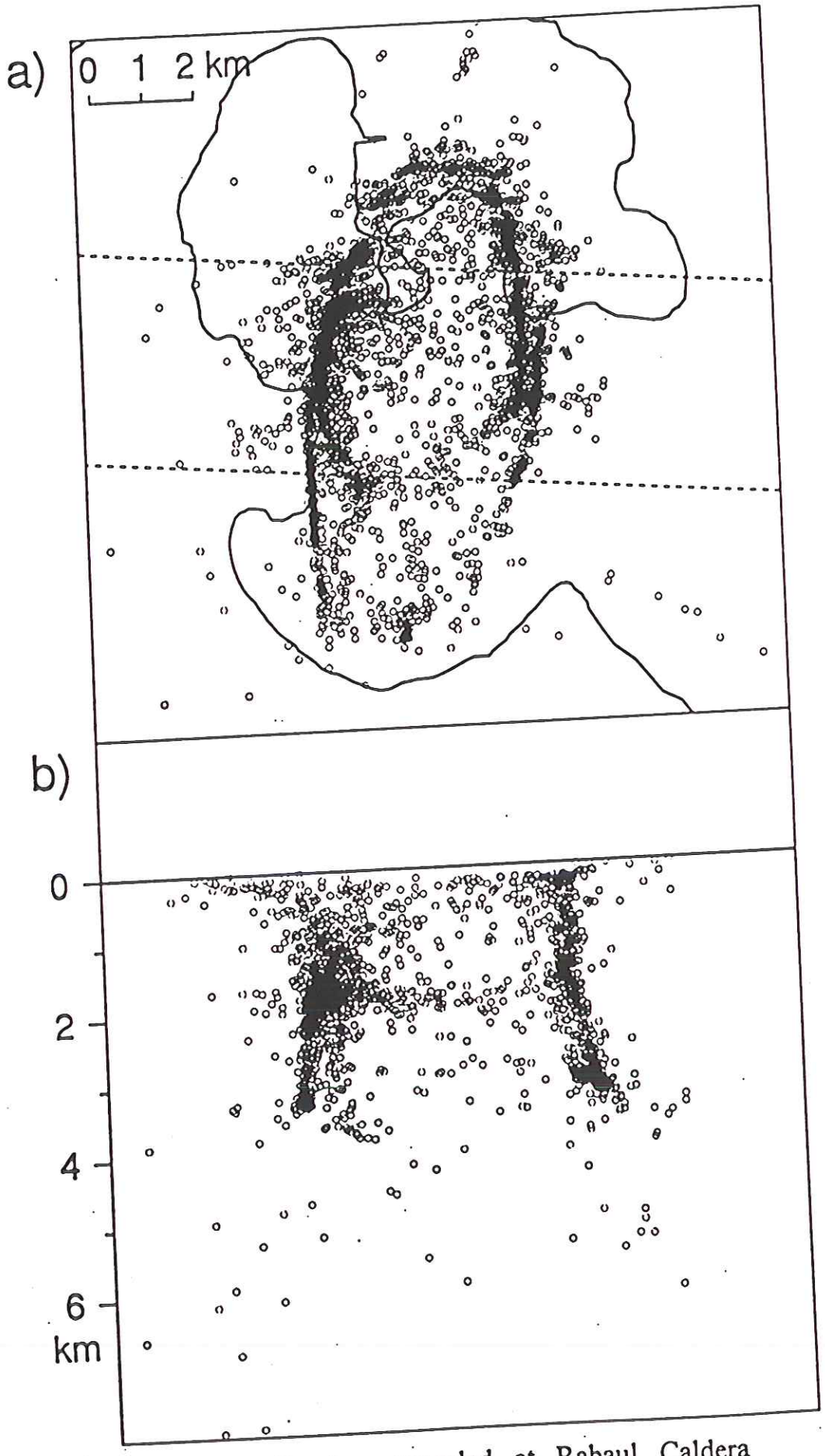

Figure 7. Earthquakes recorded at Rabaul Caldera

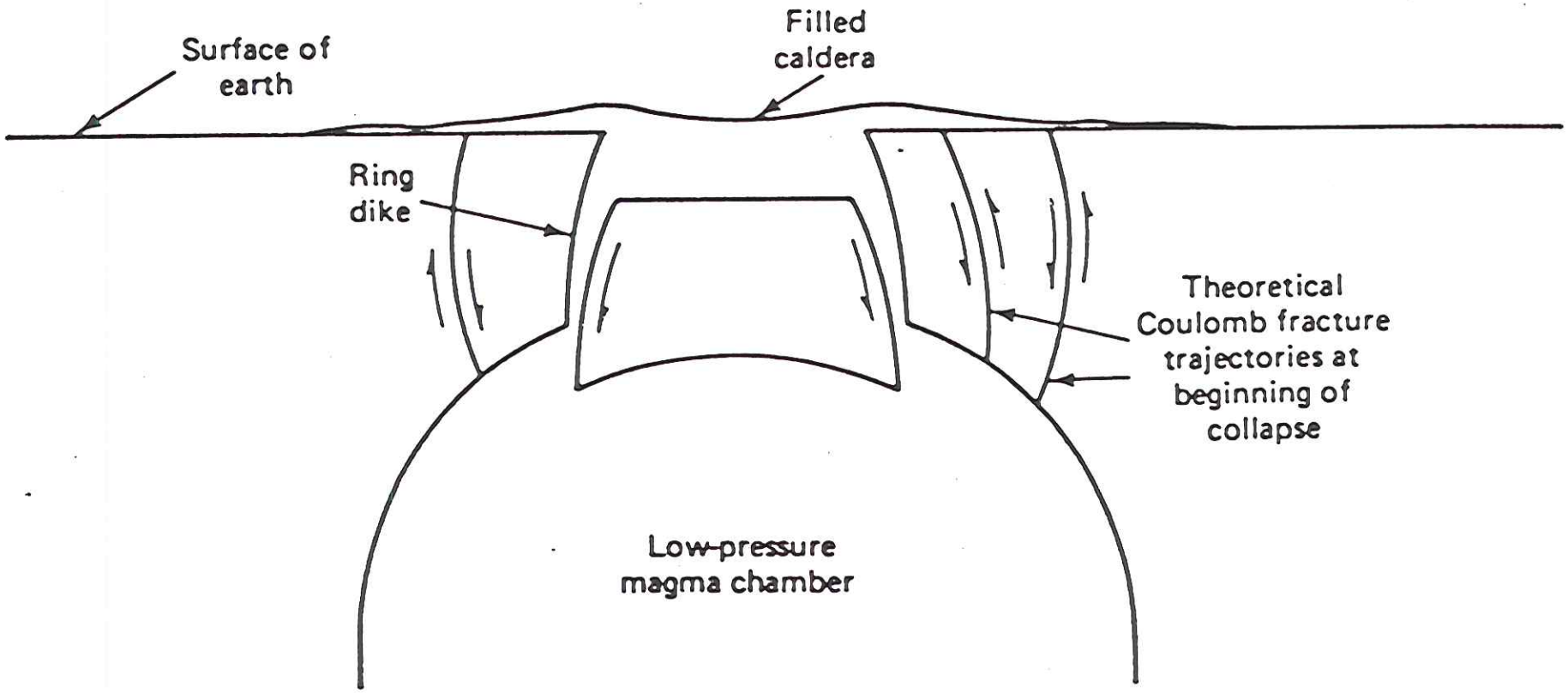

FIGURE 7–16 Schematic shear fracture trajectories around a low-pressure magma chamber leading to collapse of roof of chamber and formation of caldera and ring dike.

Mechanism of deep-focus quakes

Short slabs (e.g. Middle America)

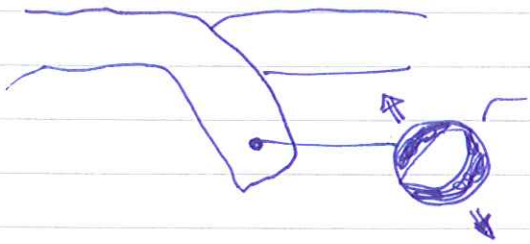

viewed from side

consistent with slab sinking under its own weight

Long slabs (e.g. Tonga)

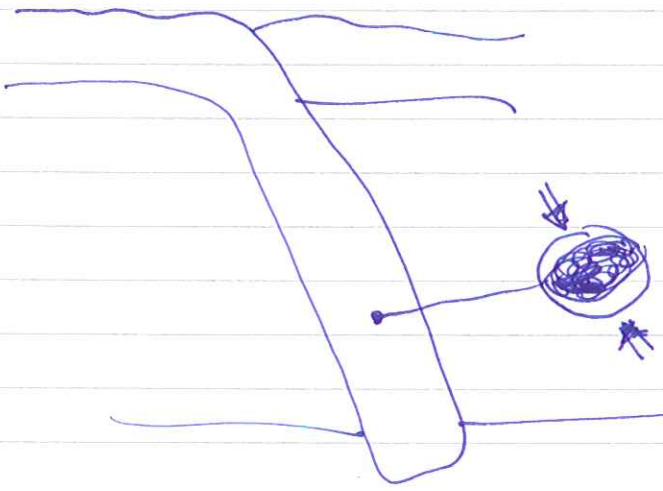

consistent with increased resistance at 670

670 km discontinuity

Detached slabs (e.g. Chile)

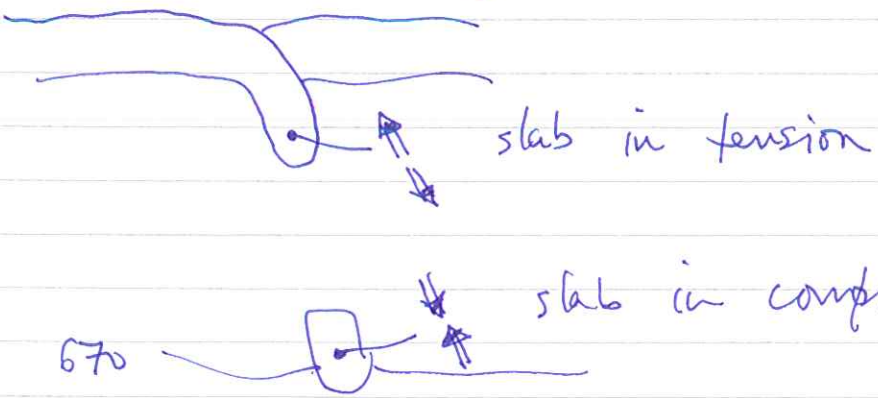

slab in tension

slab in compression

670

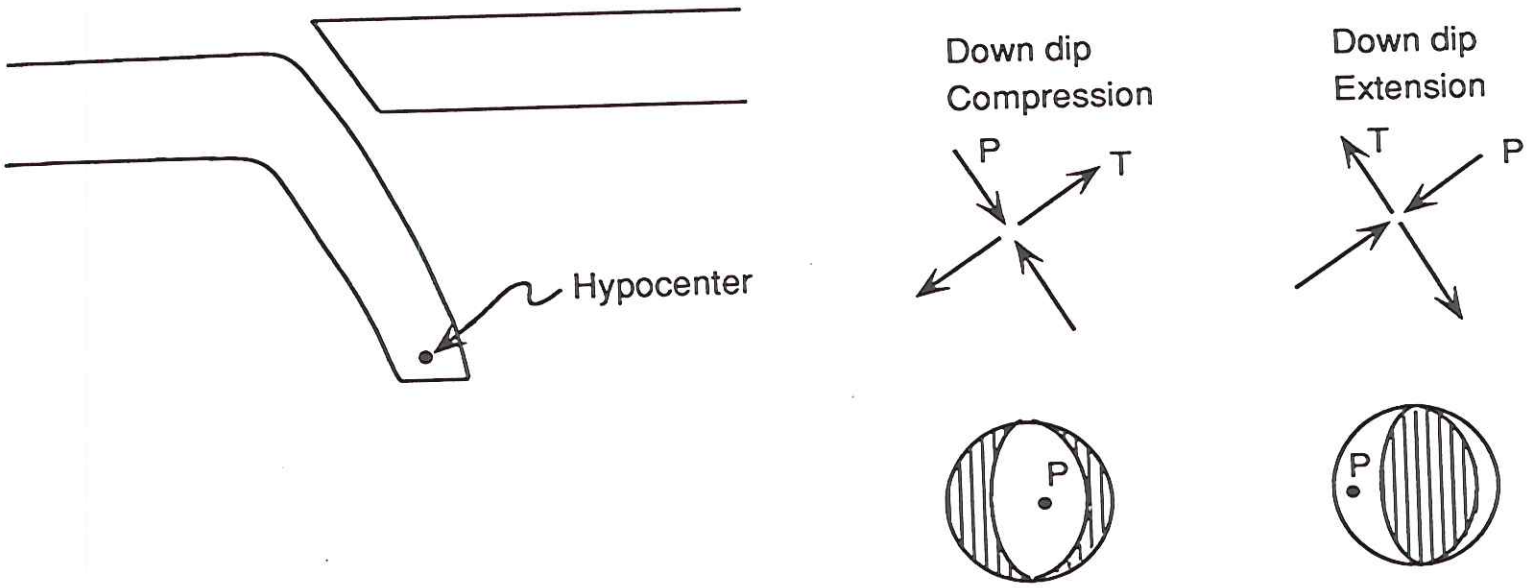

FIGURE 11.21 Focal mechanisms expected for *downdip compression* and *downdip extension*. The focal mechanism can appear to involve normal or thrust motion, depending on the slab dip and the orientation of the principal stresses. The relevant characterization of the stress regime is the direction of the *P* and *T* axes with respect to the dipping slab.

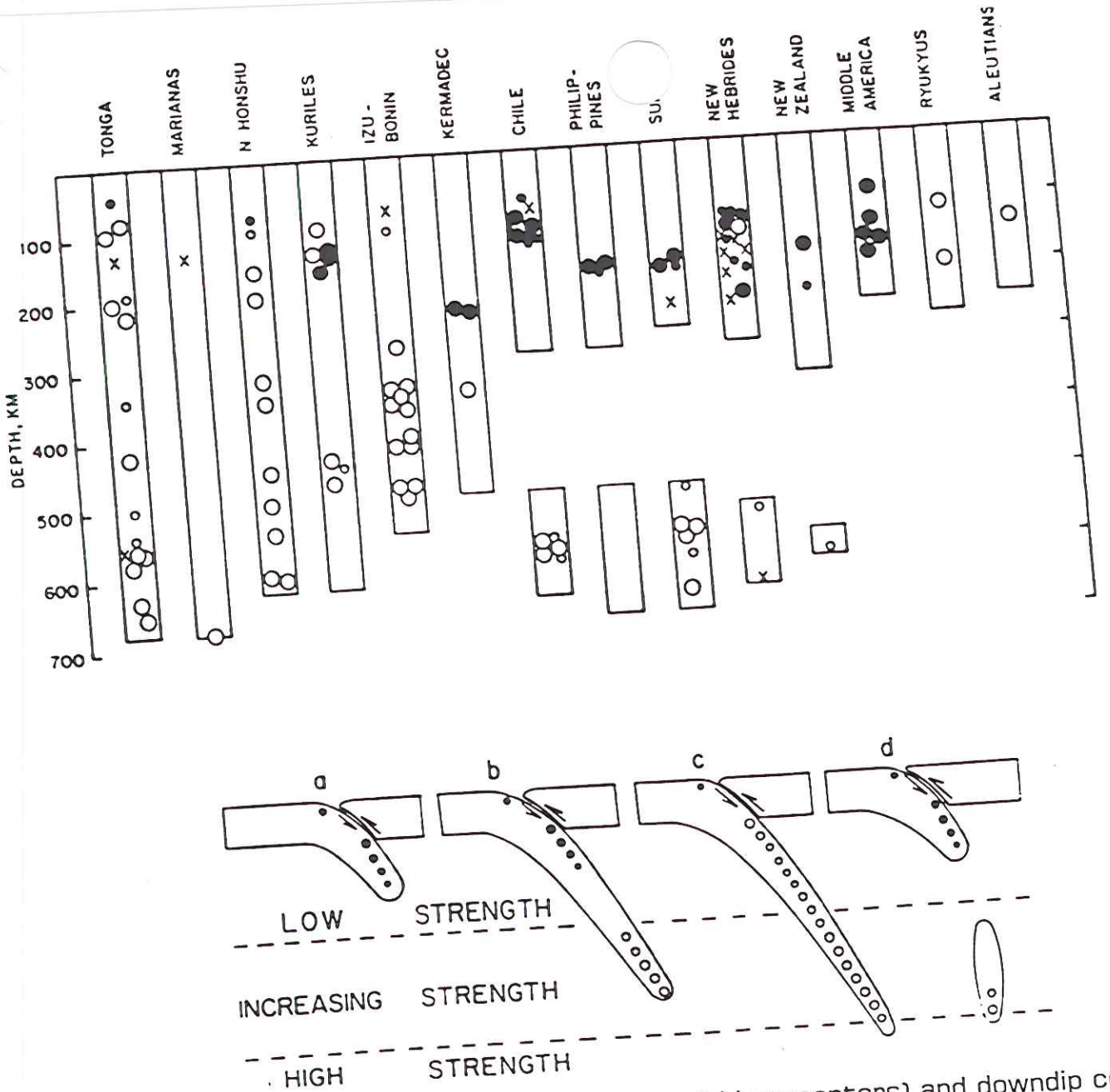

FIGURE 11.23 Distribution of downdip extension (solid hypocenters) and downdip compression (open hypocenters) in various subduction zones. The mechanical interpretation is shown below. (From Isacks and Molnar, 1971.)

Two new techniques promise to very important in study of earthquakes and faulting

(1) very precise location of microearthquakes — measure travel-times by cross-correlation; infer relative locations of clustered events to ± tens of meters (as opposed to tens of km using standard methods.

This enables one to map active faults in 3-d in the crust.

Example from Hawaii — Rubin & Gillard here at Princeton

(2) Synthetic Aperture Radar Interferometry (SAR)

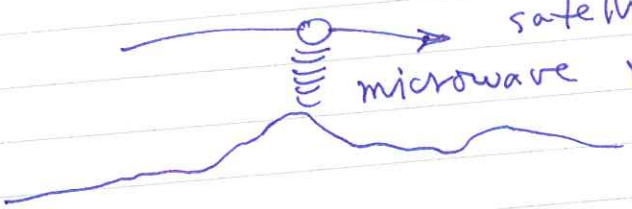

Make a map of elevation using a radar transmitter on a satellite — measure 2-way travel time to all reflecting points. After a quake fly back over and subtract the two images (form an interferogram).

Measure ground deformation in units of wavelength of radar wave

. Example – earthquake in Greece

Method developed by French group in Toulouse

Imaging slip distribution on the fault

By careful analysis of close-in stations can infer details of faulting

slip history $\Delta s(x, y, t)$ ← time

Three examples:

(1) Beroza – Loma Prieta – World Series interrupted in Candlestick Park $M = 7.0$

occurred on a dipping segment of San Andreas fault

1989

nucleation at 14 km depth

maximum dip sl
4.4 m

maximum strike slip
5.5 m

Two blocks:

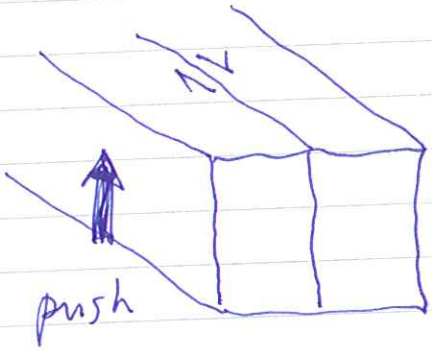

pure strike slip

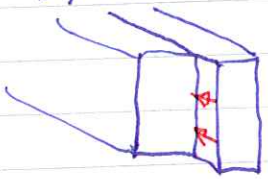

But if fault surface is inclined

dip-slip component

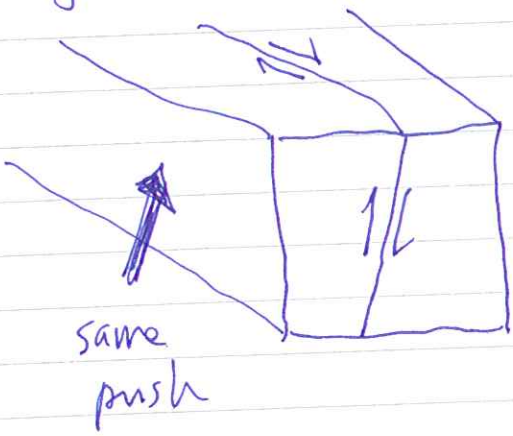

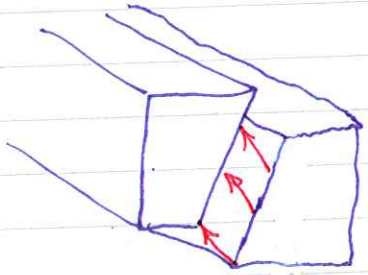

Slip distribution found to be highly variable on fault.

Aftershocks — and possibly stable afterslip — concentrated in areas that did not slip during main shock

(2) Wald — Landers 1992 — M=7.2 largest well recorded quake ever in US

occurred on 3 overlapping strike slip faults in Mojave desert

Initiated at S. end of Johnson Valley Fault, jumped to Homestead Valley fault, then to Camp Rich / Emerson faults.

Very heterogeneous slip — maximum about 6 meters — down to 15 km depth.

Rupture area observed to propagate as a pulse from S to N. Seems to get hung up at the fault jogs.

Locus of slipping area propagates at the rupture velocity

$v = 2.7$ km/sec — average

total rupture duration 24 secs

fault length 65 km

A particular point slips for only about 4–5 seconds, much less than the total rupture duration

What is typical slip velocity?

$$\frac{4\text{–}5 \text{ m of slip}}{4\text{–}5 \text{ secs}} \approx \boxed{1 \frac{\text{m}}{\text{sec}}}$$

slip velocity

So, if you were standing on the fault talking to someone and it started slipping

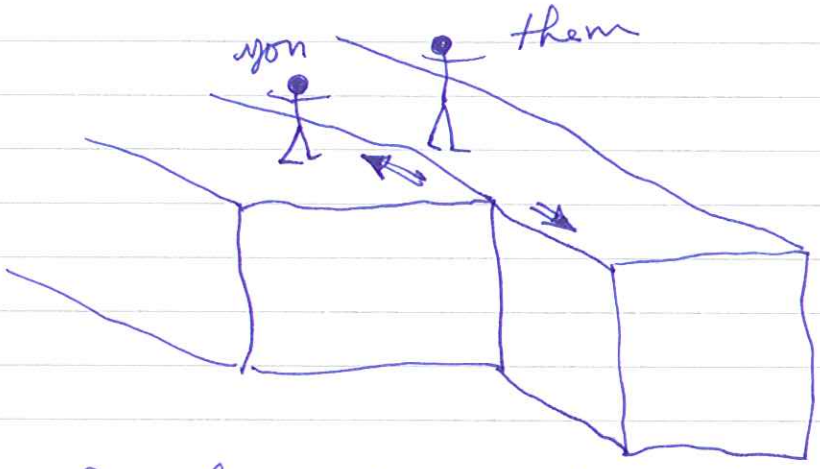

You would have to walk at 1 m/sec to keep up.

Faults slip at about the speed you can walk

(3) 1995 Kobe quake — Wald

Nucleates at 17 km — bilateral propagation

$v = 2.8$ km/sec

rupture duration 12 sec

max slip 3.5 m — average slip 1–2 m

→ slip rate 1 m/sec

local slip duration 1–2 sec

East Rift Zone of Kilauea, Hawaii — looks like a fault

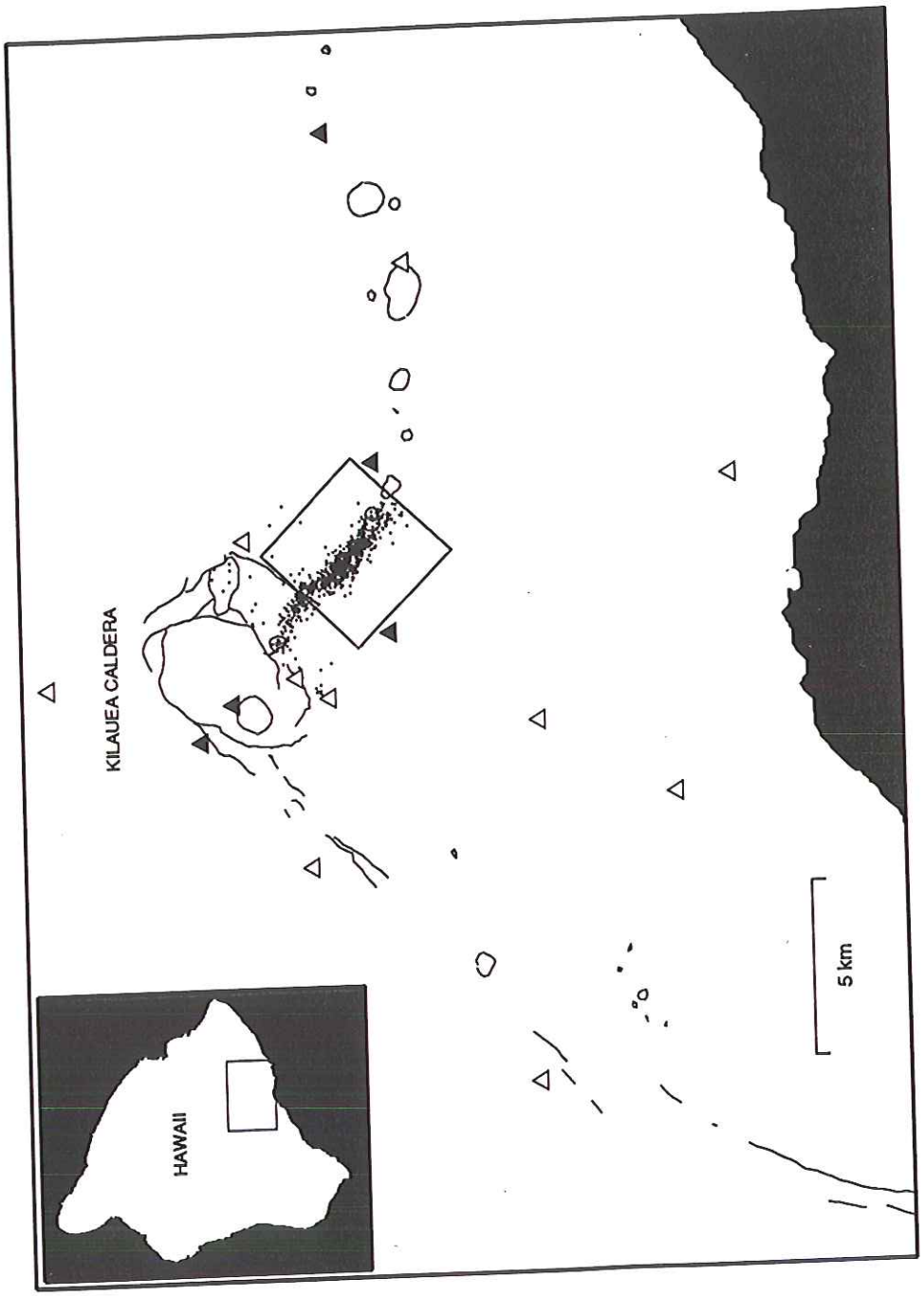

EARTHQUAKES BEFORE RELOCATION

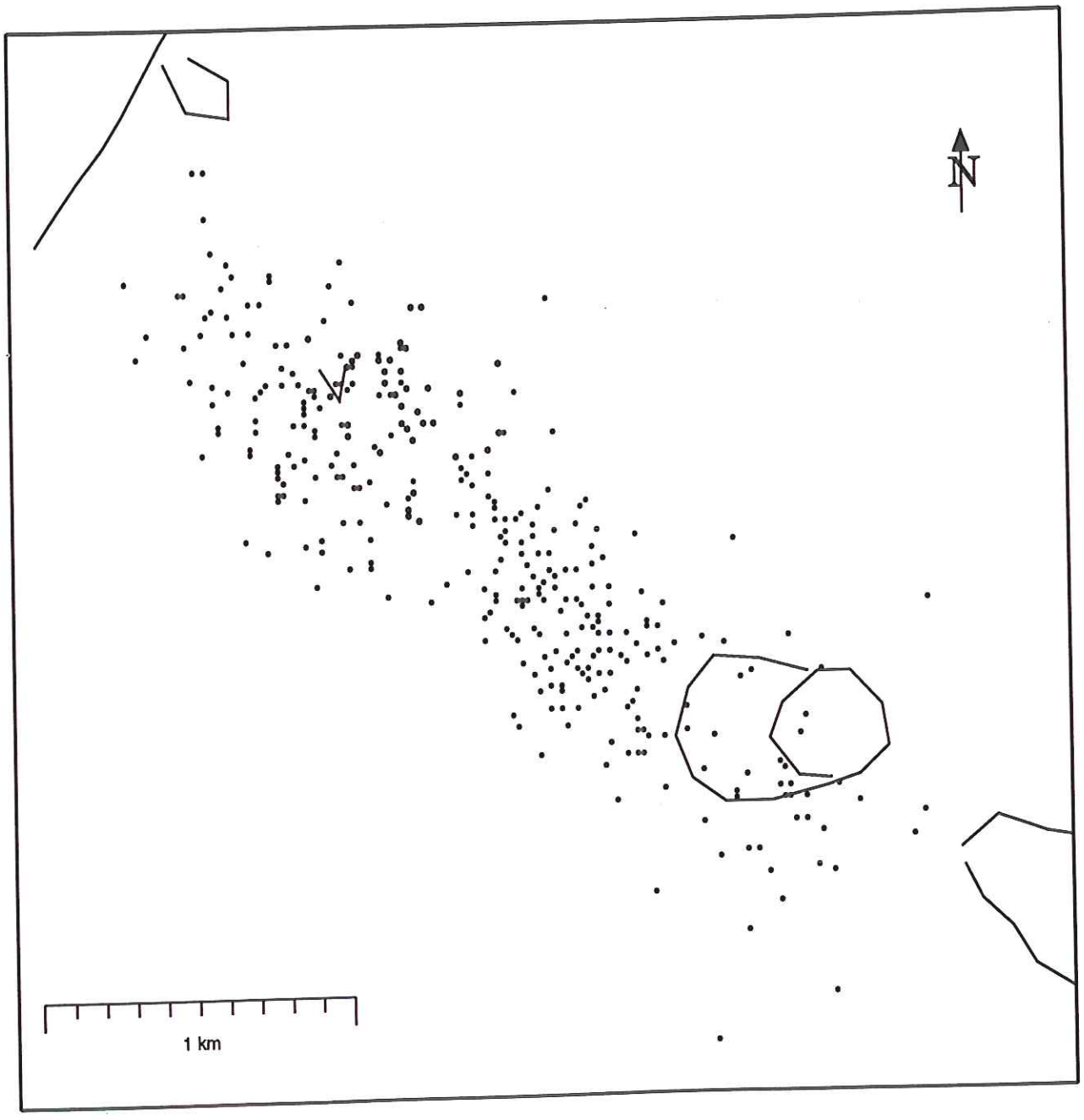

scatter due to location uncertainty ± 2–3 km

EARTHQUAKES AFTER RELOCATION

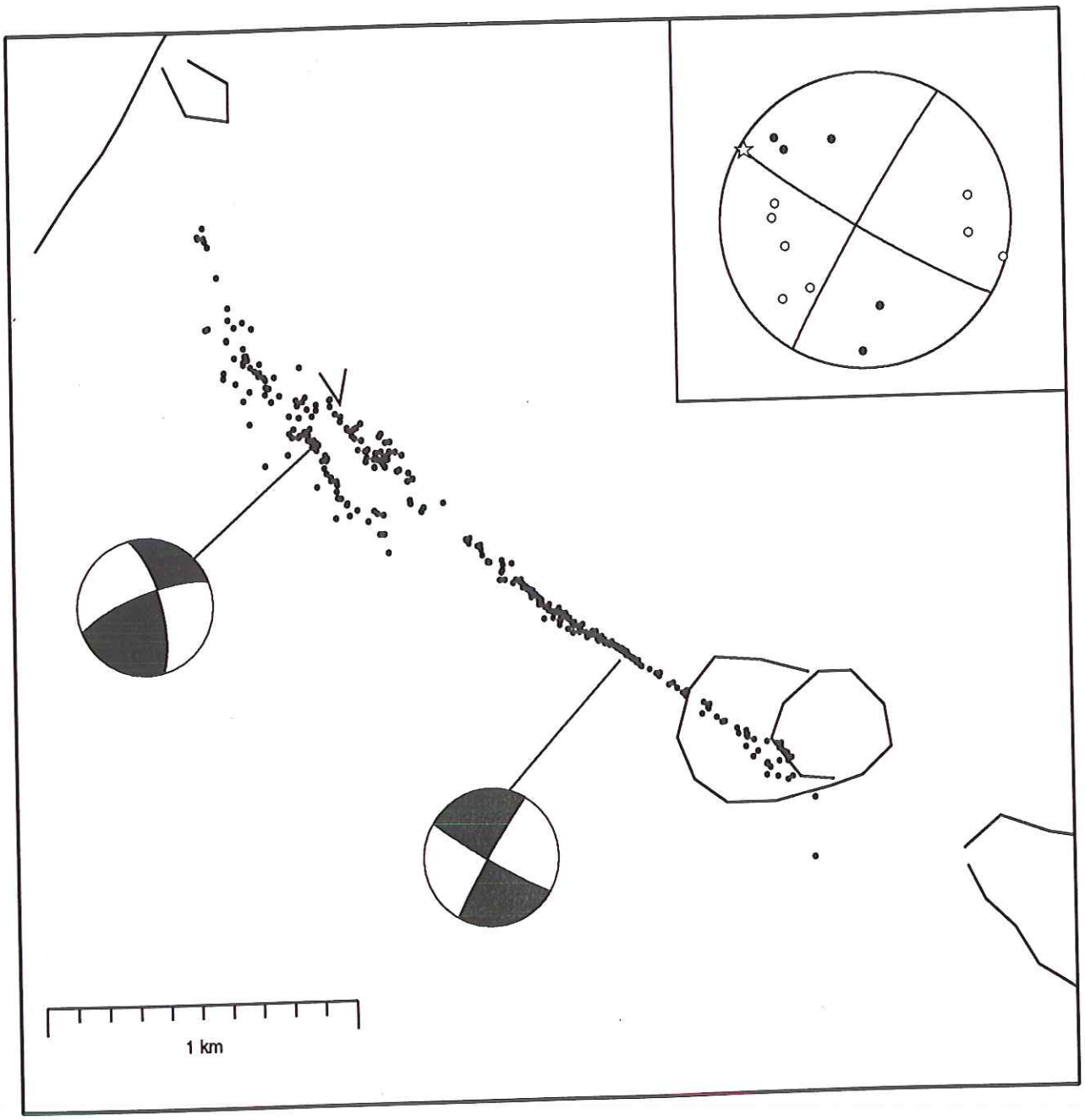

scatter reduced
to few hundred m

EARTHQUAKES BEFORE RELOCATION

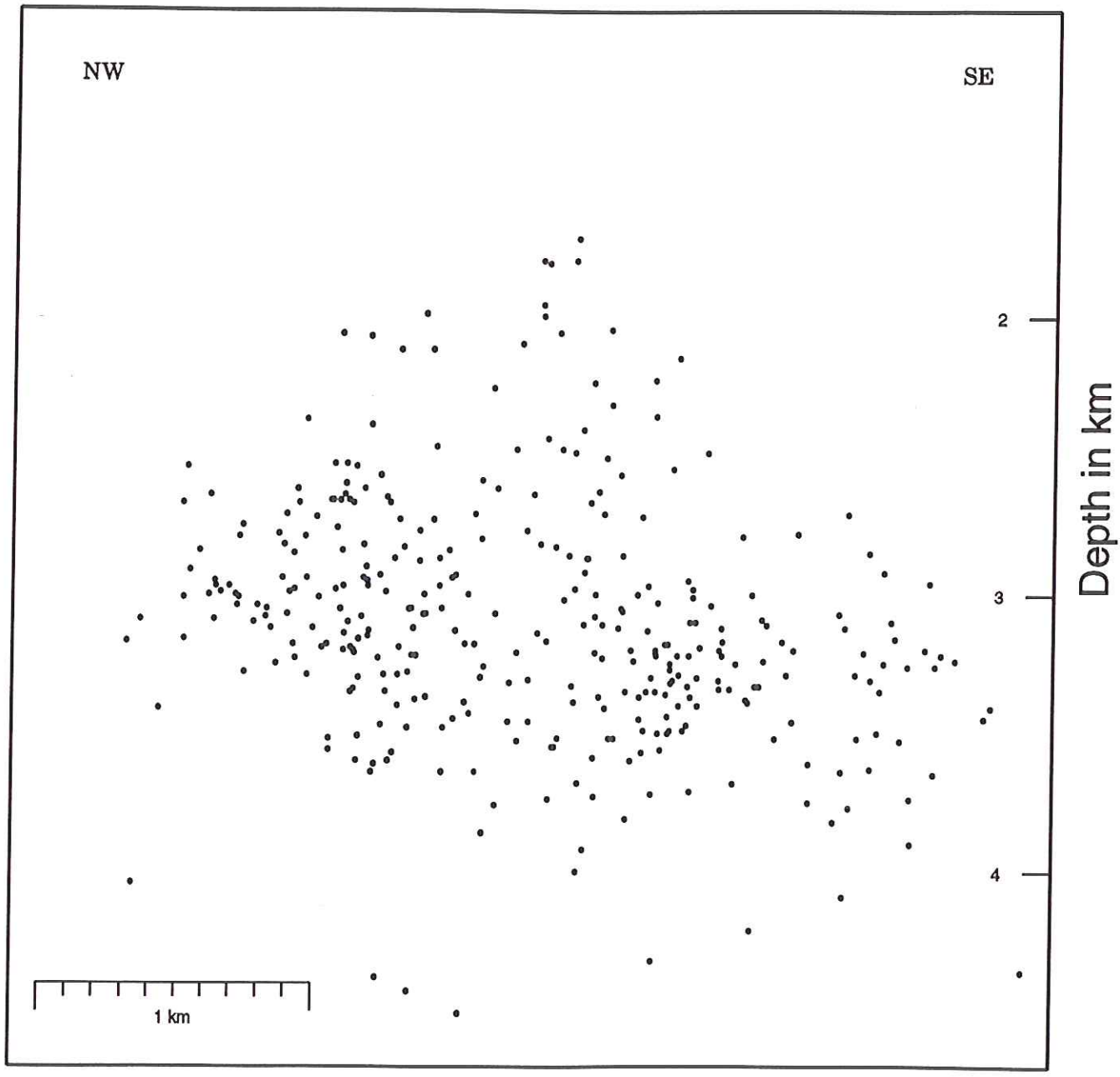

± 2 km in depth

EARTHQUAKES AFTER RELOCATION

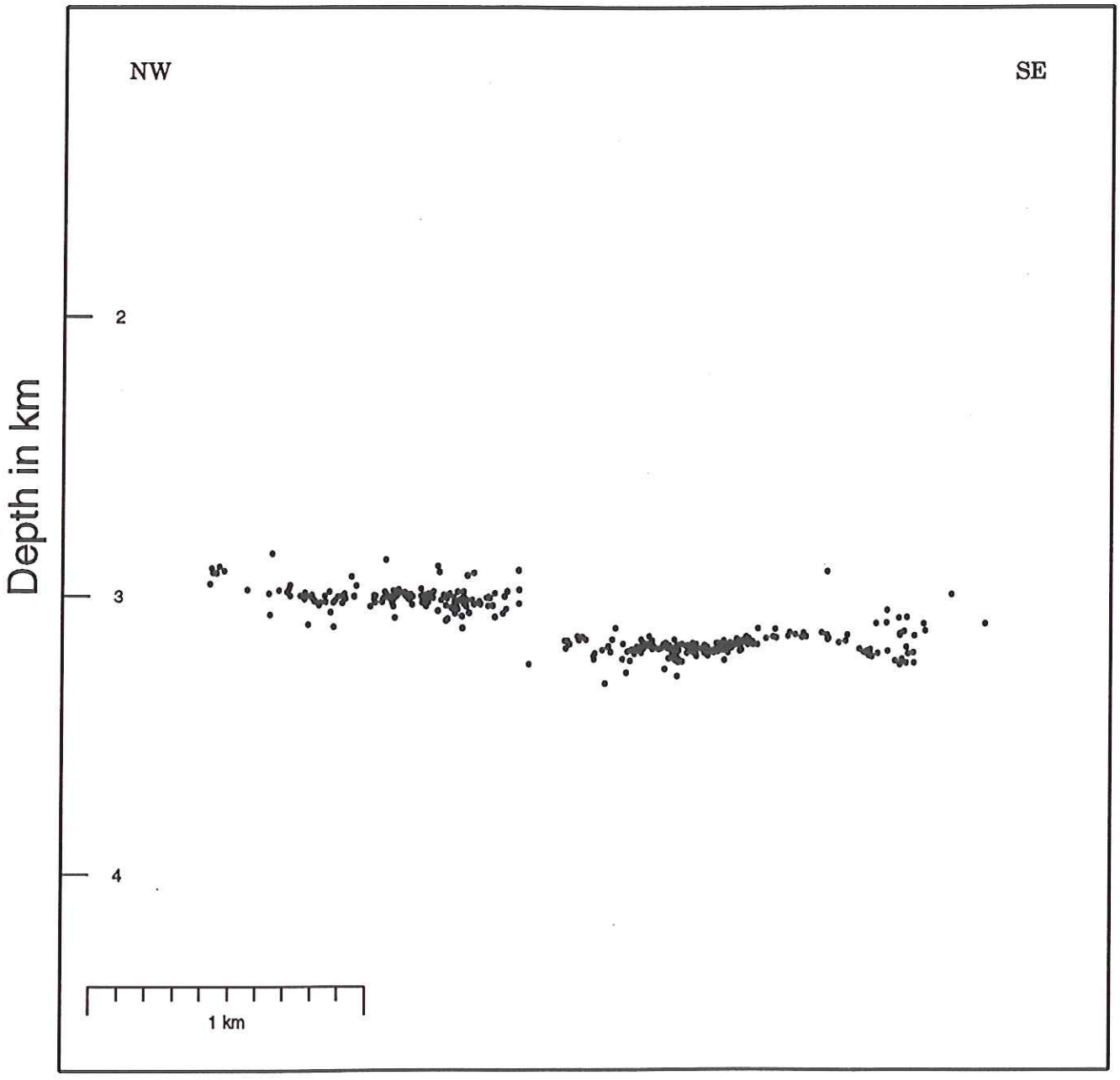

ribbon - thin fault 50-100 m high

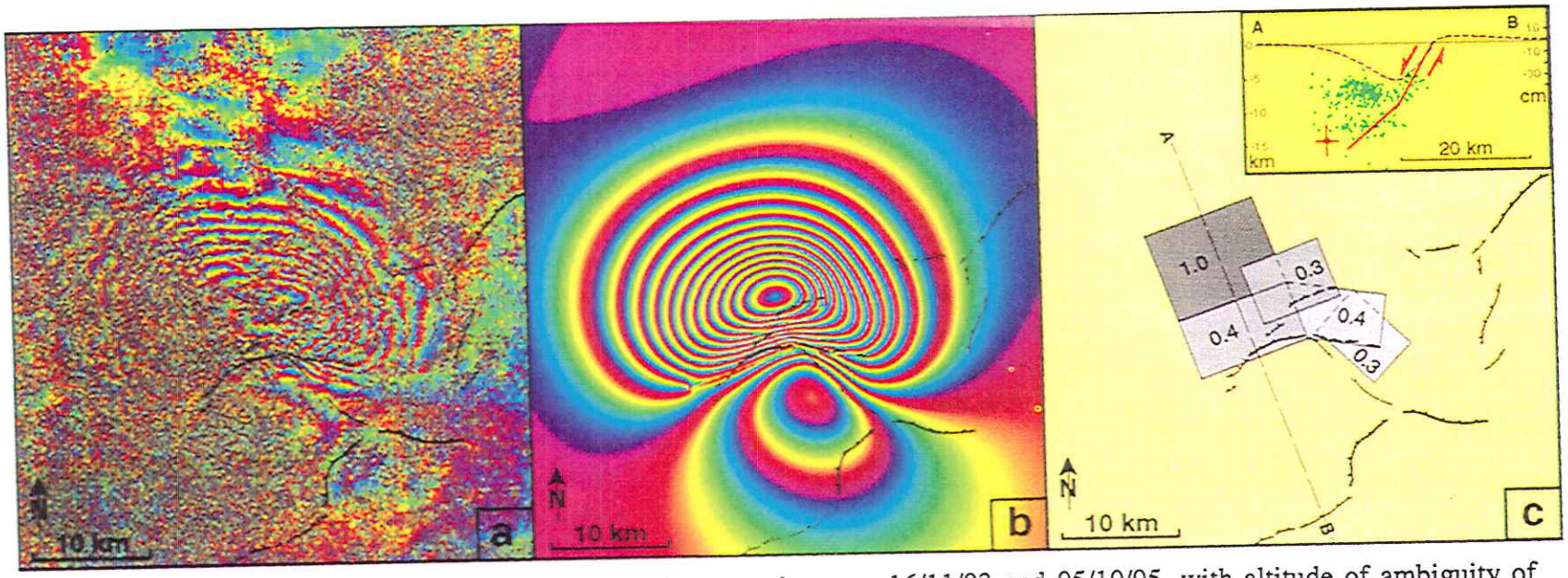

Figure 3. (a) Interferogram describing surface displacement between 16/11/93 and 05/10/95, with altitude of ambiguity of 126 m and error of less than 2 mm. Each fringe represents 28 mm displacement. Unit vector from ground to satellite [east, north, up] is [0.402, -0.083, 0.912]. (b) Synthetic fringes. (c) Fault model with average displacement (in m). The two patches with 0.4 m have variable slip, see text. Inset section: Modeled Palaeochori fault and surface vertical displacement (in cm, segmented). Main shock with error bars and aftershocks (over 14 km wide band) from Hatzfeld et al. [1996].

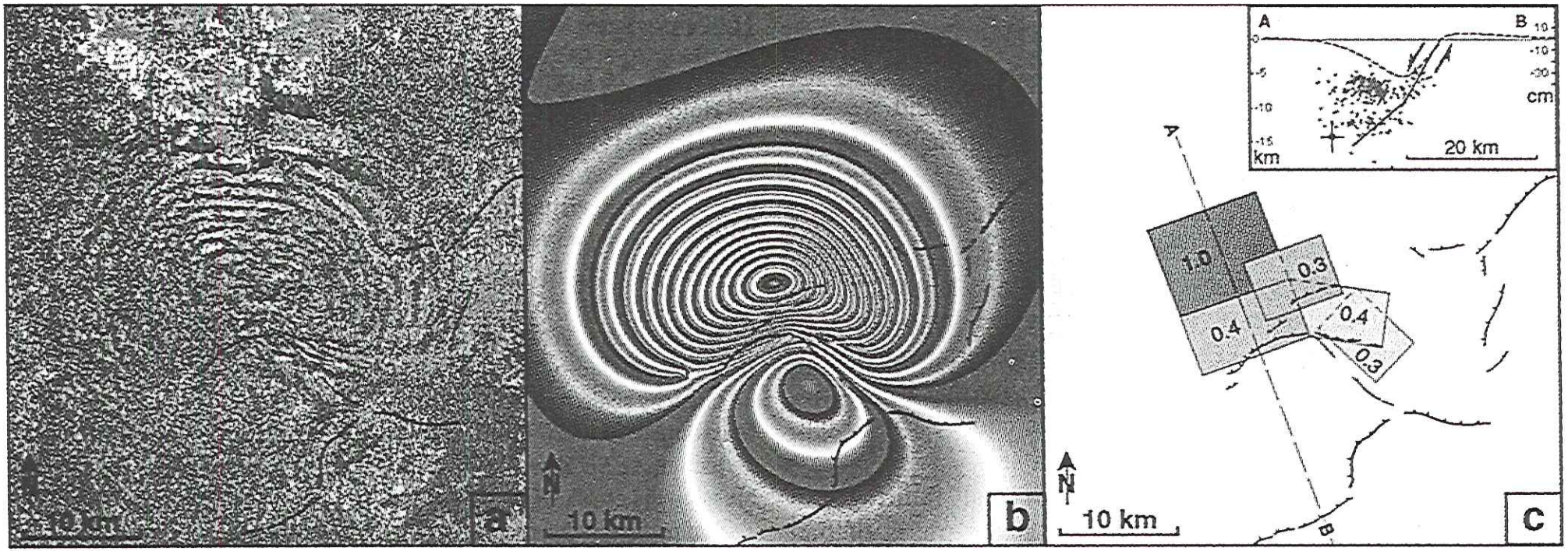

Figure 3. (a) Interferogram describing surface displacement between 16/11/93 and 05/10/95, with altitude of ambiguity of 126 m and error of less than 2 mm. Each fringe represents 28 mm displacement. Unit vector from ground to satellite [east, north, up] is [0.402, -0.083, 0.912]. (b) Synthetic fringes. (c) Fault model with average displacement (in m). The two patches with 0.4 m have variable slip, see text. Inset section: Modeled Palaeochori fault and surface vertical displacement (in cm, segmented). Main shock with error bars and aftershocks (over 14 km wide band) from Hatzfeld et al. [1996].

LOMA PRIETA STRONG MOTION STATIONS

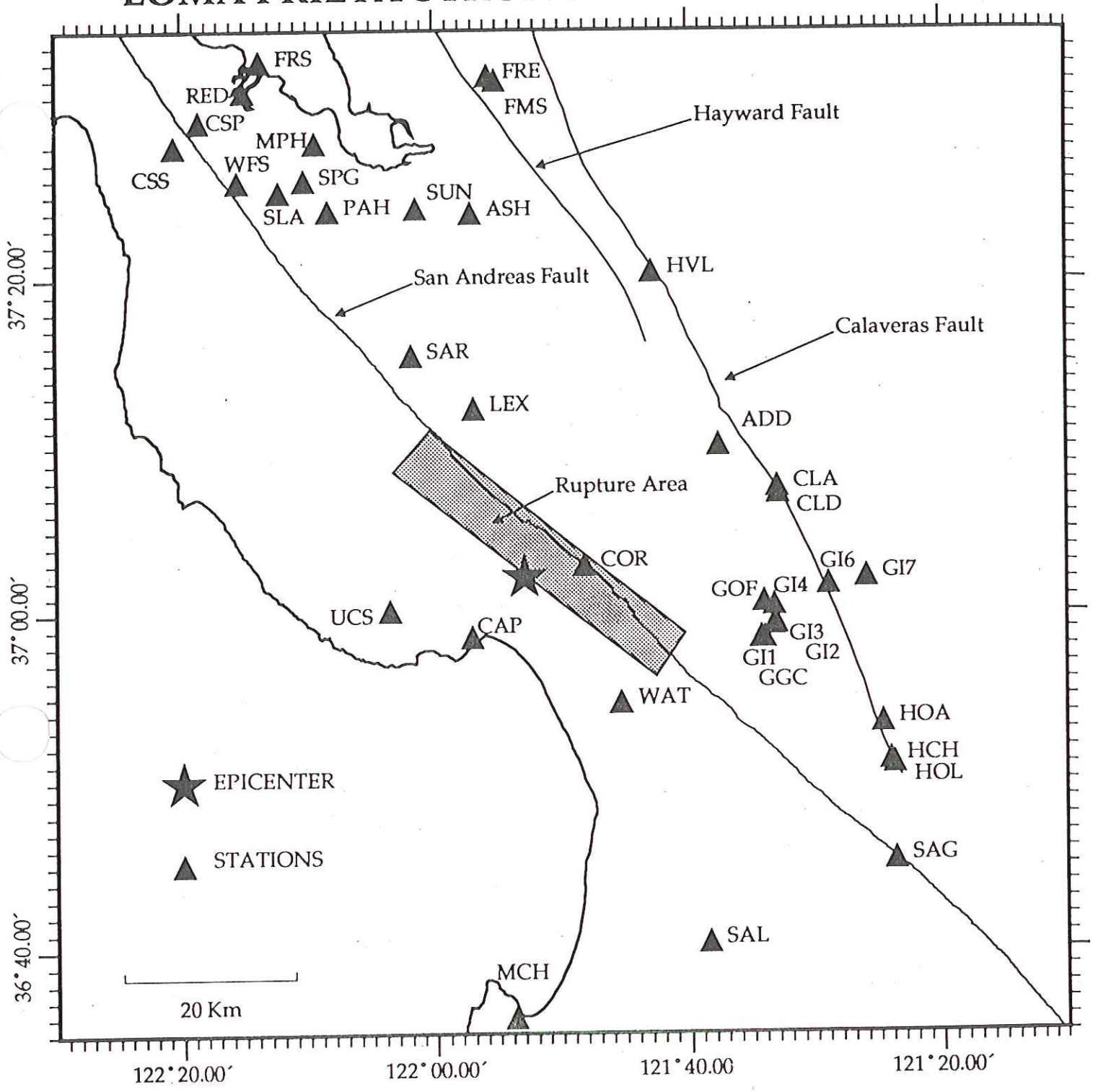

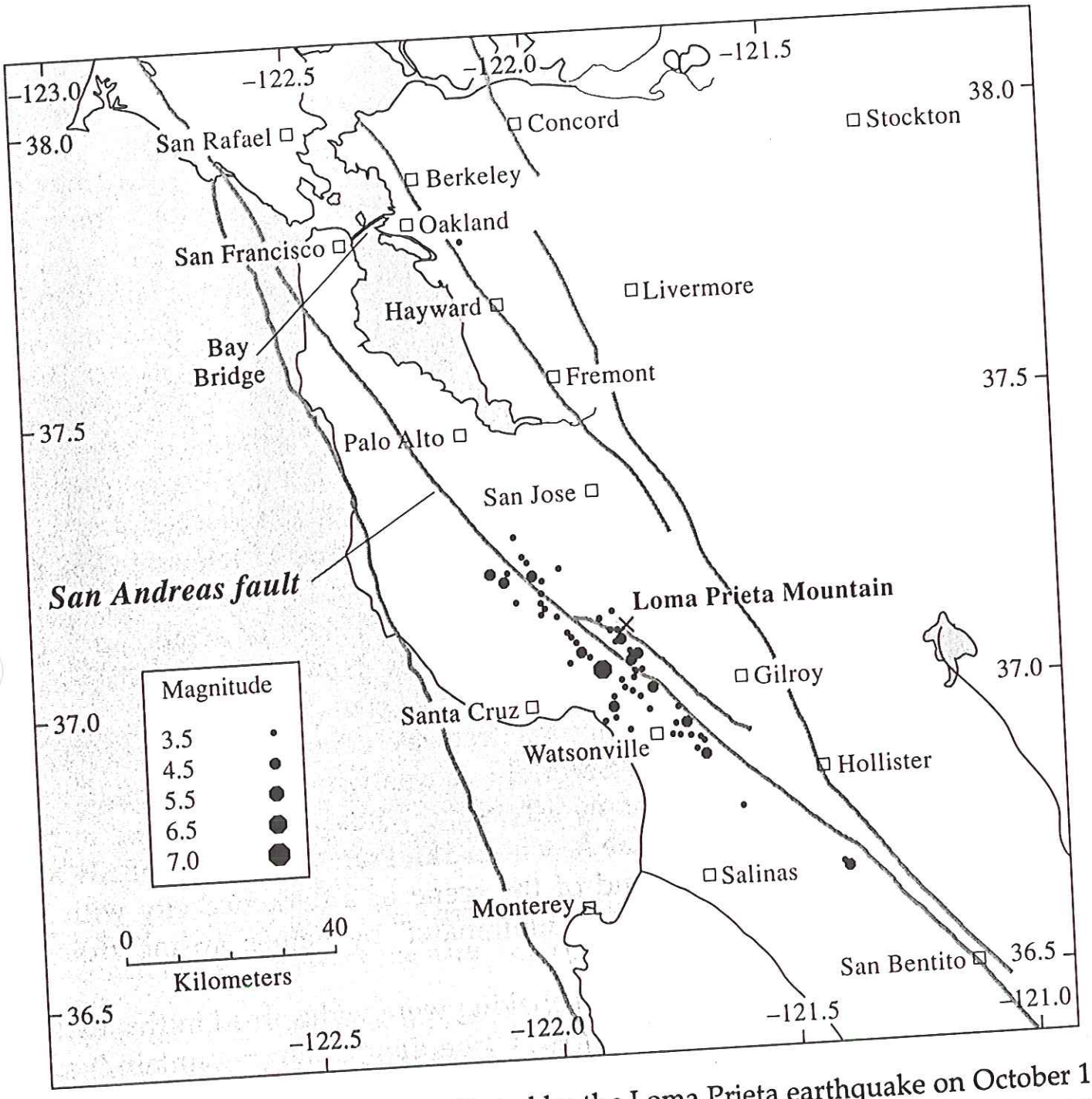

Figure 1.4 Region of California affected by the Loma Prieta earthquake on October 17, 1989. Heavy dots show the epicenters of the largest earthquakes in the sequence. The smooth lines are the main active faults in the region. The short dark line is the Bay Bridge joining San Francisco to Oakland across the Bay.

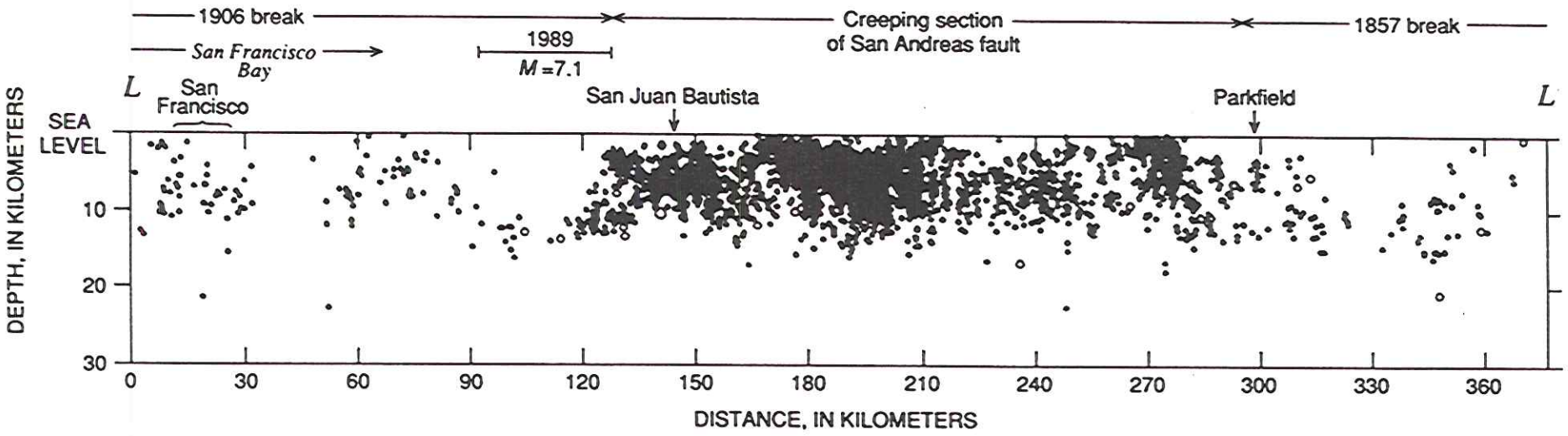

Figure 2.9 Cross-section along the San Andreas fault from north of San Francisco to south of Parkfield. Background seismicity for 20 years prior to 1989. North of San Juan Bautista the fault had been virtually aseismic since 1906. On the Loma Prieta segment the seismicity outlined a U-shaped area (Loma Prieta gap). Aftershocks of the 1989 main shock filled the former quiet zone of the Loma Prieta gap. [From Plafker and Galloway, 1989.]

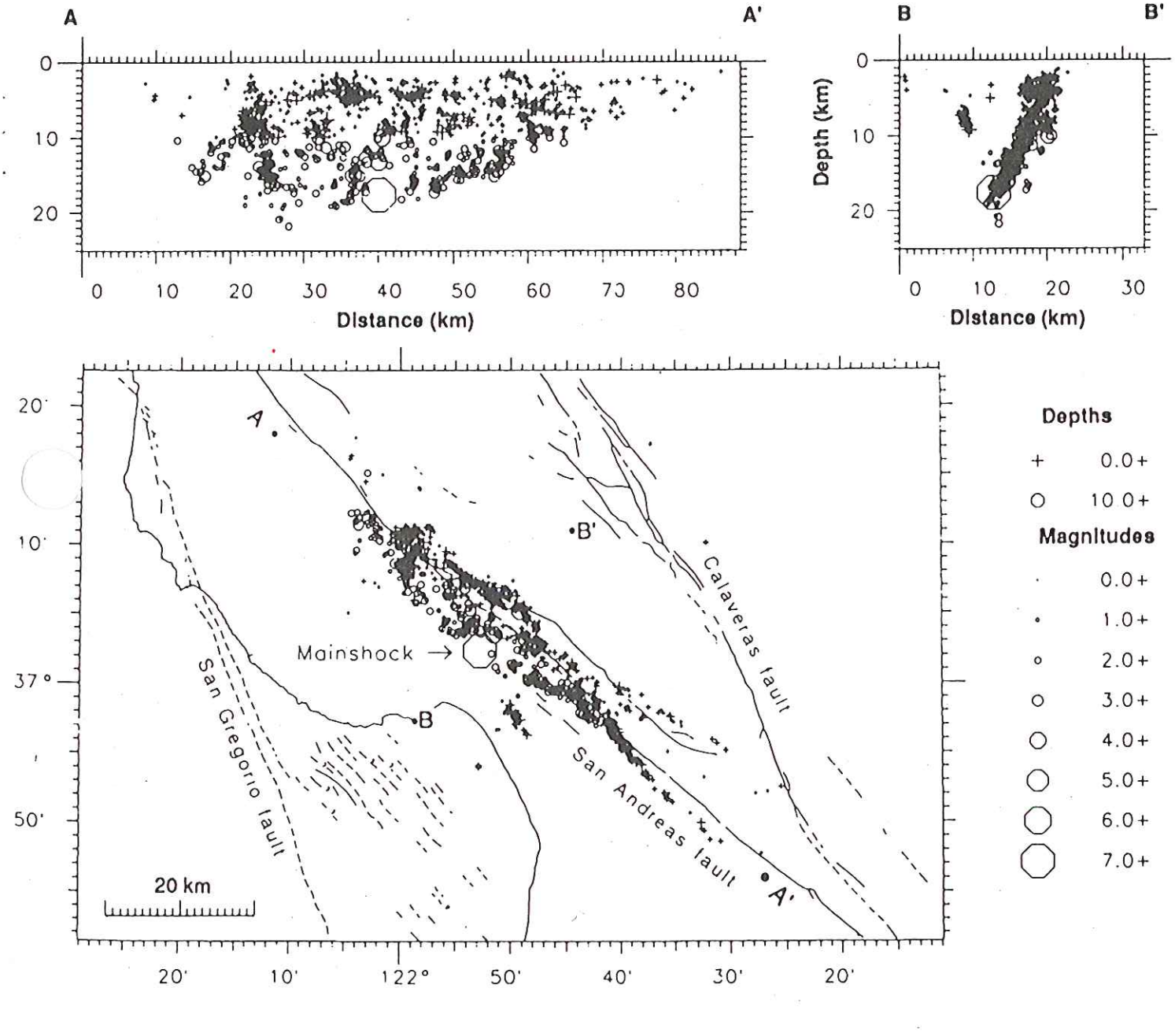
A
A'
0
10
20
0 10 20 30 40 50 60 70 80
Distance (km)
B
B'
Depth (km)
0 10 20 30
Distance (km)
20'
10'
37°
50'
A
B
B'
Mainshock
San Gregorio fault
Calaveras fault
San Andreas fault
A'
20 km
20' 10' 122° 50' 40' 30' 20'
Depths
+ 0.0+
○ 10.0+
Magnitudes
0.0+
1.0+
2.0+
3.0+
4.0+
5.0+
6.0+
7.0+

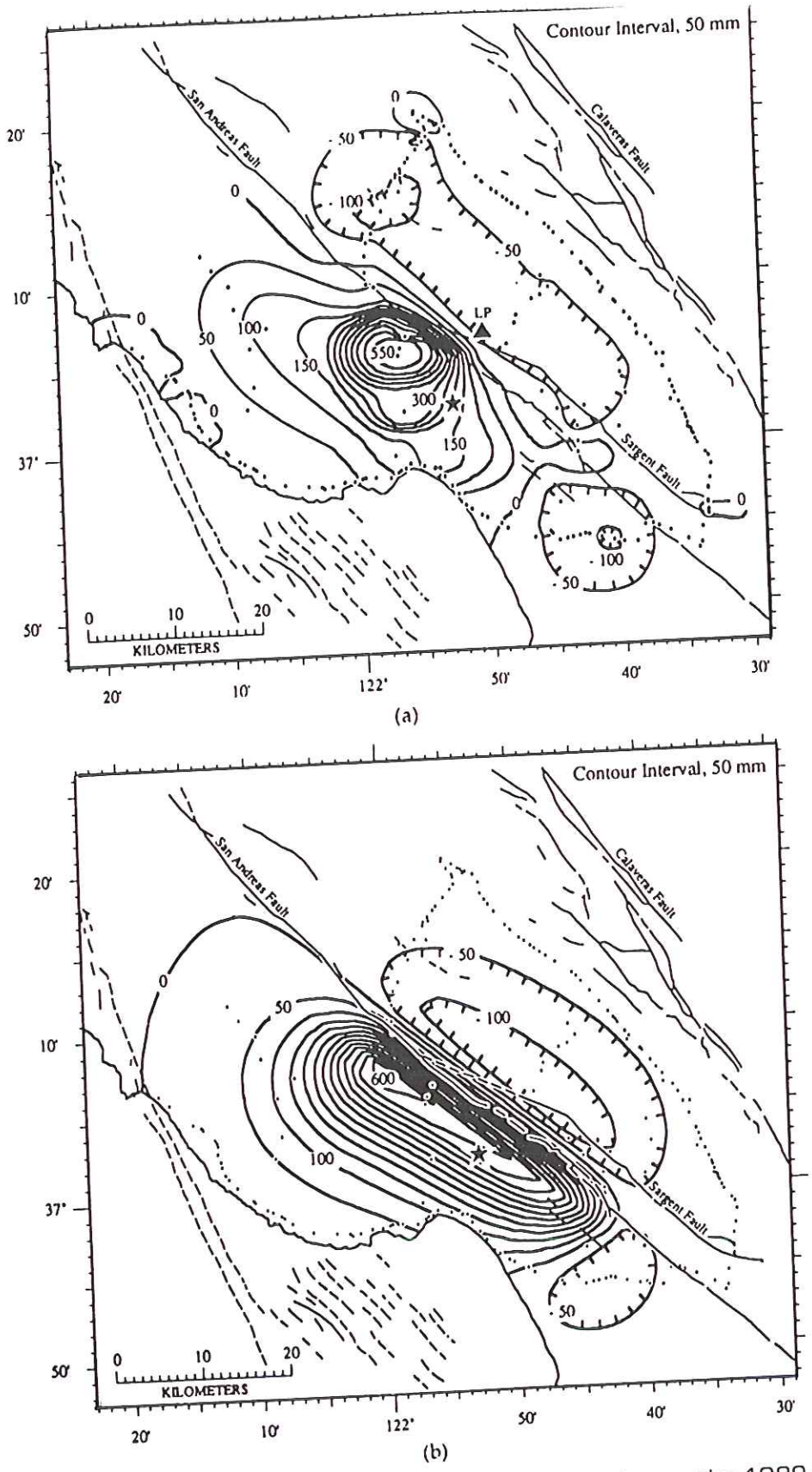

FIGURE 8.16 Observed vertical ground motions (in millimeters) near the 1989 Loma Prieta rupture zone compared to predictions of a dislocation model. The orientation of the fault zone is a 30-km-long fault parallel to the San Andreas dipping about 70° to the south. The star shows the epicenter of the event; the triangle labeled LP is the location of Loma Prieta Mountain, for which the event is named. (From Marshall *et al.*, 1991.)

Seismicity (1981-1992 M>2.5)

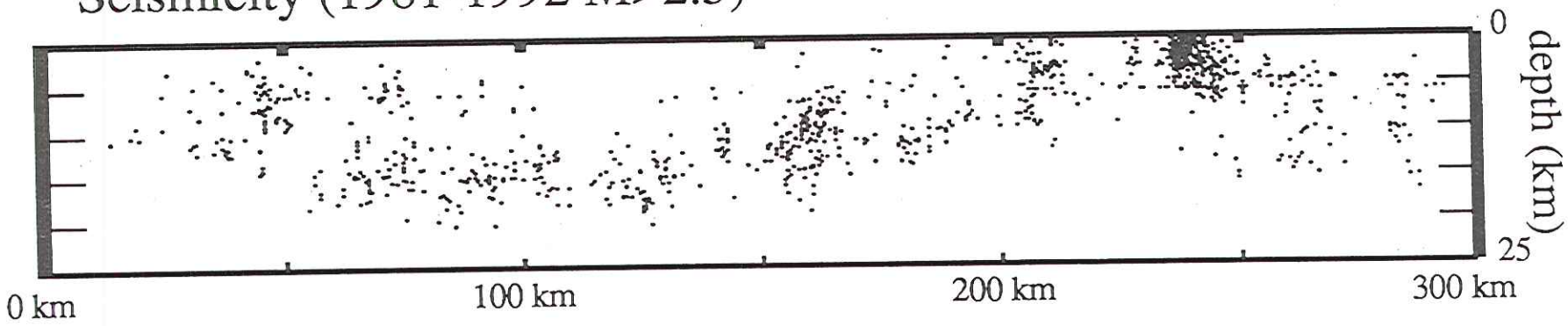

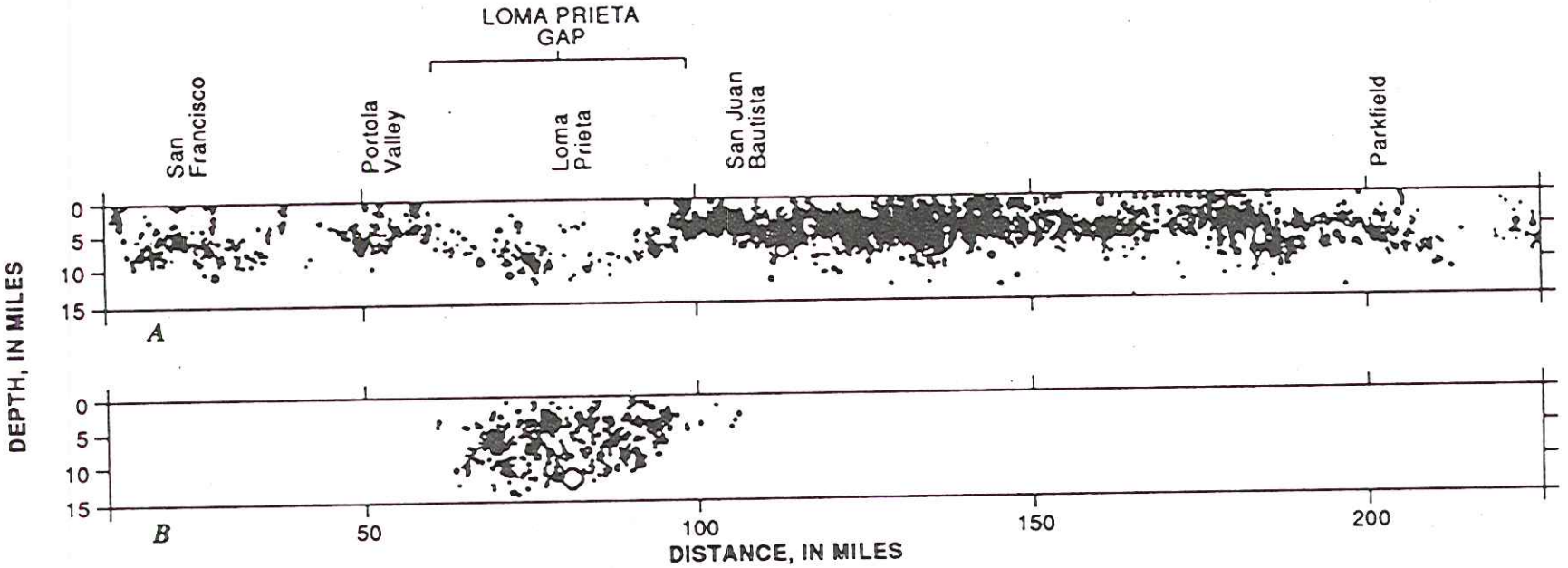

HETEROGENEOUS SLIP AT LOMA PRIETA

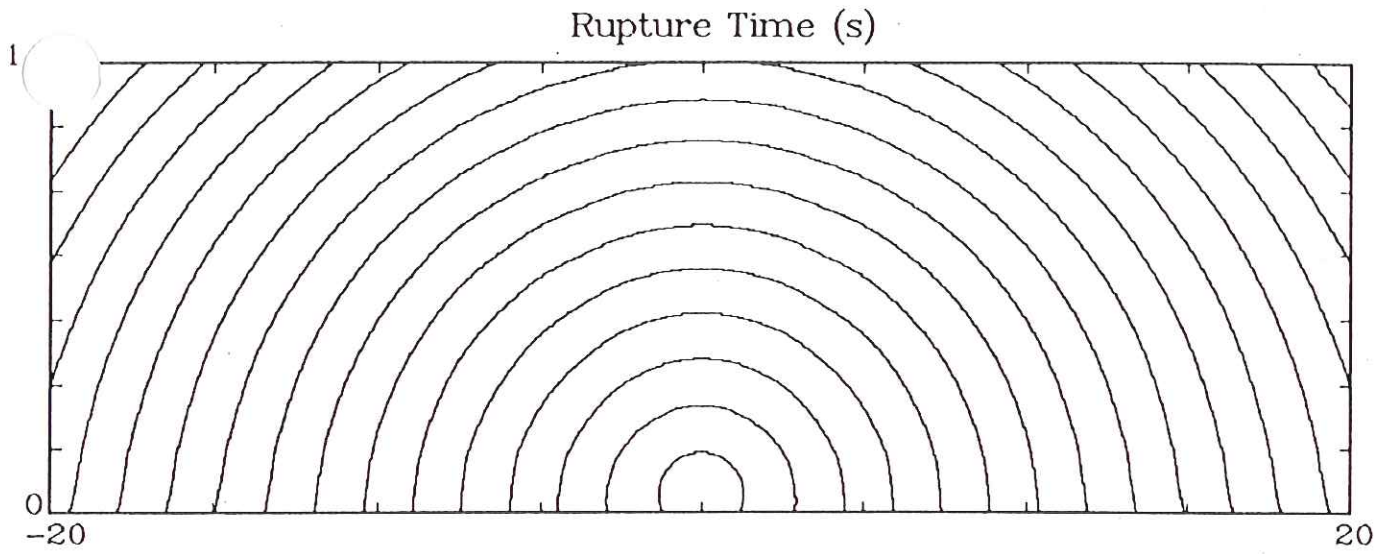

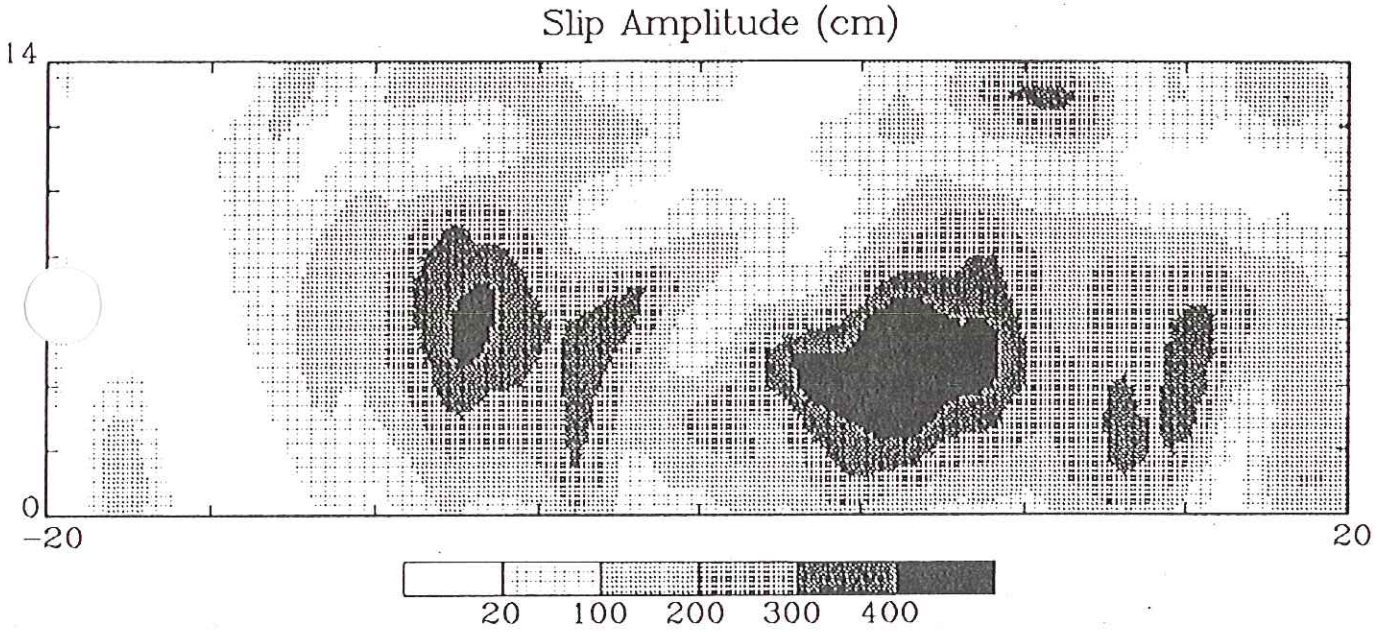

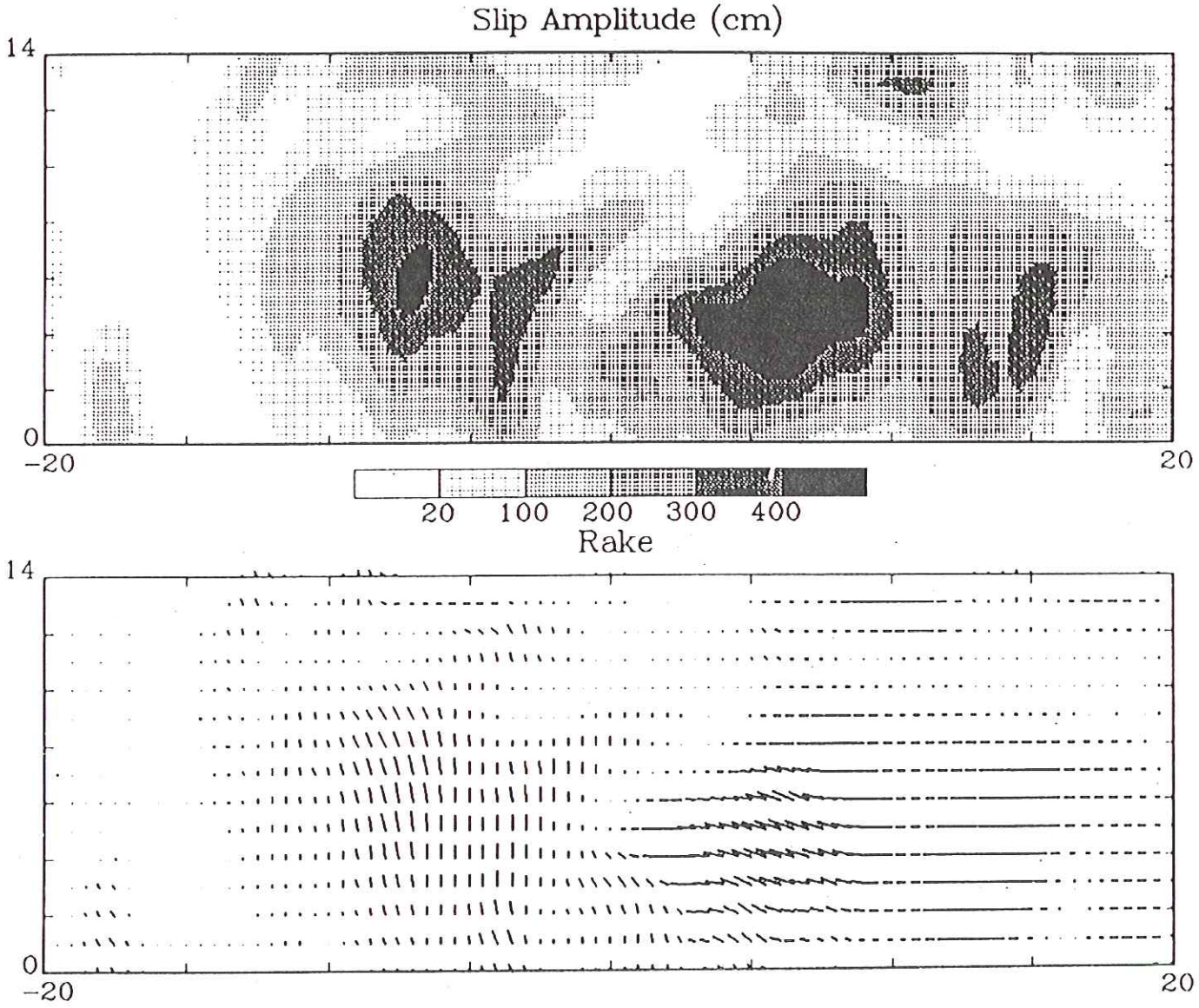
Slip Amplitude (cm)
14
0
−20
20
20
100
200
300
400
Rake
14
0
−20
20

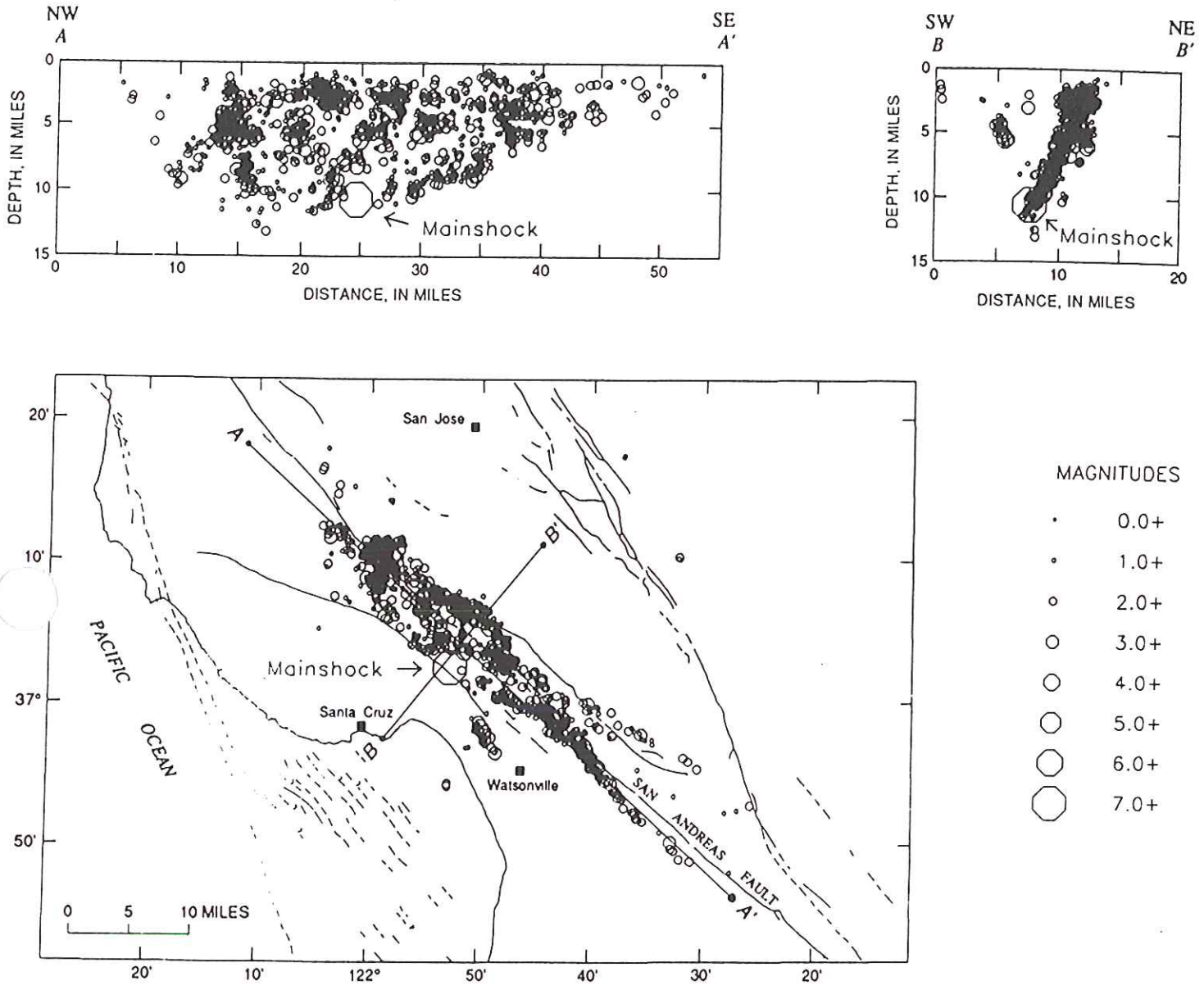

Figure 2.5 (A) Epicenters and foci of the main shock and aftershocks of the 1989 Santa Cruz (Loma Prieta) earthquake sequence. (B) Section AA′ along the San Andreas fault. (C) Section BB′ across the San Andreas fault indicating the dip of the main ruptured fault plane. [From Plafker and Galloway, 1989.]

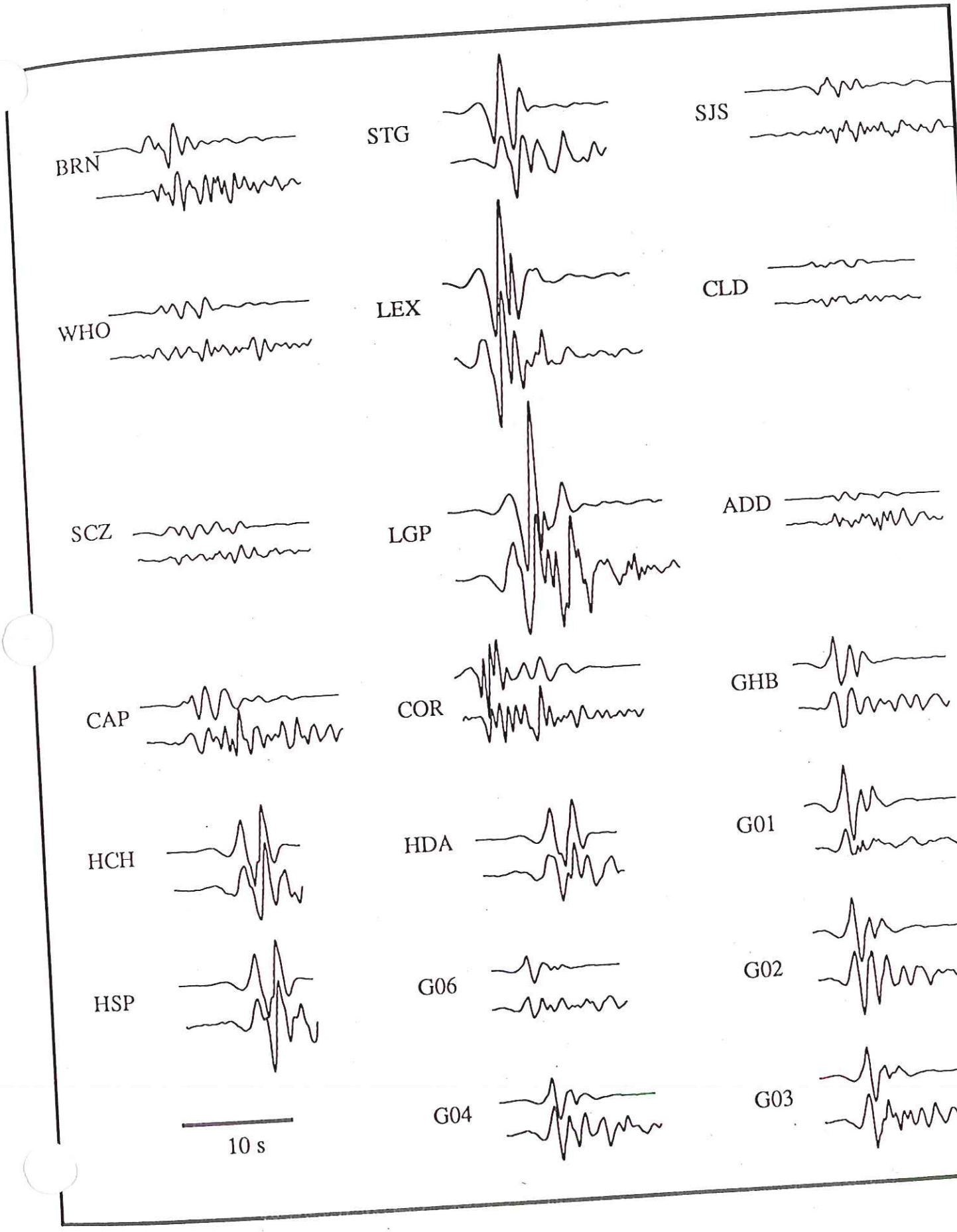
Fit to 220° Component
BRN
STG
SJS
WHO
LEX
CLD
SCZ
LGP
ADD
CAP
COR
GHB
HCH
HDA
G01
HSP
G06
G02
G04
G03
10 s

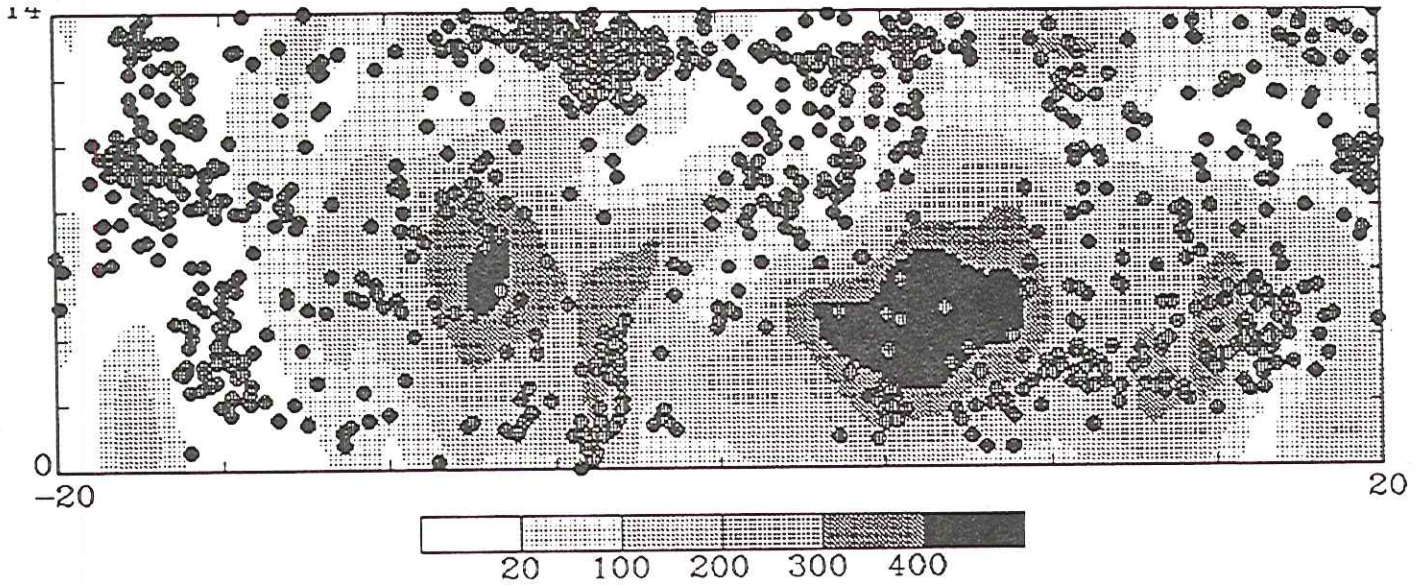
14
0
−20
20
20
100
200
300
400

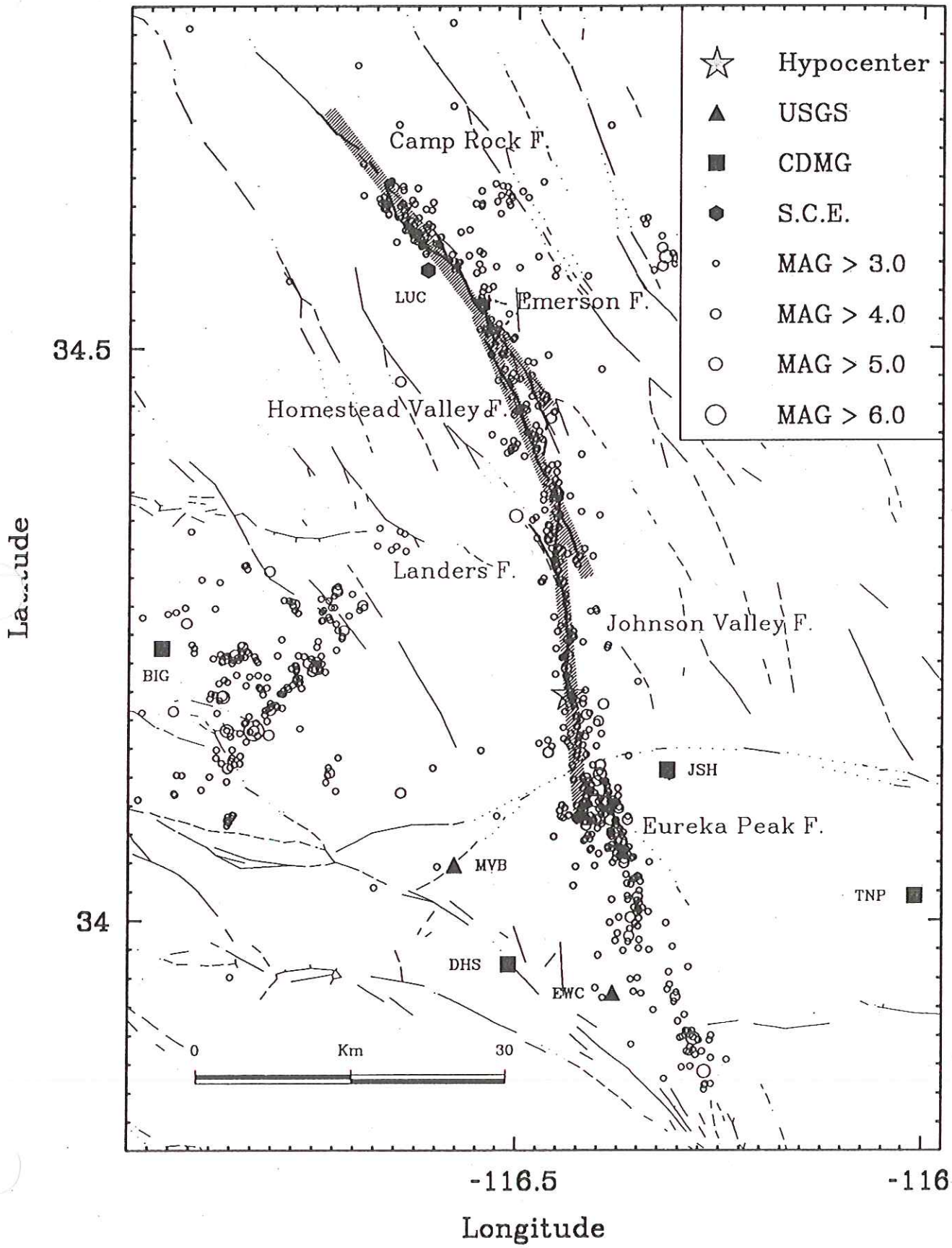
Hypocenter
USGS
CDMG
S.C.E.
MAG > 3.0
MAG > 4.0
MAG > 5.0
MAG > 6.0
Camp Rock F.
Emerson F.
Homestead Valley F.
Landers F.
Johnson Valley F.
Eureka Peak F.
LUC
BIG
JSH
MVB
TNP
DHS
EWC
0
Km
30
34.5
34
-116.5
-116
Latitude
Longitude

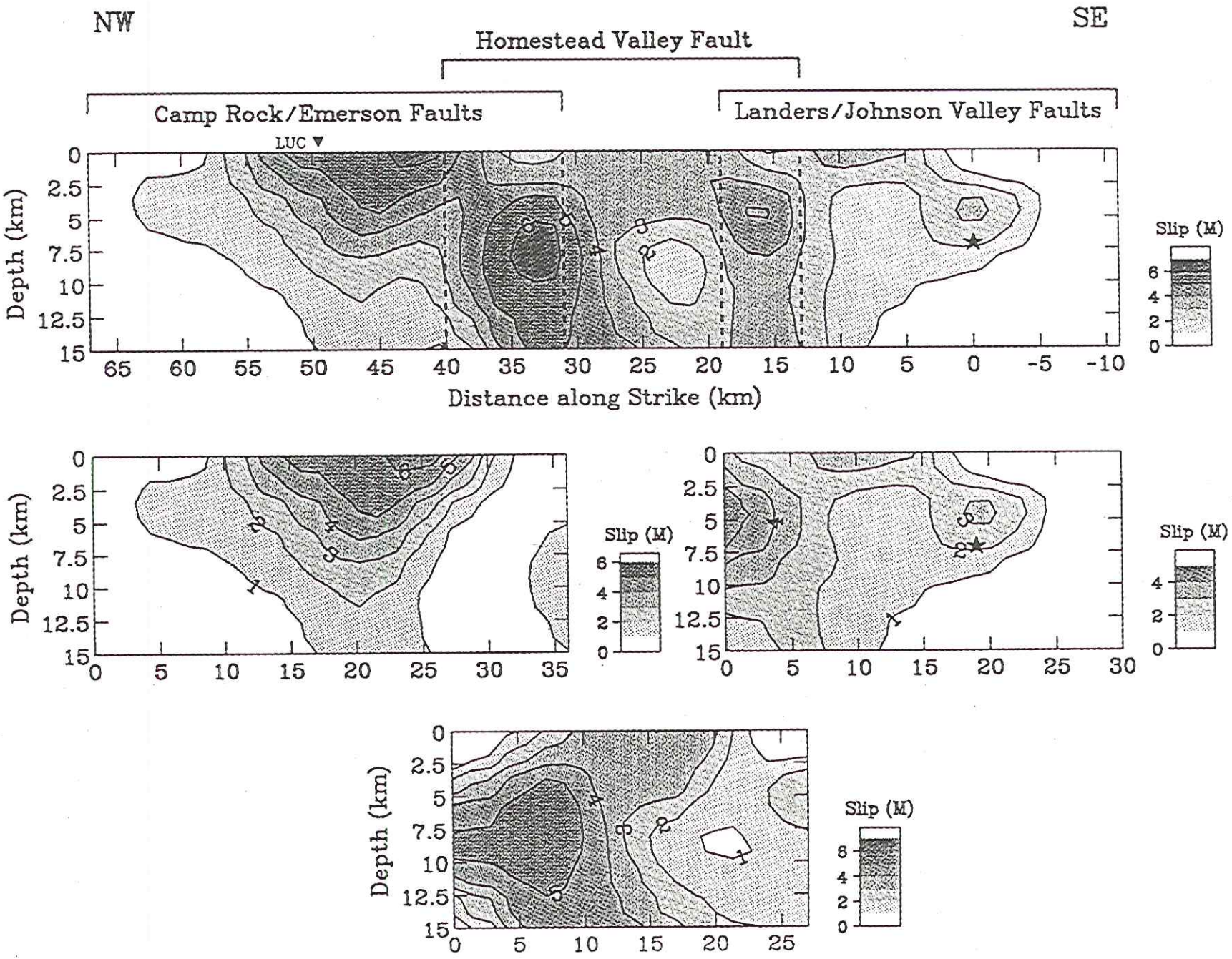
NW
SE
Homestead Valley Fault
Camp Rock/Emerson Faults
Landers/Johnson Valley Faults
LUC
Depth (km)
Distance along Strike (km)
Slip (M)

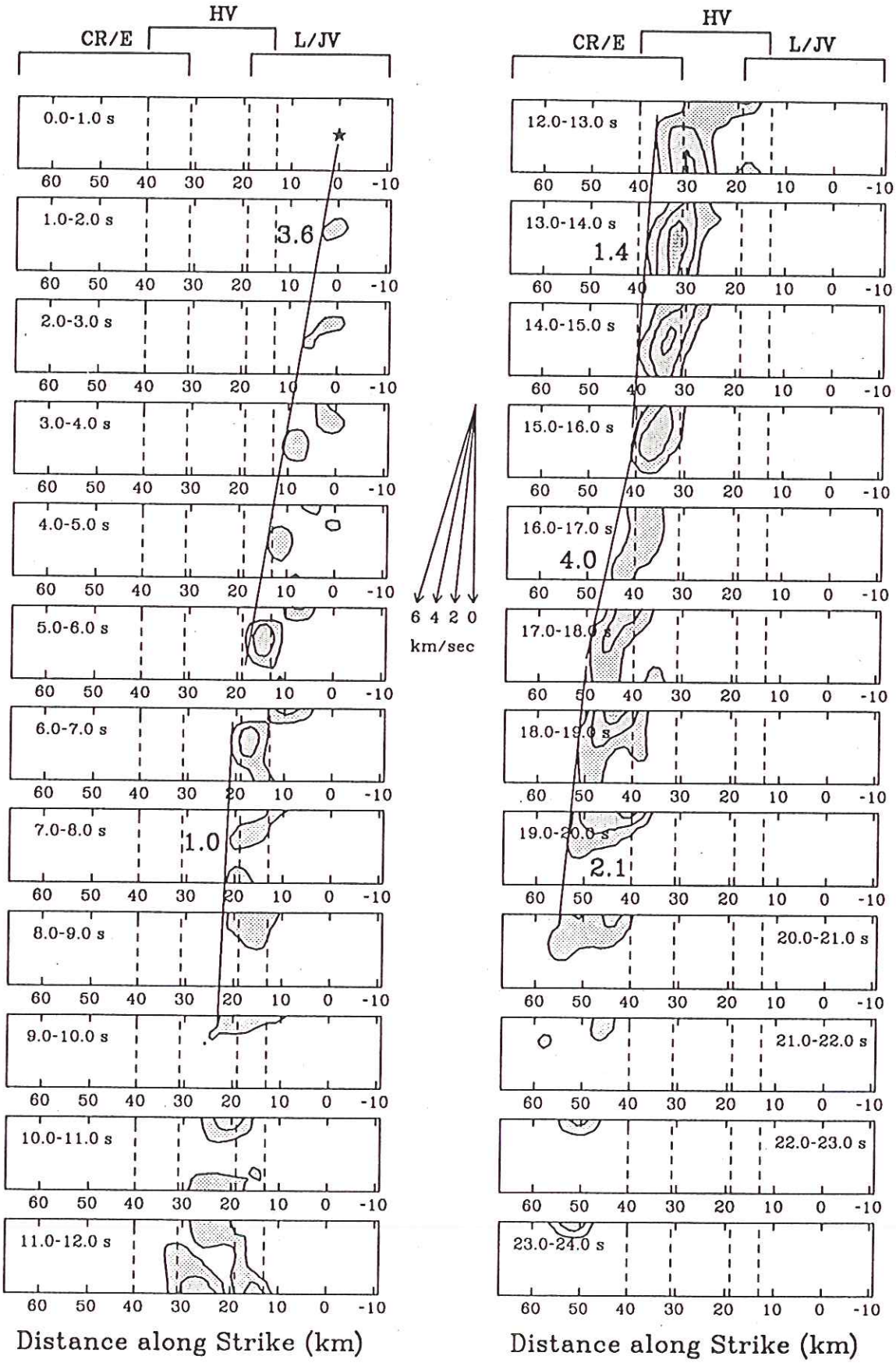
HV
CR/E
L/JV
0.0-1.0 s
1.0-2.0 s
3.6
2.0-3.0 s
3.0-4.0 s
4.0-5.0 s
5.0-6.0 s
6.0-7.0 s
7.0-8.0 s
1.0
8.0-9.0 s
9.0-10.0 s
10.0-11.0 s
11.0-12.0 s
60 50 40 30 20 10 0 -10
6 4 2 0
km/sec
12.0-13.0 s
13.0-14.0 s
1.4
14.0-15.0 s
15.0-16.0 s
16.0-17.0 s
4.0
17.0-18.0 s
18.0-19.0 s
19.0-20.0 s
2.1
20.0-21.0 s
21.0-22.0 s
22.0-23.0 s
23.0-24.0 s
Distance along Strike (km)
Distance along Strike (km)

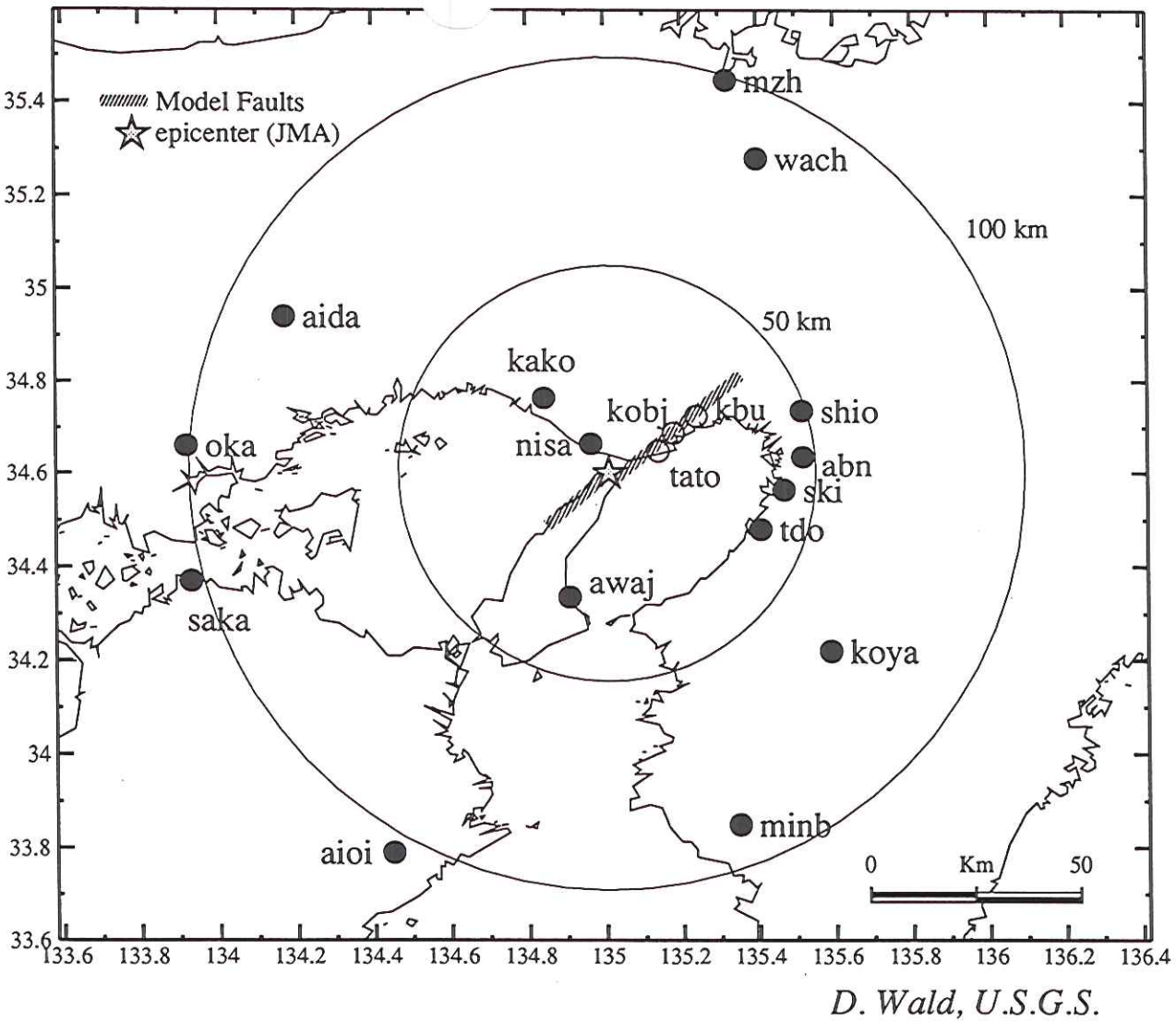

▲ **Figure 2** Map of strong motion stations and the surface location of the two model fault planes used in this study. Circles denote epicentral distances of 50 and 100 km.

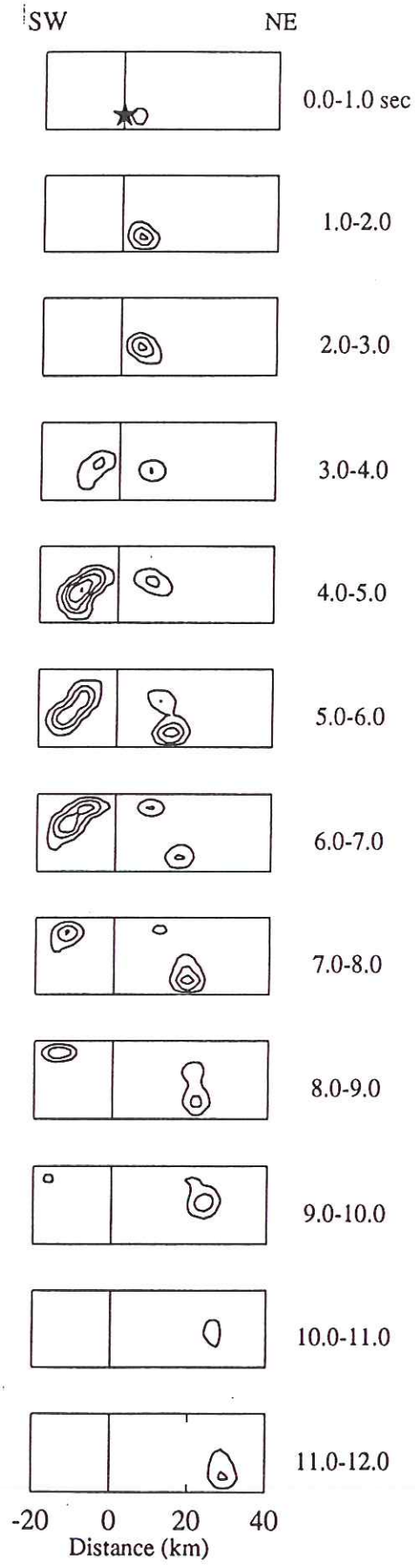

▲ **Figure 4** Rupture progression in one second time "snapshots". The Nojima and the Suma/Suwayama fault segments (left and right, respectively), depicted as rectangles, are viewed from the southeast. Slip is contoured in 0.25 meter intervals.

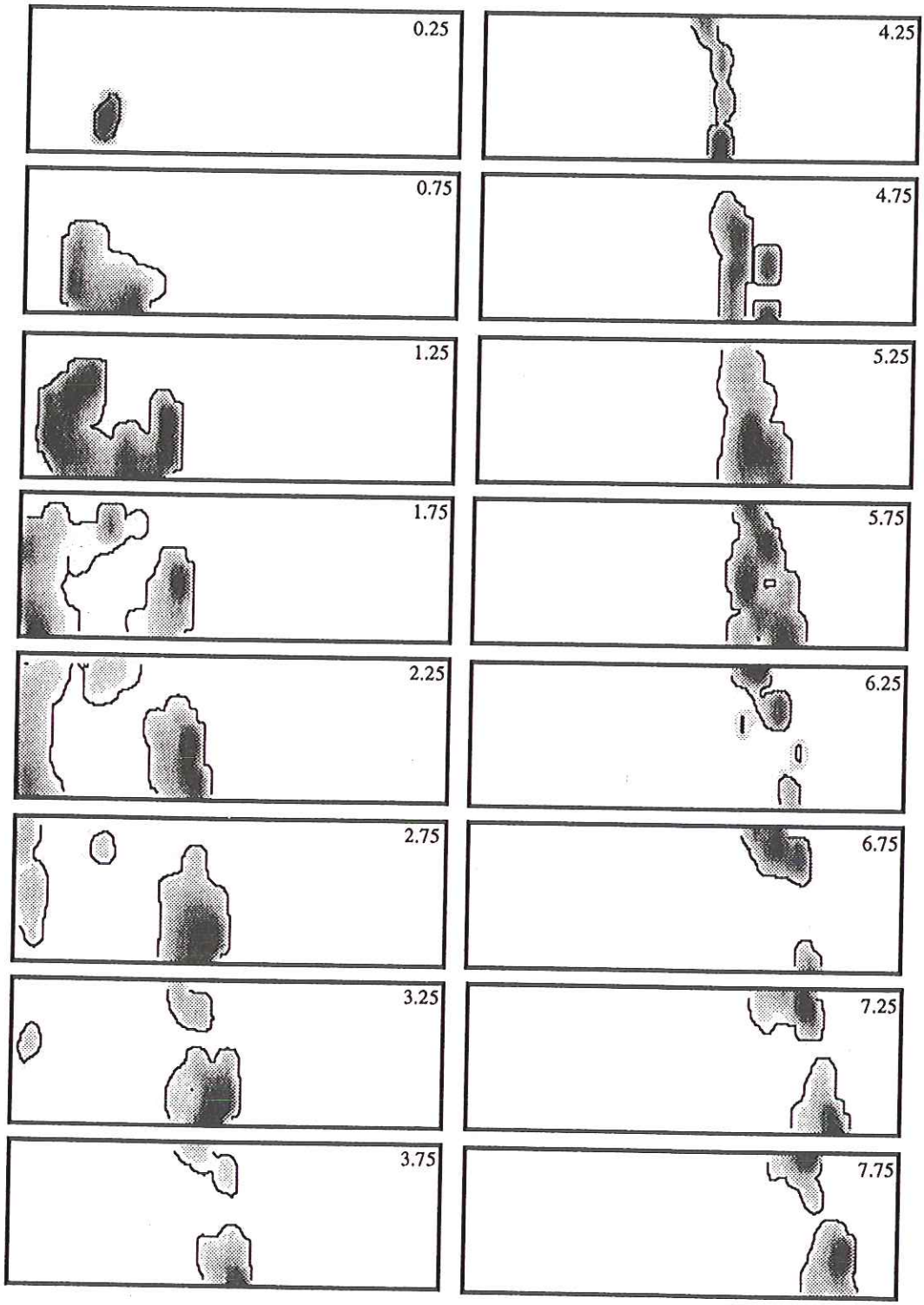

Figure 8. Snapshots of rupture. Panels show snapshots of the rupture at 0.5-s intervals starting 0.25 s into the earthquake. Times are shown in the top right corner of each panel. The darkness of shading in each panel is normalized and proportional to slip velocity. The 1 cm/s contour is shown as a contour. Once 2 s have elapsed, only a small part of the fault is rupturing at a time. By 4 s into the earthquake, slip is constricted to a very small portion of the fault. This pulse-like behavior is attributable to the rupture heterogeneity required by the strong motion data, which causes the fault to heal.

1954

What would this guy have seen?

1 m/sec

2–3 km/sec rupture propagation

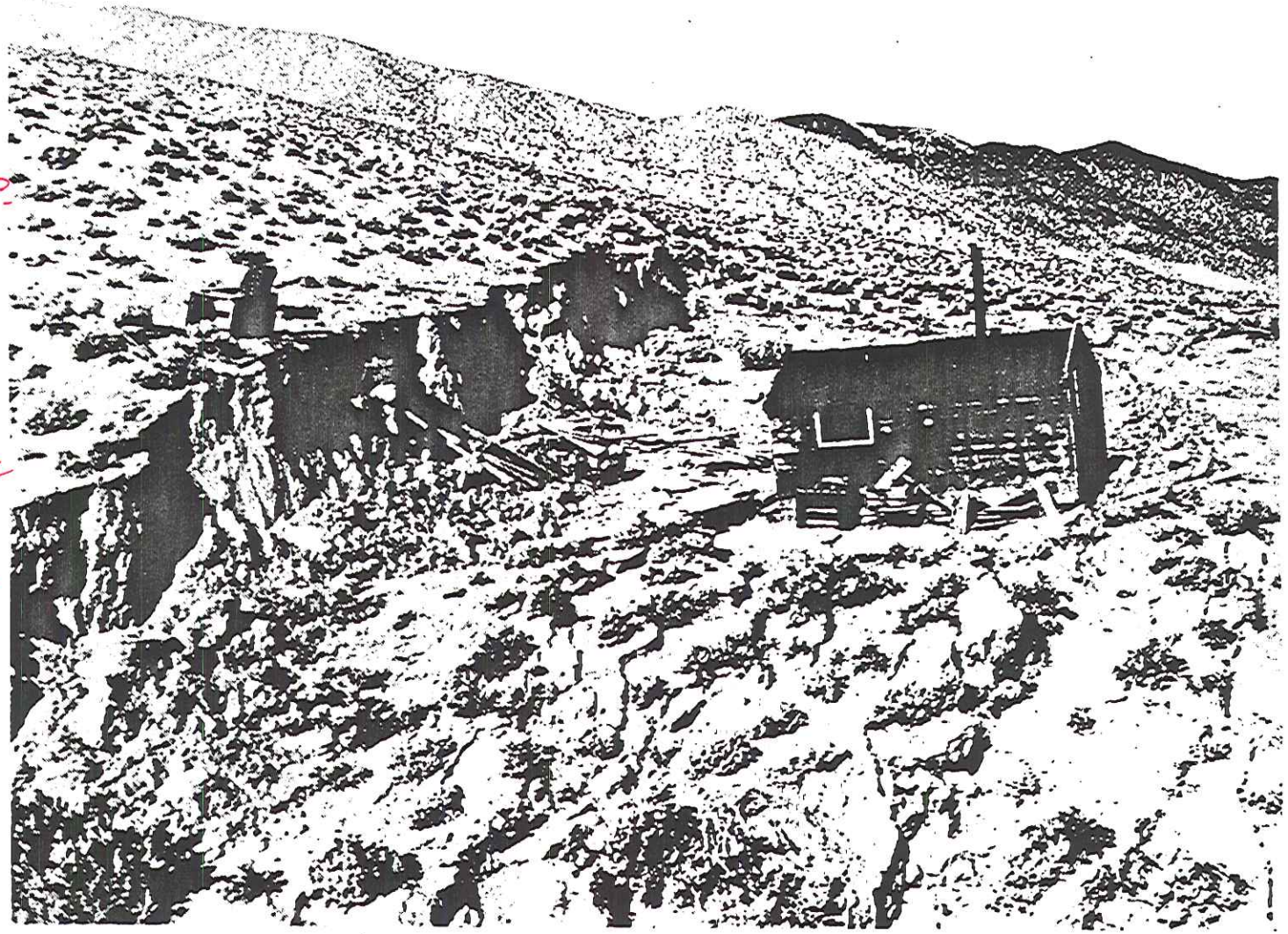

Figure 6.5 A fault scarp in Ixl Canyon, Fairview Mountain, Nevada. [Courtesy of Karl V. Steinbrugge.]